



**UNIVERSIDADE ESTADUAL DE CAMPINAS**  
Faculdade de Engenharia Mecânica

**DANIELA ANDRADE DAMASCENO**

***Nonlinear Atomic-scale Finite Element Method  
for the Modelling of Nanomaterials and  
Nanostructures***

***Modelagem de Nanomateriais e  
Nanoestruturas pelo Método não Linear de  
Elementos Finitos em Escala Atômica***

CAMPINAS  
2017

DANIELA ANDRADE DAMASCENO

*Nonlinear Atomic-scale Finite Element Method  
for the modelling of Nanomaterials and  
Nanostructures*

*Modelagem de Nanomateriais e  
Nanoestruturas pelo Método não Linear de  
Elementos Finitos em Escala Atômica*

Thesis presented to the School of Mechanical Engineering of the University of Campinas in partial fulfillment of the requirements for the degree of Doctor in Mechanical Engineering, in the area of Solid Mechanics and Mechanical Design.

Tese apresentada à Faculdade de Engenharia Mecânica da Universidade Estadual de Campinas como parte dos requisitos exigidos para a obtenção do título de Doutora em Engenharia Mecânica, na Área de Mecânica dos Sólidos e Projeto Mecânico.

Supervisor: Prof. Dr. Euclides de Mesquita Neto

Co-supervisor: Prof. Dr. Nimalsiri Dharmakeerthi Rajapakse

ESTE EXEMPLAR CORRESPONDE À VERSÃO  
FINAL DA TESE DEFENDIDA PELA ALUNA  
DANIELA ANDRADE DAMASCENO, E  
ORIENTADA PELO PROF. DR. EUCLIDES DE  
MESQUITA NETO

.....  
  
.....  
ASSINATURA DO ORIENTADOR

CAMPINAS  
2017

**Agência(s) de fomento e nº(s) de processo(s):** CNPq, 141173/2013-0

Ficha catalográfica  
Universidade Estadual de Campinas  
Biblioteca da Área de Engenharia e Arquitetura  
Luciana Pietrosanto Milla - CRB 8/8129

D18n Damasceno, Daniela Andrade, 1989-  
Nonlinear atomic-scale finite element method for the modeling of  
nanomaterials and nanostructures / Daniela Andrade Damasceno. – Campinas,  
SP : [s.n.], 2017.

Orientador: Euclides de Mesquita Neto.  
Coorientador: Nimalsiri Dharmakeerthi Rajapakse.  
Tese (doutorado) – Universidade Estadual de Campinas, Faculdade de  
Engenharia Mecânica.

1. Grafeno. 2. Nanoestrutura. 3. Quiralidade. 4. Dinâmica molecular. 5.  
Campo de força. I. Mesquita Neto, Euclides de, 1956-. II. Rajapakse, Nimalsiri  
Dharmakeerthi. III. Universidade Estadual de Campinas. Faculdade de  
Engenharia Mecânica. IV. Título.

Informações para Biblioteca Digital

**Título em outro idioma:** Modelagem de nanomateriais e nanoestruturas pelo método não  
linear de elementos finitos em escala atômica

**Palavras-chave em inglês:**

Graphene

Nanostructure

Molecular dynamics

Chirality

Force field

**Área de concentração:** Mecânica dos Sólidos e Projeto Mecânico

**Títuloção:** Doutora em Engenharia Mecânica

**Banca examinadora:**

Euclides de Mesquita Neto [Orientador]

Francisco Célio de Araújo

Munir Salomão Skaf

José Luiz Antunes de Oliveira e Sousa

Gabriel de Oliveira Ribeiro

**Data de defesa:** 27-07-2017

**Programa de Pós-Graduação:** Engenharia Mecânica

**UNIVERSIDADE ESTADUAL DE CAMPINAS**  
**FACULDADE DE ENGENHARIA MECÂNICA**  
**COMISSÃO DE PÓS-GRADUAÇÃO EM ENGENHARIA MECÂNICA**  
**DEPARTAMENTO DE MECÂNICA COMPUTACIONAL**  
**TESE DE DOUTORADO ACADEMICO**

*Nonlinear Atomic-scale Finite Element Method for  
the Modeling of Nanomaterials and Nanostructures*

*Modelagem de Nanomateriais e Nanoestruturas  
pelo Método não Linear de Elementos Finitos em  
Escala Atômica*

Autora: Daniela Andrade Damasceno

Orientador: Euclides de Mesquita Neto

Coorientador: Nimalsiri Dharmakeerthi Rajapakse

A Banca Examinadora composta pelos membros abaixo aprovou esta Tese:

**Prof. Dr. Euclides de Mesquita Neto, Presidente**  
**DMC – Faculdade de Engenharia Mecânica - UNICAMP**

**Prof. Dr. Francisco Célio de Araújo**  
**DECIV – UFOP**

**Prof. Dr. Munir Salomão Skaf**  
**IQ – UNICAMP**

**Prof. Dr. José Luiz Antunes de Oliveira e Sousa**  
**FEC – Unicamp**

**Prof. Dr. Gabriel de Oliveira Ribeiro**  
**DEES-UFMG**

A Ata da defesa com as respectivas assinaturas dos membros encontra-se no processo de vida acadêmica do aluno.

Campinas, 27 de julho de 2017.

## Dedication

*I dedicate this thesis to my nephews: Enzo, Danilo and Yago.*

*Dedico esta tese aos meus sobrinhos: Enzo, Danilo e Yago.*

## Acknowledgements

This work was carried out in four and a half years. I start by thanking everyone who directly or indirectly contributed to the completion of this thesis.

I would like to express my sincere gratitude to my advisor Prof. Dr. Euclides de Mesquita Neto for the opportunity to be developing this research, for the support during the six and a half years, in which we are working together, for the discussions and mainly for the patience and confidence throughout all those years.

I also wish to express my gratitude to my co-supervisor Prof. Dr. Nimal Rajapakse who gave me great support in the realization of this thesis over the past three and a half years. I would like to thank you for accepting to be my supervisor during my stay in Canada and encouragement extended to me.

I would like to thank the members of the jury for coming to my defense, for the discussions and for contributing to the improvement of this work. I am very thankful to Prof. Dr. Renato Pavanello for the meetings and support throughout this work.

I am also grateful to the Faculty of Mechanical Engineering of UNICAMP, in particular, to the Department of Computational Mechanics. I am thankful to Secretary Beth Viana for the support provided in administrative tasks. I would also like to thank the staffs of SIFEM, CPG and cleaning for their support during the development of this thesis.

I would like to thank Nuwan, William Vicente and Cristiano Woellner for their support and for their experienced advices to improve the methods presented on this thesis.

I would also like to express my gratitude to my graduation advisor Prof. Dr. Whisner Mamede and his wife Prof. Dr. Ana Mamede, for the support during graduation and for giving me the opportunity to undertake scientific initiation for two years at the IFSP, Sertãozinho campus, which I am also very grateful for.

I would like to thank a very special friend Tania Franzoni, who helped me and gave me great support not only for the development of this thesis, but mainly for the well-being of my day-to-day life. With your support I was able to find a way of peace, to live lighter days and mainly, I found the self-love.

I would like to express my sincere gratitude to my friends, my lab colleagues and my friends at home, in special, Priscilla Brandão, Thaís Pegoretti, Marcela Machado, Josué Labaki, Nilson Innocente, Luis Filipe, Edílson Dantas, Claudia Nobrega, Laryssa Abdala, Camila Moraes, Camila Dourado, Danilo Beli, Tyche, Emily, Polly and Zarina. Thank you so much

for the support, the conversations, the laughter, the tears, all the moments were very special and made these years unforgettable.

I am also grateful to CNPq, CEPID, Fapesp, ELAP and Capes for their financial support and research incentive.

And to finish I would like to express my eternal gratitude to the people that I love the most. Thank you father and mother for my life, for letting me dream and say that I am capable. Thank you mother for all the teachings, thank you father for the way you lead your life. To my brothers, thank you very much for giving me my nephews, they are the most valuable gifts I could receive. Thank you, Rosângela, for all your affection. I would also like to thank my boyfriend for all the support, understanding, encouragement, more life and strength throughout this final phase of this work. None of this would be so special if I could not share it with you.

## **Agradecimentos**

Este trabalho foi realizado em quatro anos e meio. Ele é o resultado de muito amor e dedicação pelos estudos que se iniciaram alguns anos atrás. Eu começo agradecendo a todas as pessoas que de forma direta ou indireta contribuíram para realização deste trabalho.

Eu gostaria de expressar a minha sincera gratidão ao meu orientador Prof. Dr. Euclides de Mesquita Neto pela oportunidade de estar desenvolvendo esta pesquisa, pelo apoio ao longo desses seis anos e meio em que estamos trabalhando juntos, pelas discussões e principalmente pela paciência e confiança ao longo de todos esses anos.

Eu gostaria também de expressar minha gratidão ao meu coorientador Prof. Dr. Nimal Rajapakse que me prestou grande apoio na realização dessa tese nos últimos três anos e meio. Gostaria de agradecer por aceitar coorientar este trabalho, por aceitar ser meu supervisor durante minha estada no Canadá e pela confiança depositada em meu trabalho.

Gostaria de agradecer aos membros da banca por virem para minha defesa, pelas discussões e por contribuírem para a melhoria deste trabalho. Sou muito grata também ao Prof. Dr. Renato Pavanello pelas reuniões e apoio ao longo deste trabalho.

Eu também sou grata à Faculdade de Engenharia Mecânica da UNICAMP, em especial, ao Departamento de Mecânica Computacional. Sou grata à secretária Beth Viana pelo apoio proporcionado em tarefas administrativas. Agradeço também aos funcionários do SIFEM, da CPG e da limpeza pelo suporte prestado durante o desenvolvimento dessa tese.

Gostaria de agradecer aos colegas de trabalho Nuwan, William Vicente e Cristiano Woellner, pelo apoio, pelas discussões e reuniões sobre os métodos apresentados nesta tese.

Eu gostaria também de expressar minha gratidão ao meu orientador da graduação Prof. Dr. Whisner Mamede e sua esposa Prof. Dr. Ana Mamede, pelo apoio durante a graduação e por ter me dado à oportunidade de realizar iniciação científica por dois anos no IFSP, campus Sertãozinho, que também sou muito grata.

Gostaria de agradecer uma amiga muito especial Tania Franzoni, que me ajudou e me deu um grande apoio não só para o desenvolvimento desta tese, mas principalmente pelo bem estar do meu dia-a-dia. Com seu apoio pude encontrar um caminho de paz, viver dias mais leves e principalmente, encontrei o amor próprio.

Eu gostaria de expressar a minha sincera gratidão aos meus amigos, colegas de laboratório e minhas amigas de casa. Em especial, Priscilla Brandão, Thaís Pegoretti, Marcela Machado, Josué Labaki, Nilson Inocente, Luis Filipe, Edilson Dantas, Claudia Nobrega, Laryssa Abdala,



Camila Moraes, Camila Dourado, Danilo Beli, Tyche, Emily, Polly e Zarina. Muito obrigada pelo apoio, pelas conversas, pelas risadas, pelos choros, todos os momentos foram muito especiais e tornaram esses anos inesquecíveis.

Eu também sou grata ao CNPq, CEPID, ELAP e a Capes pelo apoio financeiro e incentivo a pesquisa.

E para finalizar eu gostaria de expressar a minha eterna gratidão as pessoas que eu mais amo. Obrigada pai e mãe pela minha vida, por me deixar sonhar e dizer que sou capaz. Obrigada mãe por todos os ensinamentos, obrigada pai pelo modo de levar a vida. Aos meus irmãos, muito obrigada por me dar os meus sobrinhos, eles são os presentes mais valiosos que eu poderia receber. Obrigada Rosângela por todo carinho. Gostaria também de agradecer ao meu namorado por todo apoio, pela compreensão, incentivo, mais vida e força ao longo dessa fase final deste trabalho. Nada disso seria tão especial se eu não pudesse compartilhar com vocês.

*"Every choice is a renunciation."*

---

Thomas Aquinas

## Resumo

Este trabalho apresenta o comportamento mecânico de materiais em nanoescala aplicando o método de elementos finitos de escala atômica (AFEM), proposto por Liu et al., (2004), utilizando diferentes campos de potencial atômico. O método AFEM é formulado com base no conceito de campos de potenciais que descrevem a interação entre átomos. Os potenciais considerados neste estudo são o potencial de Lennard-Jones (Jones, 1924), o potencial de Tersoff (Tersoff, 1987), e o potencial REBO de segunda geração (Second-Generation Reactive Empirical Bond Order) (Brenner et al., 2002).

O objetivo de considerar e implementar o potencial de Lennard-Jones é introduzir e discutir questões fundamentais sobre a aplicação do método AFEM, como a convergência, e o tratamento consistente dos átomos nas bordas (contornos). Propomos uma abordagem para os elementos atômicos uni- e bidimensionais, para a inclusão das condições de contorno e também para explorar a ideia de relacionar o tamanho do elemento atômico ao conceito de raio de corte aplicado na Dinâmica Molecular (MD). Em oposição ao caráter local dos elementos dentro do quadro do método de elementos finitos (FEM) clássico, os potenciais utilizados no método AFEM têm caráter não-local.

Depois de examinar as questões fundamentais da formulação do método AFEM considerando o potencial de Leonard-Jones, a análise é estendida a potenciais interatômicos mais complexos, como o potencial de Tersoff e o potencial REBO de segunda geração, os quais são capazes de descrever o comportamento mecânico de folhas de grafeno. Serão consideradas folhas de grafeno com e sem defeitos, nas direções armchair e zigzag. Será analisada pelo método AFEM a influência da presença de defeitos no comportamento mecânico da folha de grafeno quando submetida a um carregamento uniaxial.

Os resultados numéricos obtidos pelo método AFEM, tais como, as relações força-deformação, são comparados com a simulação MD obtida a partir do software LAMMPS, e com os resultados apresentados na literatura. Precisão, convergência e estabilidade do AFEM serão comparadas com MD. Como a formulação básica do método AFEM é não-linear, sendo assim, o método de Newton-Raphson é usado para executar as iterações. As relações força-deformação e tensão-deformação são obtidas numericamente considerando malhas de diferentes tamanhos, defeitos e direções.

## Abstract

This work presents the mechanical behavior of materials at the nanoscale by applying the atomic-scale finite element method (AFEM), proposed by Liu et al., (2004), using different atomic potential fields. AFEM is formulated based on the concept of potentials describing the interaction among atoms. The potentials considered in this study are the Lennard-Jones potential (Jones, 1924), Tersoff potential (Tersoff, 1987) and second-generation Reactive Empirical Bond Order (REBO) potential (Brenner et al., 2002).

The purpose of considering and implementing the Lennard-Jones potential is to introduce and discuss fundamental issues about the application of the AFEM such as convergence and consistent treatment of boundary atoms. We propose a new arrangement for the atomic finite elements in one and two dimensions, for the inclusion of the boundary conditions and also to exploit the idea of linking the size of the atomic-scale element to the concept of cut-off radius applied in Molecular Dynamics (MD) simulations. Opposite to the local character of elements within the framework of classical FEM, the potentials used to generate the AFEM have non-local character.

After examining the key issues of the formulation of AFEM using Leonard-Jones potential, the analysis is extended to more complex interatomic potentials such as Tersoff potential and second-generation REBO potential, which can describe the mechanical behavior of graphene sheets. Pristine and graphene sheets with cracks with armchair and zigzag edges are considered. The influence of vacancy defects on mechanical behavior under uniaxial tensile loading is analyzed by the AFEM.

The numerical results obtained from AFEM such as the force-strain relations are compared with the MD simulation obtained from LAMMPS software, and with the results presented in the literature. Accuracy, convergence and stability of the AFEM compared to MD are examined. As the basic formulation of the AFEM is non-linear, the Newton-Raphson method is used to perform the iterations. Force-strain and stress-strain relations are obtained numerically for meshes of different sizes, defects and orientations.

## List of Figures

1.1 Schematic of the length scale of interest in nanotechnology.	22
1.2 Graphene sheet with armchair and zigzag edges.	24
1.3 (a) Buckyballs, (b) nanotubes, and (c) graphite.	24
1.4 (a) Diagram of the multi-layer graphene/PET structure. (b) Suspended graphene nanoribbon and schematic of suspended graphene.	25
1.5 Nanomechanical models.	26
3.1 Lennard-Jones Potential $U(r_{ij})$ , and internal force $F(r_{ij})$ .	34
3.2 An atomic chain with 5 atoms and distinct relations between the equilibrium distance $r_{eq}$ and the chosen cut-off radius of the LJ potentials, $r_c$ .	35
3.3 A three-node atomic-scale finite element.	37
3.4 (a) A five-node atomic-scale finite element, and (b) A seven-node atomic-scale finite element.	38
3.5 Atomic finite element with seven nodes.	39
3.6 Atomic finite elements for different two-dimensional Bravais lattices.	40
3.7 Square and Trigonal f two-dimensional Bravais lattices.	40
3.8 Example of assemblage scheme for an atomic chain of 4 atoms.	42
3.9 Introduction the boundary conditions at the 4 atoms chain.	43
3.10 Atomic structure with complete and modified elements.	44
3.11 A schematic diagram of a one-dimensional atomic chain.	46
3.12 External force by strain (3, 5 and 7 nodes elements).	47
3.13 1D AFEM results - a) force-strain relation; b) number of iterations for AFEM , c) MD-AFEM relative error, d)convergence measure	48
3.14 A schematic diagram of a two-dimensional lattice.	49
3.15 (a) Force-strain relation; (b) force-displacement relation; (c) convergence of AFEM; (d) force by number of iterations.	50
3.16 Initial and final configuration of atomic structure.	51
3.17 Internal force by r.	52
3.18 (a) Pristine mesh; (b) Defected mesh, (c) stress-strain curves, and (d) final equilibrium configuration from AFEM and MD.	53

3.19 (a) Square bravais lattice; (b) Force-strain curves obtained from AFEM and MD.	54
4.1 Part of graphene sheet.	58
4.2 (a) Graphene sheet, (b) AFEM element, (c) Atomic finite element with angle bending.	59
4.3 (a) to (f) Modified atomic elements.	60
4.4 (a) Pristine graphene sheet with 228 atoms and armchair edges, (b) Pristine graphene sheet with 228 atoms and zigzag edges, (c) and (d) Stress-strain curves obtained from AFEM and MD for armchair and zigzag sheets based on Tersoff potential	65
4.5 (a) Pristine graphene sheet with 660 atoms and armchair and zigzag edges, (c) Stress-strain curves obtained from AFEM and MD for armchair and zigzag sheets based on Tersoff potential.	66
4.6 (a) Shows a comparison of the stress-strain curves of graphene sheets with 228 and 660 atoms and armchair edges obtained from AFEM, (b) shows a comparison of the stress-strain curves of graphene sheets with 228 and 660 atoms and zigzag edges obtained from AFEM.	66
4.7 Stress-strain curves of the pristine graphene sheet having armchair zigzag edges along x direction.	68
4.8 Graphene sheet having zigzag and armchair edges with a crack of width 6.98 Å.	69
4.9 Stress-strain relation of the graphene sheet having armchair and zigzag edges with a crack of width 6.98 Å.	70
5.1 Part of graphene sheet.	75
5.2 Atomic finite element with angle bending.	80
5.3 (a) Pristine graphene sheet with 228 atoms and armchair edges, (b) Pristine graphene sheet with 228 atoms and zigzag edges, (c) and (d) Stress-strain curves obtained from AFEM and MD for armchair and zigzag sheets based on Tersoff potential.	85
5.4 (a) Pristine graphene sheet with 660 atoms and armchair and zigzag edges, (c) Stress-strain curves obtained from AFEM and MD for armchair and zigzag sheets based on Tersoff potential.	86

5.5 (a) Shows a comparison of the stress-strain curves of graphene sheets with 228 and 660 atoms and armchair edges obtained from AFEM, (b) shows a comparison of the stress-strain curves of graphene sheets with 228 and 660 atoms and zigzag edges obtained from AFEM.	86
5.6 Stress-strain curves of the pristine graphene sheet having armchair zigzag edges along x direction.	87
5.7 Comparison of stress-strain curves of pristine bulk graphene obtained from AFEM using Tersoff and second generation REBO potentials with AIREBO potential based MD results.	89
5.8 Comparison of stress-strain curves from AFEM with additional MD results from literature.	90
5.9 Graphene sheet having zigzag and armchair edges with a crack of width 6.98 Å.	91
5.10 Stress-strain relation of the graphene sheet having armchair and zigzag edges with a crack of width 6.98 Å.	92
5.11 Armchair and zigzag edges of graphene nanoribbon.	94
5.12 Stress-strain curves of armchair and zigzag GNRs.	96
5.13 Variation of elastic modulus and tensile strength of GNRs with different widths.	96
5.14 Comparison of GNR stress-strain curves obtained from AFEM with MD results.	97

## List of Tables

1.1 Comparison of total energy obtained from AFEM and MD.	45
4.1 Parameters for carbon-carbon interactions.	57
4.2 Fracture strength calculated by atomistic studies.	67
4.3 Comparison of ultimate stress-strain results of graphene for the pristine sheet and for the one with vacancy defects.	70
5.1 AFEM element and total energy value obtained from AFEM and MD	76
5.2 Fracture strength calculated by atomistic studies.	88
5.3 Comparison of ultimate stress-strain results of graphene for the pristine sheet and for the one with vacancy defects.	92



## List of Abbreviations and Acronyms

### *Superscripts*

(0)	equilibrium position
i	individual atom i
3e	element with three atoms
i-5e	atom i, considering the element with five atoms
i-7e	atom i, considering the element with seven atoms
R	repulsive
A	attractive
$\pi$	bond $\pi$
$\sigma\pi$	bond $\sigma\pi$
C	carbon
H	hydrogen
t	total
conj	conjugated

### *Subscripts*

tot	total
i	individual atom i
j	individual atom j
k	individual atom k
f	force
ext	external
ij	bond ij
c	cut-off
eq	equilibrium
i-1	position of the atom i-1 related to atom i
i+1	position of the atom i+1 related to atom i
i-2	position of the atom i-2 related to atom i
i+2	position of the atom i+2 related to atom i
i-3	position of the atom i-3 related to atom i
i+3	position of the atom i+3 related to atom i
i+4	position of the atom i+3 related to atom i
i+5	position of the atom i+3 related to atom i
i+6	position of the atom i+3 related to atom i
e	element
a	atom
R	repulsive
A	attractive

### *Latin Letters*

U	Interatomic total energy
K	Stiffness matrix

**P** Non-equilibrium force  
**E** total energy  
 $r_{\text{eq}}$  equilibrium distance  
 $U_{\text{total}}^1$  total energy of element 1  
 $U_{\text{total}}^2$  total energy of element 1  
 $U_{\text{total}}^3$  total energy of element 1  
 $U_{\text{total}}^4$  total energy of element 1  
 $U_{\text{total}}$  total energy of the system  
 $U_{\text{tot}}^{23}$  total energy of element 23  
 $U_{\text{total}}^6$  total energy of element 6  
 $U_{\text{tot}}^{25}$  total energy of element 25  
 $R^{(1)}$  and  $R^{(2)}$  are the cut-off radii.  
 $Q_{ij}$  second generation REBO parameter  
 $A_{ij}$  second generation REBO parameter  
 $B_{ij}^{(n)}$  second generation REBO parameter  
 $R^{(1)}$  second generation REBO parameter  
 $R^{(2)}$  second generation REBO parameter

### *Greek Letters*

$\sigma$  in the Lennard Jones potential is the inter-particle distance at which the potential is zero  
 $\epsilon_{\text{LJ}}$  in the Lennard Jones potential is the depth of the potential well  
 $\theta$  angle  
 $\sigma$  in the results is the stress  
 $\epsilon$  in the results is the strain  
 $\lambda^1$  Tersoff parameter  
 $\lambda^2$  Tersoff parameter  
 $\beta^n$  Tersoff parameter  
 $\beta_{ij}^{(n)}$  second generation REBO parameter

### *Acronyms*

**AFEM** - Atomic-scale finite element method  
**MD** - Molecular Dynamics  
**FEM** - Finite Element Method  
**STM** - Scanning Tunneling Microscope  
**AFM** - Atomic Force Microscope  
**CNT** - Carbon nanotubes  
**GNR** - Graphene nanoribbons  
**GM-T** - Gurtin-Murdoch theory  
**C-C** - Carbon - carbon  
**LAMMPS** - Large-scale Atomic/Molecular Massively Parallel Simulator  
**REBO** - Reactive empirical bond order  
**LJ** - Lennard Jones

**AIREBO** - Adaptive Intermolecular Reactive Empirical Bond Order  
**nm** - Nanometer

# Table of Contents

**List of Figures**

**List of Tables**

**List of Abbreviations and Acronyms**

**Resumo**

**Abstract**

**1 Introduction**

**1.1 Nanotechnology**

**1.2 Motivation**

**1.3 Nanomechanics**

**1.4 Objectives**

**1.5 Outline of Current Work**

**2 Atomic-Scale Finite Element Method Formulation**

**3 Lennard Jones Potential**

**3.1 Atomic Elements**

**3.1.1 Atomic Element in one Dimensional**

**3.1.2 Atomic Element in two Dimensions**

**3.2 AFEM Implementation**

**3.3 Results**

**3.3.1 Comparison of AFEM and MD in One Dimension**

**3.3.2 Comparison of AFEM and MD in Two Dimensions**

**3.4 Conclusions**

**4 Tersoff Potential**

**4.1 Atomic Element**

**4.2 AFEM Implementation**

**4.3 Results and discussions**

**4.3.1 Molecular dynamics simulations**

**4.3.2 Verification of the accuracy of AFEM**

**4.3.3 Effects of chirality**

**4.3.4 Effects of vacancy defects**

**4.4 Conclusions**

<b>5</b>	<b>Second-Generation Reactive Empirical Bond Order Potential</b>
5.1	Atomic Element
5.2	AFEM Implementation
5.3	Results and discussions
5.3.1	Molecular dynamics simulations
5.3.2	Verification of the accuracy of AFEM
5.3.3	Effects of chirality
5.3.4	Effects of vacancy defects
5.3.5	Modelling of mechanical behaviour of graphene nanoribbons
5.4	Conclusions
<b>6</b>	<b>General Conclusions</b>
<b>7</b>	<b>Future Works</b>
	<b>References</b>

# 1 INTRODUCTION

## 1.1 Nanotechnology

The increasing interest in understanding of the behavior of nanomaterials has brought breakthroughs in the development of nanotechnologies. In 1974, the term “nanotechnology” was first defined by Tokyo Science University Professor Norio Taniguchi in a conference paper titled “On the Basic Concept of Nanotechnology” (Taniguchi, 1974). In his definition “Nano-technology” mainly consists of the processing of, separation, consolidation, and deformation of materials by one atom or by one molecule” (Taniguchi, 1974). Nanotechnologies are also defined as “the design, characterization, production and application of materials, structures, devices and systems by controlling their shape and size at the nanometre scale” (The Royal Society and The Royal Academy of Engineering, 2004). The size range of interest in nanotechnology is from about 0.1 nm to about 100 nm. Figure 1.1 shows a schematic of the length scale of interest in nanotechnology and illustrate the comparison of systems with range from  $10^{-10}$ m to 1m.

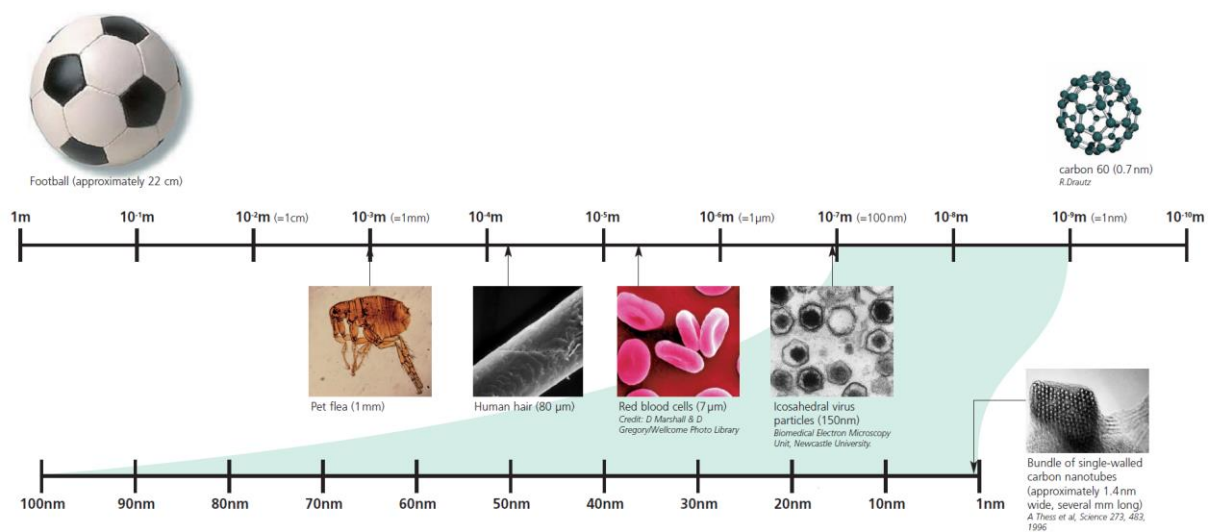


**Figure 1.1: Schematic of the length scale of interest in nanotechnology (Adapted from The Royal Society and The Royal Academy of Engineering, 2004)**

The manipulation of materials started in Pre-Modern era with the craftsmen's empirical understanding. Some examples are the Lycurgus Cup, which contains gold and silver nanoparticles, Damascus sabers, which contains carbon nanotubes and cementite nanowires, and others. Later, in the modern era, in 1857, Michael Faraday discovered colloidal "ruby" gold (Gupta, 2014). In 1959, the first lecture on nanotechnology and the possibility to control matter at the atomic scale was given by the physicist and Nobel Laureate Richard P. Feynman, in his classic lecture "There's Plenty of Room at the Bottom" (Feynman, 1959). In 1981, the Scanning Tunneling Microscope (STM) invented by Rohrer and Binnig (Binnig et al., 1983) at the IBM laboratories in Zurich, allowed researchers to observe surfaces at the atomic level for the first time, and earned the Nobel Prize in Physics for his discovery in 1986. Additionally, Binnig et al., in 1986, invented the Atomic Force Microscope (AFM) (Binnig et al., 1986). STM and AFM had important influence in the nanotechnology and nanoscience research, allowing researchers to manipulate atoms-by-atom. The Researchers Harold Kroto, Sean O'Brien, Robert Curl, and Richard Smalley in 1985 at Rice University discovered a structure made of carbon, namely Buckminsterfullerene ( $C_{60}$ ) (Kroto et al., 1985), also called buck-ball. Kroto, Curl and Smalley, for their discovery, earned the 1996 Nobel Prize in Chemistry. Later, in 1991, the carbon nanotubes (CNT) are discovered by Sumio Iijima, (Iijima, 1991), and he was awarded the Kavli Prize in Nanoscience in 2008.

The discovery of CNT (Iijima, 1991), separation of carbon allotrope "graphene" (a single flat layer of graphite) using mechanical exfoliation in 2004 (Novoselov et al., 2004) and advances in nanofabrication have opened the door for bottom-up approach to nanotechnology. In this approach, nanodevices are built from basic atomic structures such as graphene nanoribbons (GNR) and CNT. Surface defects can be minimized in the bottom-up approach to fabricate resonators with ultra-high Q-factors [Bunch et al. (2007), Garcia-Sanchez et al. (2008)]. Graphene, CNT, alumina or silicon whiskers and other nanoparticles allow for the synthesis of a new generation of composites with attractive mechanical properties that can lead to innovative breakthroughs in aerospace, construction and manufacturing industries (The Royal Society and The Royal Academy of Engineering, 2004). CNT reinforced polymer composites have been demonstrated for various applications [Njuguna et al. (2003), Goettler et al. (2007), Hu et al. (2006)].

## 1.2 Motivation

Growing understanding of nanomaterials behavior is making many advances in different fields of science, such as, engineering, medicine, biology, chemistry. In this thesis, the interest lies in the development of a computationally efficient tool for analysis of the mechanical behavior of the graphene sheet. Graphene (Novoselov et al., 2004) is a single layer of carbon atoms, connected by a covalent bond, arranged into a two dimensional hexagonal lattice. Figure 1.2 shows the graphene sheet with armchair edges (Fig. 1.2(a)) and zigzag edges (Fig. 1.2(b)).

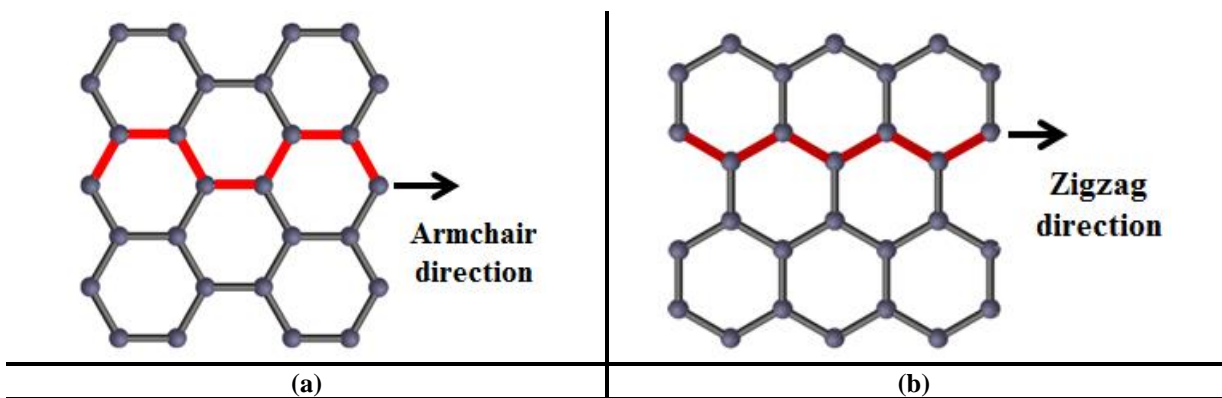


Figure 1.2: Graphene sheet with armchair and zigzag edges

Moreover, the graphene is considered the base of three carbon allotropes. As illustrated in Figure 1.3, wrapping graphene into a sphere produces buckyballs, folding into a cylinder produces nanotubes, and stacking several sheets of graphene leads to graphite. Furthermore, cutting graphene into a small ribbon results in nanoribbons.

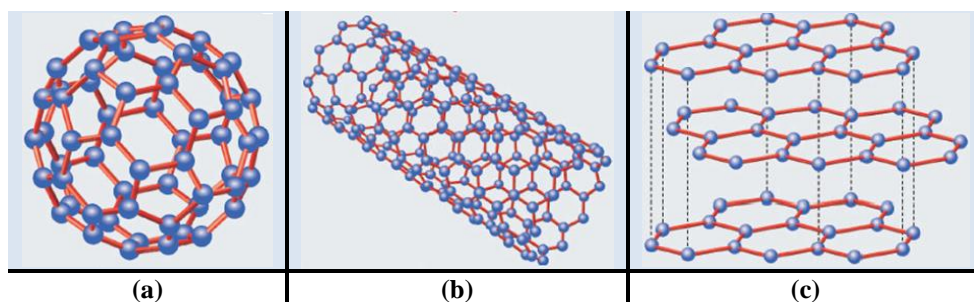
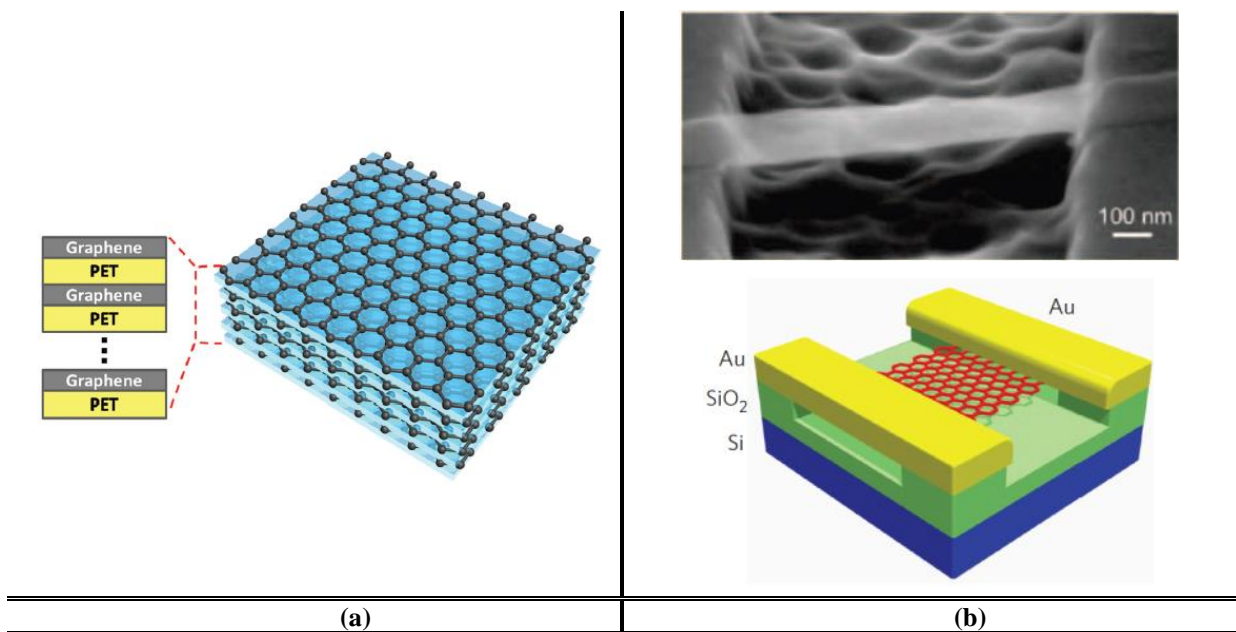


Figure 1.3: (a) Buckyballs, (b) nanotubes, and (c) graphite.



Graphene is currently receiving worldwide attention due to their extraordinary electronic, thermal, and mechanical properties that have led to revolutionary devices and applications [The Royal Society and The Royal Academy of Engineering, 2004; Novoselov et al. 2012; Iijima, 1991; Novoselov et al. 2004; Bunch et al. 2007; Garcia-Sanchez et al. 2008; Njuguna et al. 2003; Goettler et al. 2007; Hu et al. 2006; Yazdanbakhsh et al. 2009; Souza, 2012]. According to Cancino et al. (2014), carbon nanotubes have been widely applied for the development of nanomedicine. Figure (1.4) shows some graphene-based nanoelectromechanical devices. Figure 1.4(a) shows the Diagram of the multi-layer graphene/PET structure (Lu et. al., 2016), and Fig. 1.4(b) shows the suspended graphene nanoribbon and schematic of suspended graphene (Chen, 2009).



**Figure 1.4: (a) Diagram of the multi-layer graphene/PET structure. Fonte: (Lu et. al., 2016), (b) Suspended graphene nanoribbon and Schematic of suspended graphene (Chen, 2009).**

### 1.3 Nanomechanics

Nanomechanics of materials is a new branch of mechanics which studies the properties and behaviour of nanoscale materials and structures in response to applied external forces and restrictions. A structure with at least one dimension less than 100 nm is considered to be a

nanoscale, and, in this size range, in many cases, the quantum effect and the dependence of elastic properties at the atomic scale appears.

The mechanical behaviour of nanoscale systems can be analysed by using Ab-initio (first-principle) methods (Dirac, 1981), by semi-empirical quantum methods (Tadmor et al., 2011), and also by the continuum-based methods, as shown in Fig. 1.5. For nanoscale system the classical continuum mechanics breaks down at the nanoscale [Dingerville et al. (2005); Maranganti et al. (2007)]. Nanostructures greater than a few nanometres, multi-scale continuum methods such as Gurtin-Murdoch theory (GM-T) (Gurtin et al., 1975) that bridges surface and bulk energies is quite accurate and computationally inexpensive [Dingerville et al. (2005); Miller et al. (2000), Liu et al. (2010); Sapsathiarn et al. (2012)]. However, GM-T and other continuum models (e.g., non-local elasticity) are not strictly applicable to systems made of a single or few atomic layers (e.g. GNR and CNT). These have to be modelled using atomistic methods such as molecular dynamics (MD) to capture accurately the quantum mechanical effects [(Dirac, 1981); (Haile, 1992)].

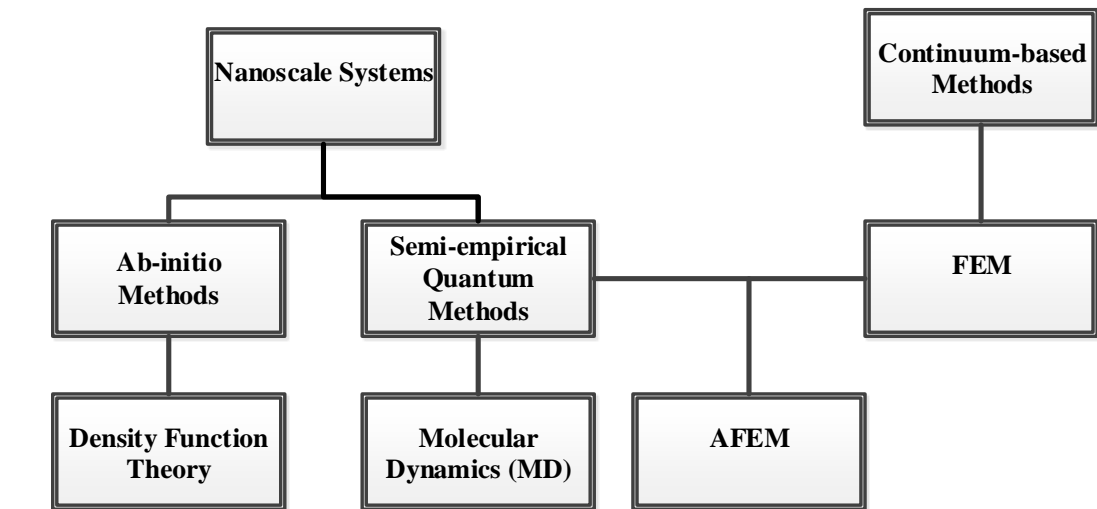


**Figure 1.5: Nanomechanical models**

Ab-initio calculation methods such as Density Function and The Hartree-Fock approximations are used to solve the Schrodinger equation, considering the Born e Oppenheimer approximation. The Hartree-Fock calculations compared with Density Function methods is more accurate, but computational more expensive. The Hartree-Fock calculations are an order  $O(N^4)$  of computational method, while for Density Function methods is an order  $O(N^3)$ ,  $N$  is a number of electrons. Ab-initio calculations are most accurate compared to semi-

empirical quantum methods, but computationally very expensive, and the analyses are limited to a few hundred or thousand atoms.

Semi-empirical quantum methods such as molecular dynamics (MD) and Tight-Binding Method are used to simplify the atomistic simulation. These methods are not accurate as Ab-initio methods, but computationally efficient. The parameters are empirical, fitted to experimental data. MD has been one of the most commonly method used to analyse the behaviour of nanomaterials. Tight-Binding Method and Ab-initio calculation are not able to analyse large size of system as MD simulation.

Molecular dynamics (MD), originally conceived by theoretical physicists in the late 1950s (Alder et al., 1959), is a simulation method used to study the motion of a system of interacting atoms. The two essential elements necessary for the analyzes are the equation of motion of the system and the potential fields, which is related with the accuracy of a MD simulation. Even MD can be applied to analyse large size of system, it is not applicable for system with million and million atoms, which are necessary to build some devices.

The literature review shows that computational cost in modelling nanomaterials is a fundamental challenge. In order to overcome this challenge, the method called atomic-scale finite element method (AFEM), proposed in (Liu et al., 2004), was first developed and applied for multiscale analysis of carbon nanotubes (CNTs) [Liu et al., (2004); Liu et al., (2005)]. The AFEM can model and analyse the mechanical behavior of materials at the nanoscale. The AFEM resembles the conventional FEM. However, in the AFEM, an atomic potential field is used to calculate the total energy of the system, making it possible to analyse system in nanoscale. Moreover, opposite to the local character of elements within the framework of classical FEM, the potentials used to generate the AFEM have non-local character. In AFEM, the choice of the potential field depends on the atomic structure and nature of atomistic interaction.

Researchers have made significant contributions by using AFEM in the study of the mechanical behavior of carbon nanotubes [Cecchi et al., (2009); Kim, (2006)], postbuckling behavior of carbon nanotubes (Leung, 2006), multiscale analysis of carbon nanotubes (CNTs) [Liu et al., (2004); Liu et al., (2005)], bending buckling of single-walled carbon nanotubes [Guo, et al. (2008); Leunget al., (2007)], study on the elastic property of bulk silicon nanomaterials (Tao et al., 2016), mechanical behavior of graphene sheet with zigzag edges (Malakouti and Montazeri, 2016).

In this thesis, the mechanical behavior of materials at the nanoscale are analyzed by applying the atomic-scale finite element method (AFEM), using different atomic potential fields. AFEM is formulated based on the concept of potentials describing the interaction among atoms. The potentials considered in this study are the Lennard-Jones potential (Jones, 1924), Tersoff potential (Tersoff, 1987; Tersoff, 1988) and second-generation Reactive Empirical Bond Order (REBO) potential (Brenner et al., 2002). Initially, the Lennard-Jones potential is considered in order to introduce and discuss fundamental issues about the application of the AFEM such as convergence, and consistent treatment of boundary atoms. We propose a new arrangement for the atomic finite elements in one and two dimensions, for the inclusion of the boundary conditions and also to exploit the idea of linking the size of the atomic-scale element to the concept of cut-off radius. After examining the key issues of the formulation of AFEM using Lennard-Jones potential, the analysis is extended to more complex interatomic potentials such as Tersoff potential and second-generation REBO potential, which can be used to describe the carbon-carbon interaction, therefore, describe the mechanical behavior of graphene sheets. Pristine and graphene sheets with cracks with armchair and zigzag edges are considered. The influence of vacancy defects on mechanical behavior under uniaxial tensile loading is analyzed by the AFEM.

## 1.5 Objectives

The main objectives of this thesis are:

- Introduction and application of the atomic scale finite element method (AFEM) to study the mechanical behavior of nanostructures in one and two dimensions using the Lennard Jones potential.
- Implement the Lennard Jones potential.
- Propose the atomic finite element in one dimension considering the Lennard Jones potential.
- Propose the atomic finite element in two dimensions considering the Lennard Jones potential.

- Introduce the concept of modified atomic finite element for the one and two dimensional cases using the Lennard Jones potential.
- Application of the atomic scale finite element method (AFEM) to study the mechanical behavior of graphene sheet with armchair and zigzag direction using the Tersoff and second generation REBO potentials.
- Implement the Tersoff potential.
- Implement the second generation REBO potential.
- Introduce the concept of modified atomic finite element.
- Validation of AFEM by comparing the force-strain behavior with MD simulation considering the potentials Lennard Jones, Tersoff and second generation REBO.
- Simulation of mechanical behavior of nanostructures in one and two dimensions considering the Lennard Jones potential.
- Simulation of mechanical behavior of graphene sheet with armchair and zigzag edges considering the potentials Tersoff and second generation REBO.
- Study the influence of vacancy defects on mechanical behavior of graphene sheet considering the potentials Tersoff and second generation REBO.

### 1.5 Outline of Current Work

This thesis is organized as follows.

In chapter 2, the basic formulation of atomic-scale finite element method (AFEM) is presented. The AFEM is based on an energy approach. It requires an interatomic energy potential, describing local or non-local bonding forces of an atom interacting with a chosen set of other surrounding atoms. The choice of the interacting surrounding atoms and their array will, ultimately, lead to the formulation of the specific Atomic Finite Element. In principle, the method can be applied to all atomic systems that may be described by an interatomic energy potential.

Chapter 3 presents an overview of the Lennard Jones potential. The purpose of this chapter is to introduce and discuss fundamental issues about the formulation and application

of the Atomic-Scale Finite Element Method (AFEM). This methodology will be applied, exemplary, to analyze the mechanical behavior of one-dimensional (1D) and two-dimensional (2D) atomic structures and lattices. The Lennard-Jones interatomic potential will be used in the formulation and analysis. In particular, the chapter describes how to relate the number of nodes of a 1D Atomic Finite Element with the cut-off radius of the Lennard-Jones potential. It also addresses, in detail, the modifications at the element level that have to be performed to model bounded atomic domains and to introduce proper boundary conditions. The obtained numerical results are compared with classical MD simulations. Accuracy and computational costs involved in both methodologies are addressed.

Chapter 4 and 5 present an overview of the Tersoff and the second-generation reactive empirical bond order (REBO) potentials formulations. In these two chapters, the mechanical behavior of a single-layered graphene sheet having armchair and zigzag edges is studied using the atomistic finite element method (AFEM). The Tersoff interatomic potential model and the second generation REBO potential are used to calculate the energy of interaction between carbon atoms of the graphene sheets. The atomic finite element is revised, and the concept of modified atomic finite element is introduced to account for the inclusion of boundary conditions in bounded domains. The modified elements are also required to model defects and vacancies in the graphene sheets. The results obtained by the AFEM are compared and validated with those obtained by a Molecular Dynamics (MD) simulation software. The mechanical behavior of pristine graphene in terms of force-strain relation is reported and comparisons between AFEM and MD simulations are presented. The influence of chirality and vacancy defects on mechanical behavior under uniaxial tensile loading are analyzed by the AFEM. It is shown that AFEM presents a good agreement with MD, especially at lower strains, and that chirality and vacancy defects have a significant effect on the mechanical behavior of graphene.

Finally, the general conclusions regarding the work developed in this thesis are presented in Section 6. The section 7 indicates some suggestions for further research.

## 2 ATOMIC-SCALE FINITE ELEMENT METHOD FORMULATION

The AFEM, as described by (Liu et al., 2004), is based on an energy approach. It requires an interatomic energy potential,  $U$ , describing local or non-local bonding forces of an atom interacting with a chosen set of other surrounding atoms. The choice of the interacting surrounding atoms and their array will ultimately lead to the formulation of the specific atomistic finite element. In principle, the method can be applied to all atomic systems that may be described by an interatomic energy potential. The interatomic energy potentials are described in terms of the coordinates of the individual atoms,  $x_i$ , and some constitutive parameters of the considered atomic elements and arrays.

For a system with  $N$  atoms the interatomic total energy considers the contribution of all interacting atoms:

$$U_{\text{tot}} = \sum_{i < j}^N U(\underline{x}_j - \underline{x}_i) \quad (2.1)$$

The energy,  $W_f$ , related to the work of external forces,  $\underline{F}_i^{\text{ext}}$ , acting on one individual atoms is given by:

$$W_f = \sum_{i=1}^N \underline{F}_i^{\text{ext}} \cdot \underline{x}_i \quad (2.2)$$

The total energy in this approach,  $E_{\text{tot}}$ , is composed of the interatomic bonding energy and the (eventual) work of external forces.

$$E_{\text{tot}} = \sum_{i < j}^N U(\underline{x}_j - \underline{x}_i) - \sum_{i=1}^N \underline{F}_i^{\text{ext}} \cdot \underline{x}_i \quad (2.3)$$

As usual, the desired equilibrium condition is obtained by determining the stationary value of the total energy in the system with respect to the position  $\underline{x}_i$  of the individual atoms:

$$\frac{dE_{\text{tot}}}{d\underline{\mathbf{x}}} = 0 \quad (2.4)$$

The total energy  $E_{\text{tot}}$  can be expanded in a Taylor series around the equilibrium position of the atoms,  $\underline{\mathbf{x}}^{(0)}$ :

$$E_{\text{tot}}(\underline{\mathbf{x}}) \approx E_{\text{tot}}(\underline{\mathbf{x}}^{(0)}) + \left. \frac{dE_{\text{tot}}}{d\underline{\mathbf{x}}} \right|_{\underline{\mathbf{x}}=\underline{\mathbf{x}}^{(0)}} (\underline{\mathbf{x}} - \underline{\mathbf{x}}^{(0)}) + \frac{1}{2} (\underline{\mathbf{x}} - \underline{\mathbf{x}}^{(0)})^T \left. \frac{d^2E_{\text{tot}}}{d\underline{\mathbf{x}}d\underline{\mathbf{x}}} \right|_{\underline{\mathbf{x}}=\underline{\mathbf{x}}^{(0)}} (\underline{\mathbf{x}} - \underline{\mathbf{x}}^{(0)}) \quad (2.5)$$

Defining the displacement  $\underline{\mathbf{u}}$  as the difference between the actual,  $\underline{\mathbf{x}}$ , and the equilibrium position,  $\underline{\mathbf{x}}^{(0)}$ :

$$\underline{\mathbf{u}} = (\underline{\mathbf{x}} - \underline{\mathbf{x}}^{(0)}) \quad (2.6)$$

and substituting the Equation (5) into Equation (4) leads to the AFEM equation system:

$$[\mathbf{K}(\underline{\mathbf{u}})] \{\underline{\mathbf{u}}\} = \{\mathbf{P}(\underline{\mathbf{u}})\} \quad (2.7)$$

where  $[\mathbf{K}(\underline{\mathbf{u}})]$  corresponds to the nonlinear stiffness matrix,  $\{\underline{\mathbf{u}}\}$ , the displacement increment vector and  $\{\mathbf{P}(\underline{\mathbf{u}})\}$  the non-equilibrium load vector, respectively, given by:

$$[\mathbf{K}(\underline{\mathbf{u}})] = \left[ \left. \frac{d^2E_{\text{tot}}}{d\underline{\mathbf{x}}d\underline{\mathbf{x}}} \right|_{\underline{\mathbf{x}}=\underline{\mathbf{x}}^{(0)}} \right] = \left[ \left. \frac{d^2U_{\text{tot}}}{d\underline{\mathbf{x}}d\underline{\mathbf{x}}} \right|_{\underline{\mathbf{x}}=\underline{\mathbf{x}}^{(0)}} \right] \quad (2.8)$$

$$\{\mathbf{P}(\underline{\mathbf{u}})\} = \left\{ - \left. \frac{dE_{\text{tot}}}{d\underline{\mathbf{x}}} \right|_{\underline{\mathbf{x}}=\underline{\mathbf{x}}^{(0)}} \right\} = \left\{ \mathbf{F} - \left. \frac{dU_{\text{tot}}}{d\underline{\mathbf{x}}} \right|_{\underline{\mathbf{x}}=\underline{\mathbf{x}}^{(0)}} \right\} \quad (2.9)$$

The implementation procedure of AFEM will be described in the next sections.



### 3 LENNARD JONES POTENTIAL

In this chapter, a brief review of the Lennard Jones (LJ) potential proposed by Jones (1924) is introduced. It is used to calculate the potential energy of interaction between two non-bonding atoms based on their distance of separation,  $r_{ij}$ ,

$$U(r_{ij}) = \begin{cases} 4\varepsilon_{LJ} \left[ \left( \frac{\sigma}{r_{ij}} \right)^{12} - \left( \frac{\sigma}{r_{ij}} \right)^6 \right] & \text{for } r_{ij} < r_c \\ 0 & \text{for } r_{ij} \geq r_c \end{cases} \quad (3.1)$$

where  $r_{ij} = \sqrt{(x_i - x_j)^2 + (y_i - y_j)^2}$  is the bond length, and the  $r_c$  is some prescribed cut-off radius, which switches off the interaction when the bond length is exceeded. Only two Lennard Jones parameters are suffice to describe the intermolecular interactions,  $\sigma$  and  $\varepsilon_{LJ}$ , as shown in the Figure (3.1). The parameter  $\varepsilon_{LJ}$  is the depth of the potential well and  $\sigma$  is the inter-particle distance at which the potential is zero. The  $(1/r_{ij})^{12}$  term represents the strong repulsion and the high energy on the bond, as the distance between the pair of atoms decrease. The  $(1/r_{ij})^6$  term represents the attractive term, which gives the weak attraction on the bond, as the distance between the pair of atoms increase.

The internal force,  $F(r)$ , between the two atoms is obtained by differentiating the potential with respect to the intermolecular distance,  $r_{ij}$ :

$$F(r) = - \frac{dU(r)}{dr} = 4 \varepsilon_{LJ} \left[ 12 \frac{\sigma^{12}}{r^{13}} - 6 \frac{\sigma^6}{r^7} \right] \quad (3.2)$$

Figure (3.1) shows the LJ potential,  $U(r)$ , and the interatomic force,  $F(r)$ , as a function of the distance,  $r_{ij}$ . By setting the force  $F(r) = 0$ , the equilibrium distance between the atoms,  $r_{eq}$  is found to be:

$$r_{\text{eq}} = 2^{\frac{1}{6}} \sigma = 1.1225\sigma \quad (3.3)$$

If the distance between two atoms is less than  $r_{\text{eq}}$ , the Lennard Jones force is repulsive. If the distance is greater than  $r_{\text{eq}}$ , the force is attractive. The maximal force is obtained at the intermolecular distance,

$$r_{\text{fmax}} = \frac{1}{\sqrt[6]{\frac{7}{26}}} \sigma = 1.2445\sigma \quad (3.4)$$

It should be noted that for intermolecular distances larger than  $r_{\text{fmax}}$  the interatomic bonding force decreases continuously. When the distance between atoms reaches the equilibrium distance between the atoms,  $r_{\text{eq}}$ , the bonding force is assumed to vanish.

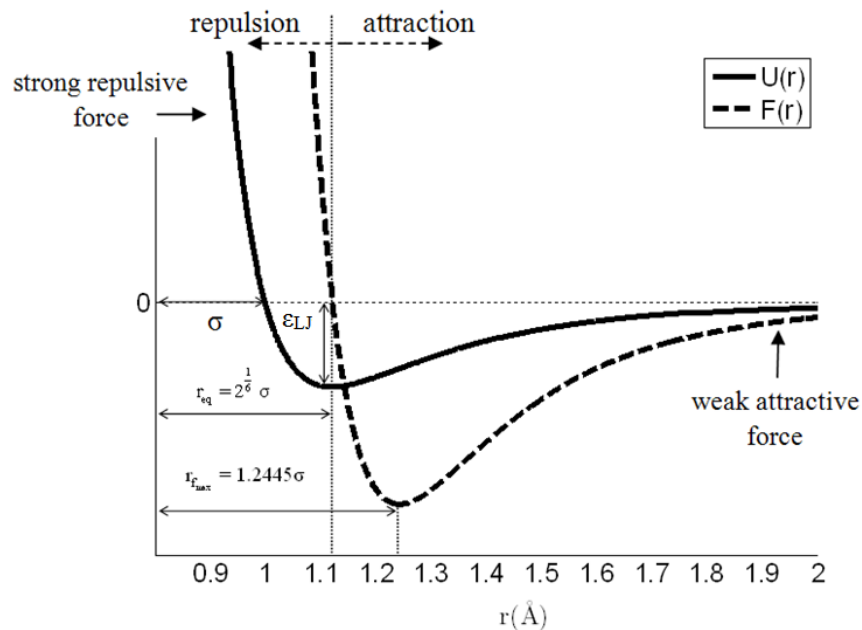


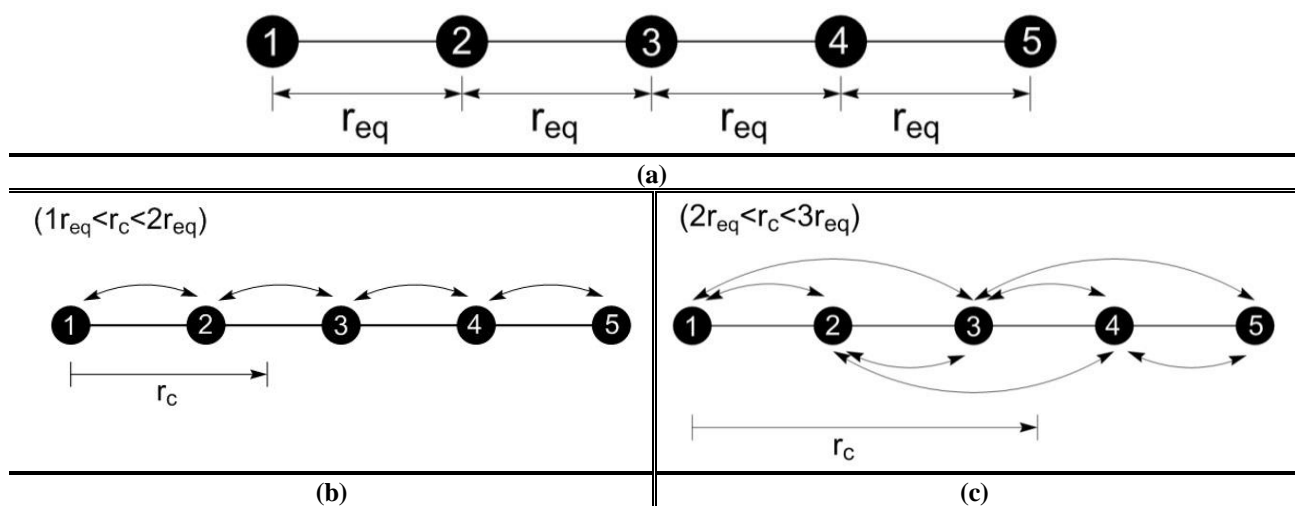
Figure 3.1: Lennard Jones Potential  $U(r_{ij})$ , and internal force  $F(r_{ij})$ .

The cut-off radius  $r_c$  is an important parameter to be chosen. It determines with how many neighboring atoms, a given atom is interacting. The cut-off radius  $r_c$  also determines whether the atomic interaction has a local or non-local character. In this chapter the cut-off radius of the interatomic bonding will be related to the number of nodes within a specific Atomic Finite

Element (AFE). This will be illustrated in the next paragraphs within the context of 1D elements.

Consider an atomic chain with 5 atoms in equilibrium position, as shown in Figure 3.2(a). Every considered atom interacts with one or more of its neighbors, according to the relation between the interatomic equilibrium distance  $r_{eq}$  and the chosen cut-off radius  $r_c$ . Three distinct conditions will be analyzed. First, consider that the cut-off radius obeys the relation ( $r_{eq} < r_c < 2r_{eq}$ ). This means that one atom only interacts with the first nearest neighboring atoms, as shown in Figure 3.2(b). For the second condition, ( $2r_{eq} < r_c < 3r_{eq}$ ), every atom interacts with the first and the second nearest neighboring atoms, as shown in Figure 3.2(c). The third condition, ( $3r_{eq} < r_c < 4r_{eq}$ ), is illustrated in Figure 3.2(d).

Two aspects should be stressed. First, when the cut-off radius is smaller than two times the equilibrium distance,  $r_c < 2r_{eq}$ , the atomic bonding have a local character. For larger cut-off radius,  $r_c > 2r_{eq}$ , the bonding extends to the second or more distant neighbors and gives a non-local character to the interatomic interactions. The second comment is related to the finitude of the atomic chain considered. The atoms 1 and 5, indicated in Figure 3.2(a), represent the physical limit of the considered chain. The lack of atoms to the left of atom number 1 and to the right of atom number 5 impacts directly the energy bonds of the chain. If  $r_c > 2r_{eq}$ , non-local bonds exist and not only the bond energy of the most external atoms (1 and 5, at the present case) is affected. This must be carefully considered when modelling a bounded atomic domain with the AFEM.



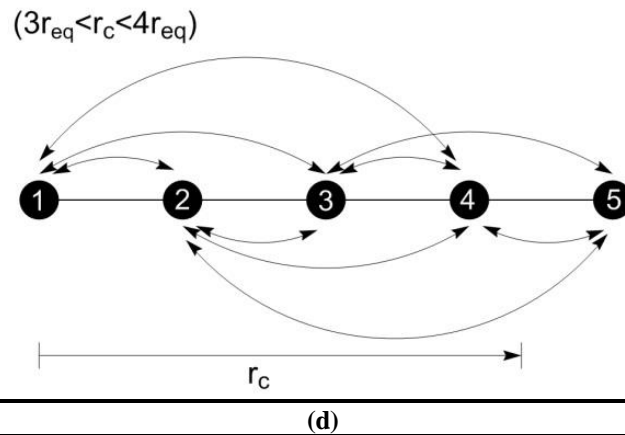


Figure 3.2: An atomic chain with 5 atoms and distinct relations between the equilibrium distance  $r_{eq}$  and the chosen cut-off radius of the LJ potentials,  $r_c$ .

The first and second derivatives in relation to  $x_i$  and  $y_i$  are available in Appendix A.

### 3.1 Atomic Elements

In this section the formulation for 1D and 2D Atomic Finite Elements are, exemplarily, presented for the case the Lennard-Jones interatomic potential. The idea is to focus on the fundamental issues of the AFEM formulation and not on material properties of the domains to be analyzed.

#### 3.1.1 Atomic Element in One Dimensional

The notion of the **atomic finite element** will be introduced based on three examples. Consider Figure (3.3), showing an atomic finite element with three nodes, designated as  $i-1$ ,  $i$  and  $i+1$ . The definition of the atomic finite element and all the derived calculations, such as internal forces and stiffness matrix, are related to the central node, in this case, node  $i$ . It is assumed that the relation between the equilibrium distance and the potential cut-off radius satisfies  $(r_{eq} < r_c < 2r_{eq})$ . The arrows in Figure (3.3) show that the central atom  $i$ , is only

connected to its first neighbor atom to the left (i-1) and to the right (i+1). The total bonding energy for this 3 node atomic finite element i is composed of the bonding (i-1, i) and (i, i+1):

$$U_{\text{tot}}^i = U_{i,i-1} + U_{i,i+1} \quad (3.5)$$



Figure 3.3: A three-node atomic-scale finite element.

The expressions for element stiffness matrix,  $K_i^{3e}$  and non-equilibrium force vector,  $P_i^{3e}$  for this atomic three node finite element are obtained by substituting the expression for the bonding energy (3.5) and the external forces in Equations (2.8) and (2.9), resulting delivering, respectively:

$$K_i^{3e} = \begin{bmatrix} 0 & \frac{1}{2} \frac{d^2 U_{\text{tot}}}{d x_{i-1} d x_i} & 0 \\ \frac{1}{2} \frac{d^2 U_{\text{tot}}}{d x_{i-1} d x_i} & \frac{d^2 U_{\text{tot}}}{d x_i d x_i} & \frac{1}{2} \frac{d^2 U_{\text{tot}}}{d x_{i+1} d x_i} \\ 0 & \frac{1}{2} \frac{d^2 U_{\text{tot}}}{d x_{i+1} d x_i} & 0 \end{bmatrix}_{3 \times 3} \quad (3.6)$$

$$P_i^{3e} = \begin{bmatrix} 0 \\ \underline{F}_i^{\text{ext}} - \frac{d U_{\text{tot}}}{d x_i} \\ 0 \end{bmatrix}_{3 \times 1} \quad (3.7)$$

The Lennard-Jones potential is a pairwise potential, describing the interaction between two atoms, that is the interaction of atom (i) over atom (i+1) and the reciprocal interaction of atom (i+1) on atom (i). In the present formulation the atomic element is represented by node (i) and only the interaction of node (i) with (i-1) and (i) with (i+1) will be considered. This is implied by the directions of the arrows in Figure (3.3). The reciprocal interaction, of the neighboring atomic element centered in the node (i-1) on the node (i), of the present element,

will be added later at the mesh assembly procedure. So only half of the bonding energy between (i) and (i-1), and (i) and (i+1) has to be considered. . This is expressed by the 1/2 factor in the element stiffness matrix.

Figure 3.4(a) shows a 5-node atomic finite element. The central node is denoted by (i) and it interacts with the two nearest nodes, (i-1) and (i-2) to the left and (i+1) and (i+2) to the right. For this element the condition ( $2r_{eq} < r_c < 3r_{eq}$ ) is considered. Analogously, for the 7-node element, shown in Figure 3.4(b), the relation between equilibrium distance and cut-off radius is ( $3r_{eq} < r_c < 4r_{eq}$ ).

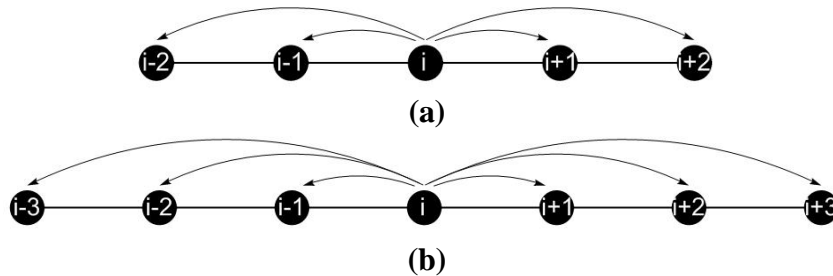


**Figure 3.4:** (a) A five-node atomic-scale finite element, (b) a seven-node atomic-scale finite element.

The total bonding energy of these elements are, respectively, given by:

$$U_{tot}^{i-5e} = U_{i,i-1} + U_{i,i-2} + U_{i,i+1} + U_{i,i+2} \quad (3.8)$$

$$U_{tot}^{i-7e} = U_{i,i-1} + U_{i,i-2} + U_{i,i-3} + U_{i,i+1} + U_{i,i+2} + U_{i,i+3} \quad (3.9)$$

### 3.1.2 Atomic Element in Two Dimensions

In this section two-dimensional atomic finite elements are presented. The starting point is the 7-node 2D element shown in Figure (3.5). As it will be shown, it may be used to model the geometry of hexagonal Bravais type lattices (Liu et al., 2006). The central atom, (i), has connection with all of surrounding atoms, (i+1), (i+2), (i+3), (i+4), (i+5) and (i+6). The total

energy for this basic 2D 7-node atomic finite element is the sum of all pairwise interacting nodes:

$$U_i^{\text{tot}} = U_{i,i+1} + U_{i,i+2} + U_{i,i+3} + U_{i,i+4} + U_{i,i+5} + U_{i,i+6} \quad (3.10)$$

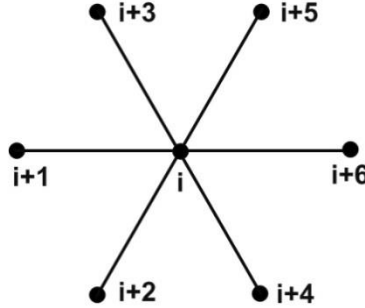


Figure 3.5: Atomic finite element with seven nodes.

The element stiffness matrix and the element non-equilibrium force vector for the atomic finite element with seven nodes are given by, respectively:

$$\underline{\mathbf{K}}_e = \begin{bmatrix} 0 & \dots & 0 & \frac{d^2 U_{\text{tot}}}{dx_{(i+3)} dx_i} & \frac{d^2 U_{\text{tot}}}{dy_{(i+3)} dx_i} & 0 & \dots & 0 \\ \vdots & \ddots & \vdots & \frac{d^2 U_{\text{tot}}}{dx_{(i+3)} dy_i} & \frac{d^2 U_{\text{tot}}}{dy_{(i+3)} dy_i} & \vdots & \ddots & \vdots \\ 0 & \dots & 0 & \vdots & \vdots & 0 & \dots & 0 \\ \frac{d^2 U_{\text{tot}}}{dx_{(i+3)} dx_i} & \frac{d^2 U_{\text{tot}}}{dy_{(i+3)} dx_i} & \dots & \frac{d^2 U_{\text{tot}}}{dx_i dx_i} & \frac{d^2 U_{\text{tot}}}{dy_i dx_i} & \dots & \frac{d^2 U_{\text{tot}}}{dx_{(i+6)} dx_i} & \frac{d^2 U_{\text{tot}}}{dy_{(i+6)} dx_i} \\ \frac{d^2 U_{\text{tot}}}{dx_{(i+3)} dy_i} & \frac{d^2 U_{\text{tot}}}{dy_{(i+3)} dy_i} & \dots & \frac{d^2 U_{\text{tot}}}{dx_i dy_i} & \frac{d^2 U_{\text{tot}}}{dy_i dy_i} & \dots & \frac{d^2 U_{\text{tot}}}{dx_{(i+6)} dy_i} & \frac{d^2 U_{\text{tot}}}{dy_{(i+6)} dy_i} \\ 0 & \dots & 0 & \vdots & \vdots & 0 & \dots & 0 \\ \vdots & \ddots & \vdots & \frac{d^2 U_{\text{tot}}}{dx_{(i+6)} dx_i} & \frac{d^2 U_{\text{tot}}}{dy_{(i+6)} dx_i} & \vdots & \ddots & \vdots \\ 0 & \dots & 0 & \frac{d^2 U_{\text{tot}}}{dx_{(i+6)} dy_i} & \frac{d^2 U_{\text{tot}}}{dy_{(i+6)} dy_i} & 0 & \dots & 0 \end{bmatrix} \quad (3.11)$$

$$\underline{P}_e = \begin{bmatrix} (0)_{6 \times 1} \\ \underline{F}_i^{\text{ext}} - \frac{dU_{\text{tot}}}{dx_i} \\ \underline{F}_i^{\text{ext}} - \frac{dU_{\text{tot}}}{dy_i} \\ (0)_{6 \times 1} \end{bmatrix} \quad (3.12)$$

Figures 3.6(a) and 3.6(b) illustrate two other 2D atomic finite elements. These atomic finite elements are defined based on the types of Bravais lattices (Liu et al., 2006) shown in Figure 3.7(a) and 3.7(b) respectively. The extension of the AFEM to these elements is straight forward.

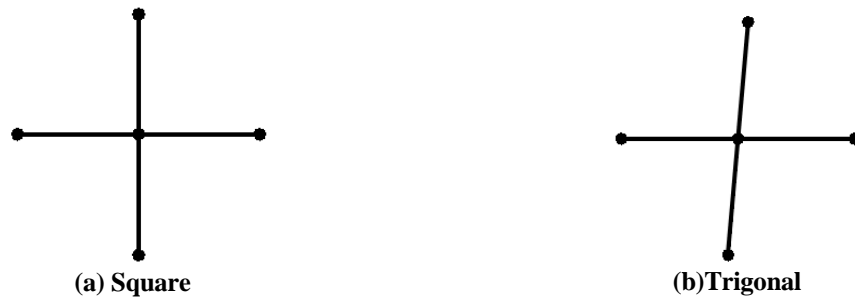


Figure 3.6: Atomic finite elements for different two-dimensional Bravais lattices



Figure 3.7: Square and Trigonal f two-dimensional Bravais lattices.

### 3.2 AFEM Implementation



In this section is described the computational procedure of AFEM implementation. Once known the atomic structure, the first two steps are:

- (a) Construct the  $[K_e]$  matrix, Eq. (2.8), and the  $\{P_e\}$  vector, Eq. (2.9);
- (b) Next, assemble the global stiffness matrix and global non-equilibrium force vector, taking into account the prescribed boundary conditions.

The stiffness matrix and the force vector depend on the second and first derivative of the total energy. Therefore, the potential energy that better describes the interactions between the atoms is chosen, and the atomic finite element is defined. Before go to the next step of AFEM implementation, the assemblage procedure in one and two dimensions, application of boundary conditions and the concept of modified atomic finite element are discussed.

Figure (3.8) illustrates the AFEM assemblage procedure for a 1D atomic chain containing 4 atoms. The atomic finite element with three nodes is considered. The atomic chain is bounded so that to the left side of atom 1 and to the right side of atom 4 there are no atoms. Because of this lack of neighboring atoms, the atomic finite elements on the edges of the mesh must be modified. So even before the imposition of the boundary conditions, the potential energy of the edge element must be modified to account for the non-existence of one or more neighboring atoms.

Using a 3-node atomic finite element, the assemblage procedure for the 4 element chain, shown in Figure (3.8), requires 4 atomic finite elements, called, respectively,  $EI=1$ ,  $EI=2$ ,  $EI=3$ ,  $EI=4$ . Initially, all the atomic elements have three local nodes, designated by (-1), (0) and (+1). In the sequence, the atomic elements,  $EI=1$  and  $EI=4$ , must be modified. For the atomic  $EI = 1$ , the contribution of energy from the central node (0) onto left node (-1) does not exist and, therefore, must be eliminated from the calculations of the stiffness matrix and global non-equilibrium force vector. Also, the degree of freedom of node (-1) of  $EI=1$  must be eliminated from the assemblage procedure. This is graphically indicated by the dashed arrow between node (0) and node (-1) for  $EI=1$ . Analogously, for  $EI=4$ , the energy contribution of node (0) to the node (+1) must be eliminated from the energy calculation procedure. Again, the dashed arrow in  $EI=4$ , between node (0) and node (+1) illustrates the required modification.

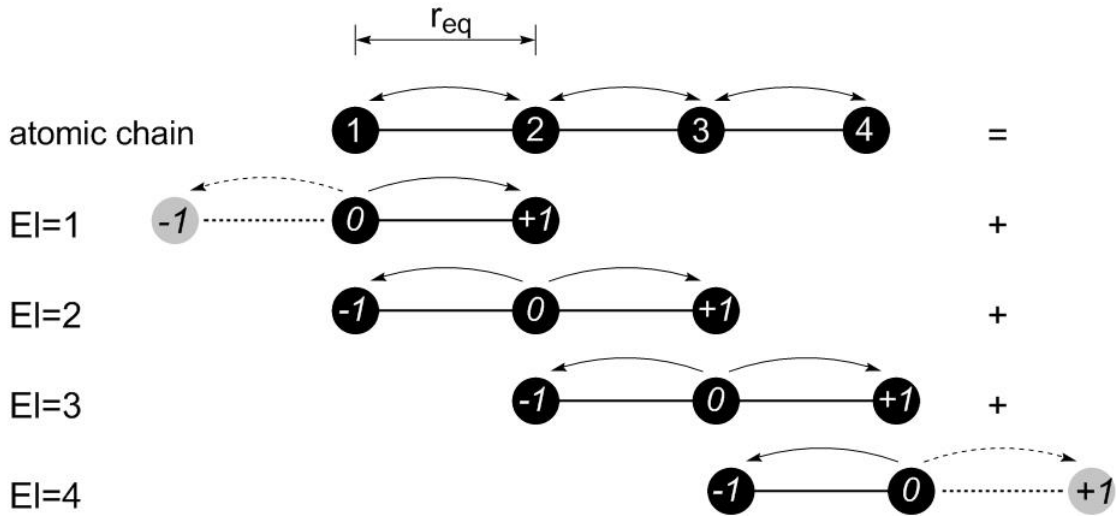


Figure 3.8: Example of assemblage scheme for an atomic chain of 4 atoms.

The expression for the total energy of the 4 atom chain,  $U_{\text{total}}$ , is given by the sum of the contributions of the energy of individual elements,  $U^{\text{EI}}$ , as shown in equation (3.13):

$$U_{\text{total}} = \frac{1}{2} (U^{\text{EI}=1} + U^{\text{EI}=2} + U^{\text{EI}=3} + U^{\text{EI}=4}) \quad (3.13)$$

The expressions for the energy of each of the 4 atomic elements used to model the 4-atom chain of Figure (3.8) are given in the expressions (3.14) to (3.17):

$$U_{\text{total}}^{\text{EI}=1} = 4\epsilon_{\text{LJ}} \left[ \left( \frac{\sigma}{r_{12}} \right)^{12} - \left( \frac{\sigma}{r_{12}} \right)^6 \right] \quad (3.14)$$

$$U_{\text{total}}^{\text{EI}=2} = 4\epsilon_{\text{LJ}} \left[ \left( \frac{\sigma}{r_{21}} \right)^{12} - \left( \frac{\sigma}{r_{21}} \right)^6 \right] + 4\epsilon_{\text{LJ}} \left[ \left( \frac{\sigma}{r_{23}} \right)^{12} - \left( \frac{\sigma}{r_{23}} \right)^6 \right] \quad (3.15)$$

$$U_{\text{total}}^{\text{EI}=3} = 4\epsilon_{\text{LJ}} \left[ \left( \frac{\sigma}{r_{32}} \right)^{12} - \left( \frac{\sigma}{r_{32}} \right)^6 \right] + 4\epsilon_{\text{LJ}} \left[ \left( \frac{\sigma}{r_{34}} \right)^{12} - \left( \frac{\sigma}{r_{34}} \right)^6 \right] \quad (3.16)$$

$$U_{\text{total}}^{\text{EI}=4} = 4\epsilon_{\text{LJ}} \left[ \left( \frac{\sigma}{r_{43}} \right)^{12} - \left( \frac{\sigma}{r_{43}} \right)^6 \right] \quad (3.17)$$

It should be noticed that the energy expressions for the elements in equations (3.14) to (3.17) are given in terms of the distance between the atoms, considering the global numbering scheme. Elements EI=1 and EI=4 only present the energy contribution from one bond. On the other hand, elements EI=2 and EI=3 present two energy contributions, because these elements present neighboring atoms to the right and to the left.

The third important stage of the assemblage produce in AFEM is the application of the boundary conditions. Figure (3.9) illustrates the same atomic chain of Figure (3.8) but including a set of boundary conditions. In this case, the displacement of atom 1 is blocked, so, the degree of freedom of this atom must be excluded from the global stiffness matrix, and from of the global non-equilibrium force vector.

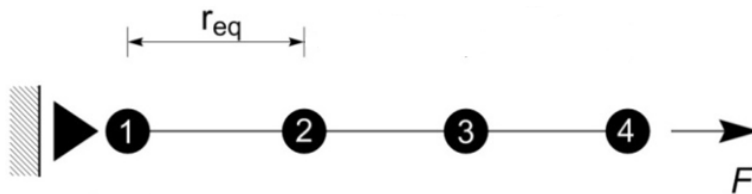


**Figure 3.9: Introduction the boundary conditions at the 4 atoms chain.**

The assemblage procedure of AFEM in two dimensions system is the same used for the one dimensional system. Figure (3.10) illustrates an example, which consists of a triangular (hexagonal) mesh with 38 atoms. The basic atomic finite element considered has 7 nodes, and was shown in Figure (3.5). In order to apply boundary conditions or to analyze meshes with defects and missing atoms, the basic atomic elements must also be modified to account for the missing neighboring atoms. This is illustrated in Figure (3.10). Element number 23 is an example of a complete atomic element. Elements 1, 6 and 25 are incomplete, or modified elements. Just like the 1D case, the bond energy of the missing neighboring atoms must be excluded from the total energy of the element.

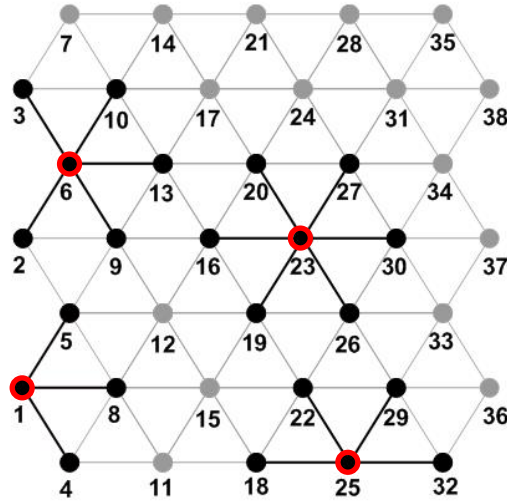


Figure 3.10: Atomic structure with complete and modified elements.

The total energy expression for the mentioned elements 23, 1, 6, and 25 are:

$$U_{\text{tot}}^{23} = U_{23,16} + U_{23,19} + U_{23,20} + U_{23,26} + U_{23,27} + U_{23,30} \quad (3.18)$$

$$U_{\text{tot}}^1 = U_{1,4} + U_{1,5} + U_{1,8} \quad (3.19)$$

$$U_{\text{tot}}^6 = U_{6,2} + U_{6,3} + U_{6,9} + U_{6,10} + U_{6,13} \quad (3.20)$$

$$U_{\text{tot}}^{25} = U_{25,18} + U_{25,22} + U_{25,29} + U_{25,32} \quad (3.21)$$

The total bond energy of the complete element 23 and of the modified elements 1, 6 and 25 is given in Table 1. The element energy determined within the atomistic finite element procedure and the corresponding energy obtained by the Molecular Dynamics (MD) package LAMMPS (Plimpton, 1995) are also indicated. It can be seen that the energy for each AFE is distinct, according to the number of missing surrounding atoms. Table 1 also shows that the energy values calculated by AFEM and MD are in accordance.

**Table 1.1: Comparison of total element energy obtained from AFEM and MD.**

	<b>Total Energy</b>			
	$U_{\text{tot}}^{23}$ (eV)	$U_{\text{tot}}^1$ (eV)	$U_{\text{tot}}^6$ (eV)	$U_{\text{tot}}^{25}$ (eV)
<b>AFEM</b>	-3.0	-1.50	-2.50	-2.0
<b>MD</b>	-3.0	-1.50	-2.50	-2.0

The matrices and load vectors for the complete or modified elements are assembled and, in the sequence, the boundary conditions are imposed. It is stressed again, that modifying the atomic elements to account for missing bonds and the imposition of boundary conditions are two distinct solution steps within the AFEM.

The next steps of the AFEM implementation are:

(c) Solve  $\{\underline{u}\} = [\mathbf{K}(\underline{u})]^{-1} \{\mathbf{P}(\underline{u})\}$ ;

(d) Update  $\mathbf{x}$  by  $\mathbf{x} = \{\underline{u}\} + \mathbf{x}_0$ .

where  $[\mathbf{K}(\underline{u})]$  is the global stiffness matrix,  $\{\mathbf{P}(\underline{u})\}$  is the global non-equilibrium force vector,  $\mathbf{x}_0$  represents the initial position and  $\mathbf{x}$  the final position of the atoms. In the present implementation the resulting non-linear system, Equation (2.7) was solved iteratively by the Newton-Raphson method until the non-equilibrium force vector,  $\{\mathbf{P}(\underline{u})\}$ , reaches zero or a prescribed error tolerance.

For results in the form of a stress-strain diagram, the stress  $\sigma$  is approximated by dividing the sum of the external forces applied at the atoms  $n_a F_{\text{ext}}$  by an assumed area  $A$ . This area is considered to be formed by the length of mesh orthogonal to the traction direction,  $L_y$ , and a thickness  $t$ .

$$\sigma = \frac{n_a F_{\text{ext}}}{A} = \frac{n_a F_{\text{ext}}}{L_y t} \quad (3.22)$$

### 3.3 Results

#### 3.3.1 Comparison of AFEM and MD in One Dimension

In this section, the 1D AFEM is investigated. Initially, the influence of the number of element nodes in the atomic elements is addressed. As already discussed, the number of nodes in the AFE is related to the chosen cut-off radius for the Lennard Jones potential. The first example is shown in Figure (3.11). It consists of a 7 atom chain, fixed at atom 1 and loaded by a force  $F$  at node 7. This example will be solved using atomic elements with 3, 5 and 7 nodes. Before imposing the boundary conditions, the distance between the atoms is set to be equal to the equilibrium position,  $r_{eq} = 1.122 \text{ \AA}$ . After applying the boundary conditions, the load vector is increased until the atomic chain fails by bond breaking. At every load step the non-linear Equation (2.7) is solved iteratively.

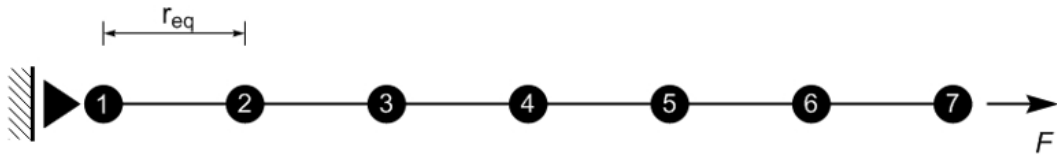


**Figure 3.11: A schematic diagram of a one-dimensional atomic chain.**

Figure (3.12) shows the resulting force-strain relations. The strain measure  $\varepsilon$  is obtained by dividing the displacement of atom 7,  $u_7$  by the original chain length  $L_0$ ,  $\varepsilon = u_7/L_0$ . The curves show that there is very little difference between the results obtained considering the atomic elements with 5-nodes and 7-nodes. It suggests that 1D AFEM simulations using atomic finite element with 5 nodes is almost as accurate as atomic finite element with 7-nodes.

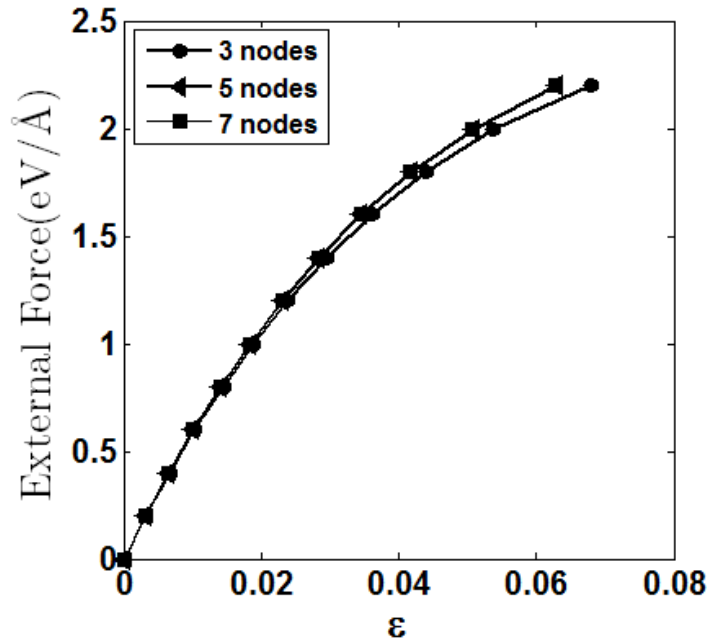


Figure 3.12: External force by strain (3, 5 and 7 nodes elements).

In the sequence, the accuracy of the obtained AFEM results will be validated by comparison with the results obtained from MD package LAMMPS. To simplify, the values of parameters of the LJ potential were assigned unit values,  $\sigma = 1$  and  $\epsilon_{LJ} = 1$ . The AFEM results were determined for the 5 node element. In the MD simulations, the Lennard Jones potential was used at a temperature of 1 K. Non-periodic boundary conditions were used. For the AFEM and MD simulations the cut-off radius is set equal to  $r_c = 2.5\sigma$  (Smit, 1992). The time integration step for the MD simulations is 0.05 fs.

Figure 3.13(a) shows force-strain curves obtained by both methodologies. Figure 3.13(c) depicts the relative error between strains obtained by both solutions. There is a good agreement between both solutions, with a relative error smaller than  $10^{-5}$ , except at the initial equilibrium position. The MD simulation needed 1000 iterations to achieve the equilibrium position for every load step. On the other hand, the number of iterations for the AFEM to reach a non-equilibrium force vector smaller than  $10^{-11}$  for distinct values of the load force is shown in Figure 3.13(b). The number of iterative steps for every force in the AFEM varied from 4 to 8 according to the loading stage.

Figure 3.13(d) shows a typical behavior of the quantity  $\mathbf{u} \cdot \mathbf{P}$ , that is the dot product between displacement vector and the global non-equilibrium force vector. It also represents a measure of convergence of the iterative solution (Kim, 2006). The figure shows that convergence obtained for the present results is very fast.

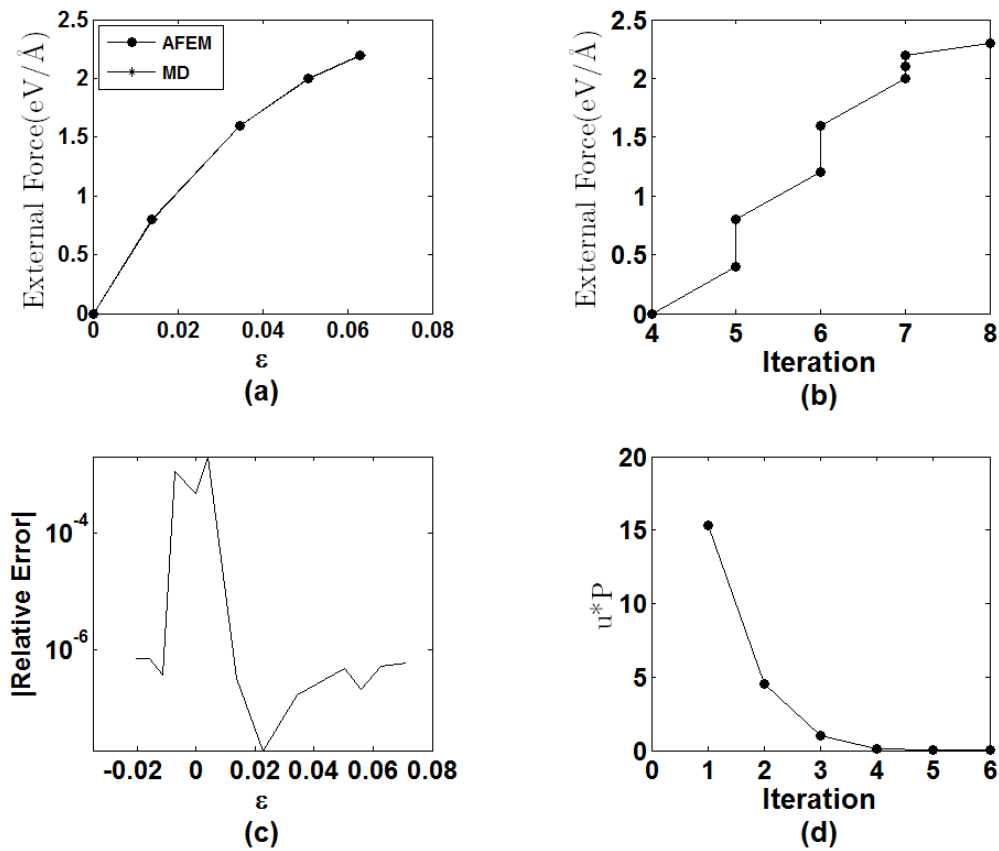


Figure 3.13: 1D AFEM results - a) force-strain relation; b) number of iterations for AFEM , c) MD-AFEM relative error, d)convergence measure

The results of Figures 3.13(a) to 3.13(d) suggest that the 1D AFEM formulation and implementation is correct, that the results are accurate and the number of iterative steps, required for the solution, is significant smaller than those of the typical MD simulations.

### 3.3.2 Comparison of AFEM and MD in Two Dimensions

This section is dedicated to the study of a 2D AFE. A two-dimensional hexagonal (or triangular) lattice, shown in Figure (3.14), presenting 655 atoms is analyzed. The 2D atomic finite element (AFE) with 7 nodes, given in Figure (3.5), is considered. Zero displacement boundary conditions are imposed on all atoms on the left edge, shown inside of the red dashed box. External force with the same amplitude are applied on all atoms on the right edge in x



direction, as shown by the arrows in Figure (3.14). The Lennard Jones potential was used in MD at a temperature of 1 K. The Lennard-Jones potential parameters are,  $\sigma = 1$  and  $\epsilon_{LJ} = 1$ . The cut-off radius for the MD simulations is set to  $r_c = 1.5\text{\AA}$ . Non-periodic boundary conditions were used.

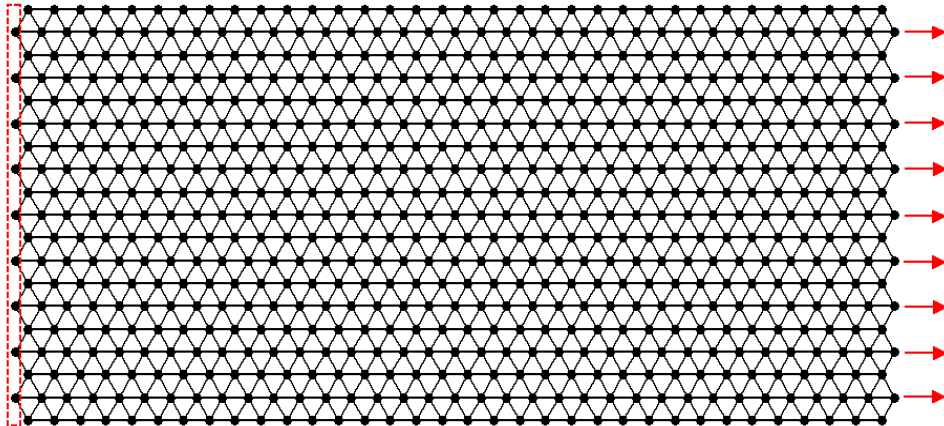


**Figure 3.14: A schematic diagram of a two-dimensional lattice.**

Figure 3.15(a) shows a force-strain diagram obtained by AFEM and MD. The results are obtained for the central atom at the left border of the mesh. A similar result, showing the change in total length of the atomic mesh,  $\Delta L$ , is given in Figure 3.15(b). The AFEM and MD solutions agree very well. The residual ( $u \cdot P$ ) is shown in Figure 3.15(c) and the number of iterations required to solve the non-linear system for every load step can be found in Figure 3.15(d). The MD simulation required 50000 iterative steps to achieve a final configuration with 4 significant digits, whereas the AFEM never needed more than 7 steps to achieve the same accuracy.

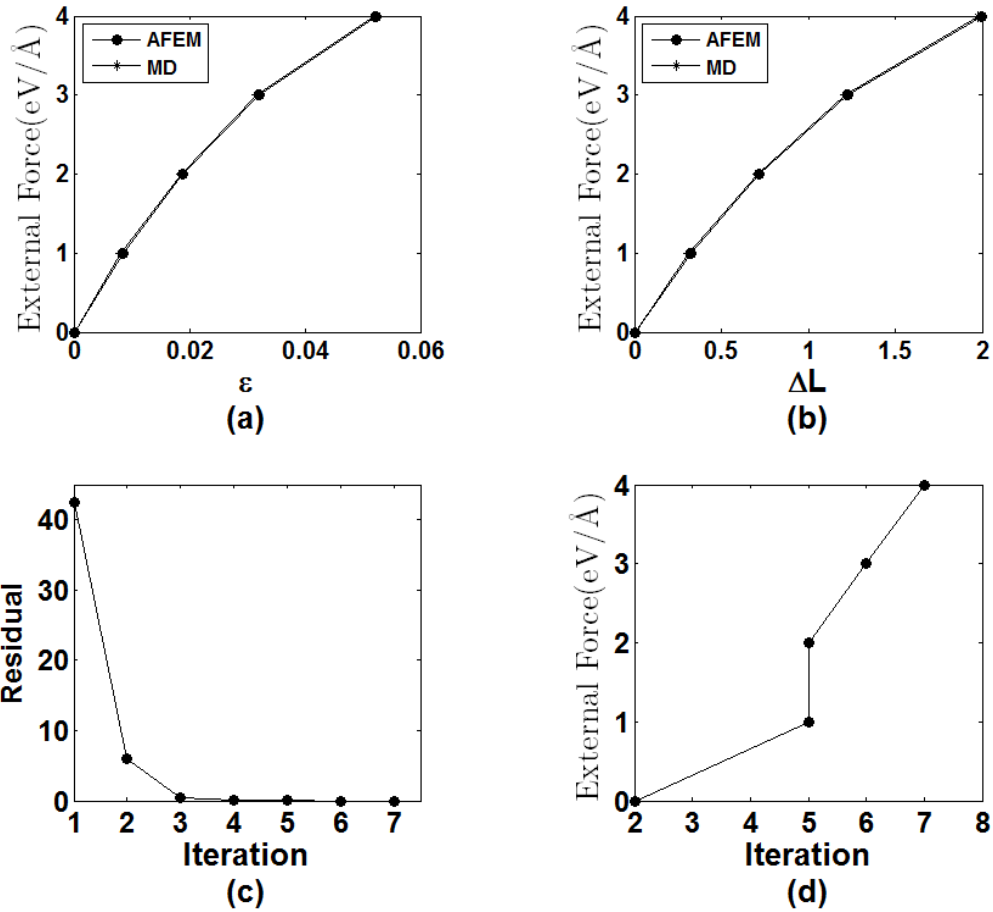


Figure 3.15: (a) Force-strain relation; (b) force-displacement relation; (c) convergence of AFEM; (d) number of iterations for distinct force levels.

As a second 2D example, consider the same mesh of the previous example, shown in Figure (3.16). Zero displacement boundary condition imposed to the atoms within the red dashed box at the left border. An external force  $F_{\text{ext}}$  is applied in the vertical direction upon atom number 739. The black lattice in Figure (3.16) represents the original atomic mesh. The blue mesh shows the deformed mesh at its last loading step before bond breaking. The atom 739 is connected to atoms 728 and 729 as illustrated in the detail shown in Figure (3.16). It is simple to see that the bonding force between atoms 739 and 729 is in compression and that the force between atoms 739 and 728 is traction.

Figure (3.17) shows in dashed lines the interatomic bonding force developed by the Lennard-Jones potential as a function of the interatomic distance  $r_{ij}$ , as anticipated by Equation (3.2). This Figure also show the bonding forces between atoms 739-729 (compression) and between atoms 739-728 (traction) for distinct amplitude stages of the external force,  $F_{\text{ext}}$ . Traction is marked in blue color and compression in red color.

As expected, the interatomic bonding forces start with a zero value at the equilibrium position and increase continuously in traction and compression for increasing values of the external load. The bonding forces follow exactly the path predicted in Equation (3.2). It should be noticed that this is a highly non-linear behavior, in which interatomic displacements for compressed bonds is much smaller than those of the traction bonds for the same external loading level. Figure (3.17) also shows the break bonding situation. After the condition, in which the traction bond, in blue, reaches the maximum bonding force at  $r_{f_{\max}} = 1.2445\sigma$ , given by Equation (3.4), the bonding forces decrease for larger distances, the bond can no longer withstand the imposed external loads and breaks. The iterative system will no longer converge, unless a new mesh without the lost atom is considered.

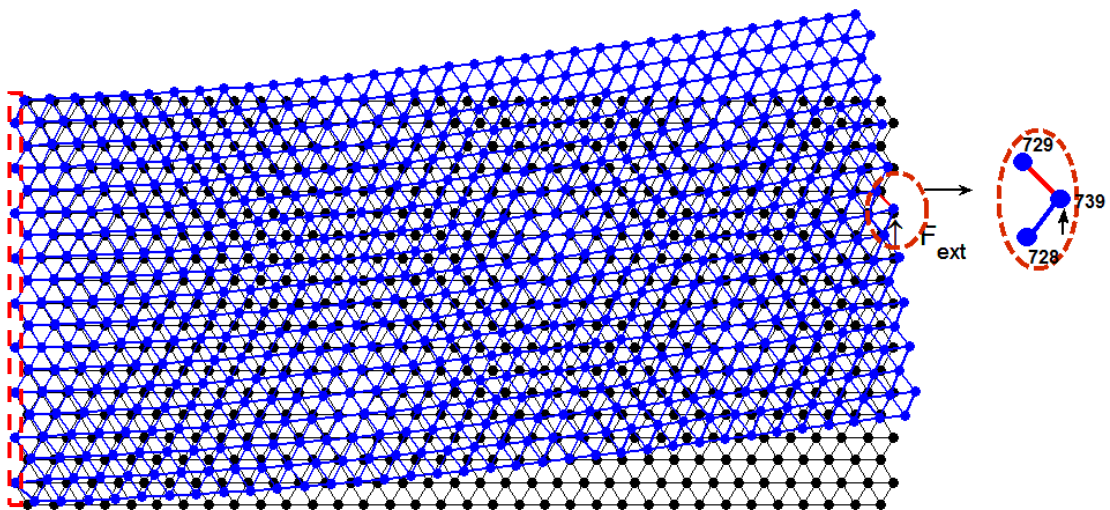


Figure 3.16: Initial and final configuration of a 2D atomic mesh.

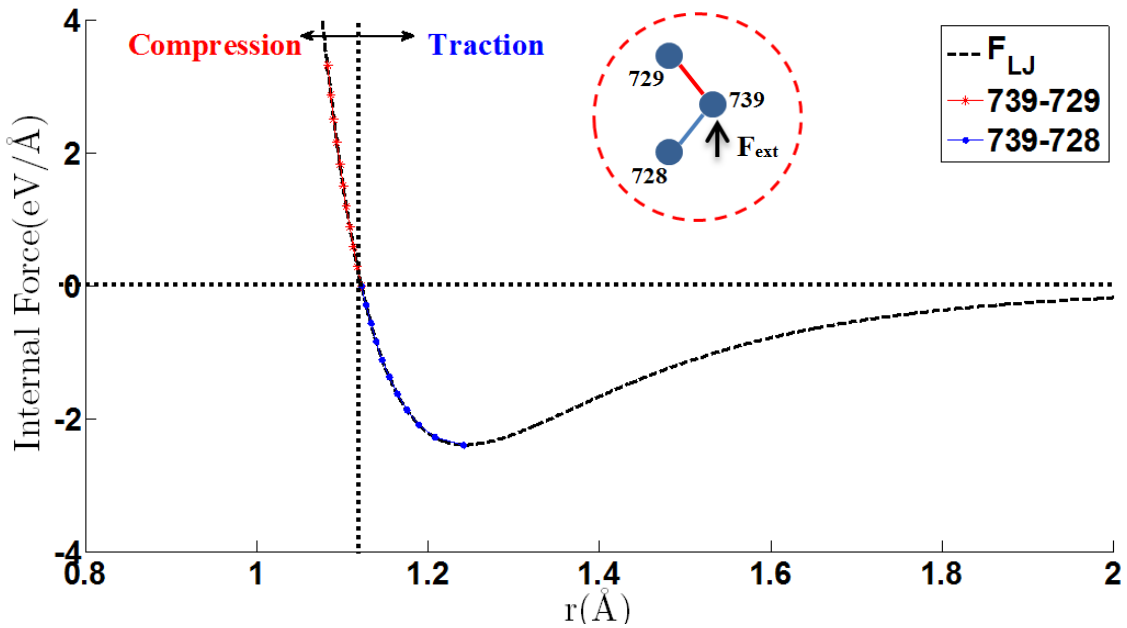
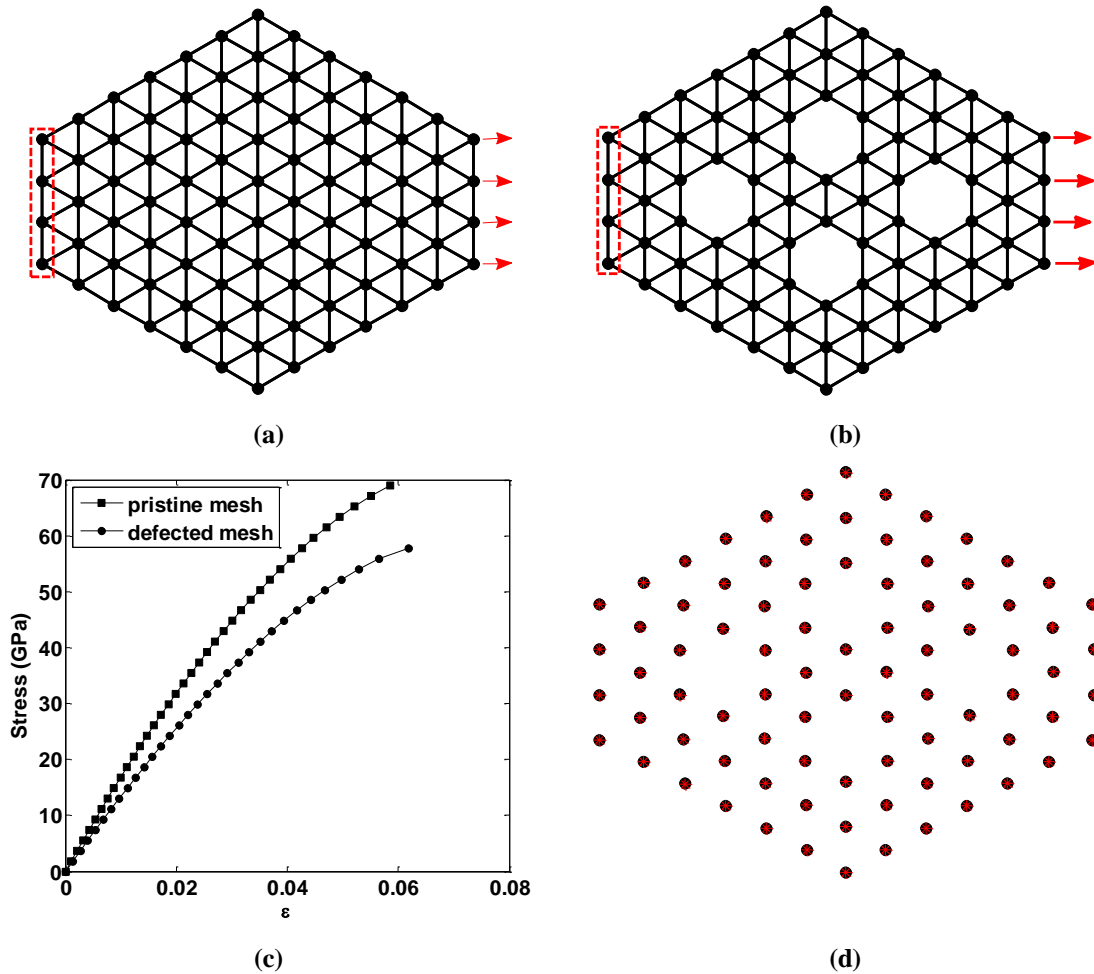


Figure 3.17: internal force by  $r$ .

In the third example, the effect of missing atoms or vacancies on the mechanical behavior of an atomic mesh is investigated. Figure 3.18(a) shows a pristine mesh, with no vacancies. On the other hand, Figure 3.18(b) depicts the same mesh but with 4 missing atoms. In both cases, zero displacement boundary conditions are prescribed for the atoms in the right edge within the red dashed box. A force of equal, increasing amplitude is applied to the 4 atoms at the left border. The external load is increased incrementally until one or more atomic bonds within the mesh break. Figure 3.18(c) shows the stress (force)-strain behavior of the pristine and of the defect mesh. The same strain measure of the previous examples is used. It can be seen that vacancies do have a large effect on the force-strain behavior. For validation purposes, Figure 3.18(d) depicts the deformed configuration of the defect mesh (Figure 3.16(b)), determined by AFEM and MD. There is a good visual agreement between the two methodologies.



**Figure 3.18: (a) Pristine mesh; (b) Defected mesh, (c) stress-strain curves, and (d) final equilibrium configuration from AFEM and MD.**

As a last example, consider the square Bravais lattice shown in Figure 3.19(a). The square 2D AFE with 5 nodes, shown in Figure 3.6(a), is used to model the atomic domain. The displacements of all atoms with the box at the left edge of the mesh are blocked. Upon all atoms within the dashed box at the right side, an equal and increasing force is applied. Figure 3.19(b) shows the resulting force-strain curves obtained by both methodologies. Both curves show the same trend, but there is no perfect agreement. This should be further investigated, because all previous and even more complex meshes had presented a much better agreement between both methodologies.

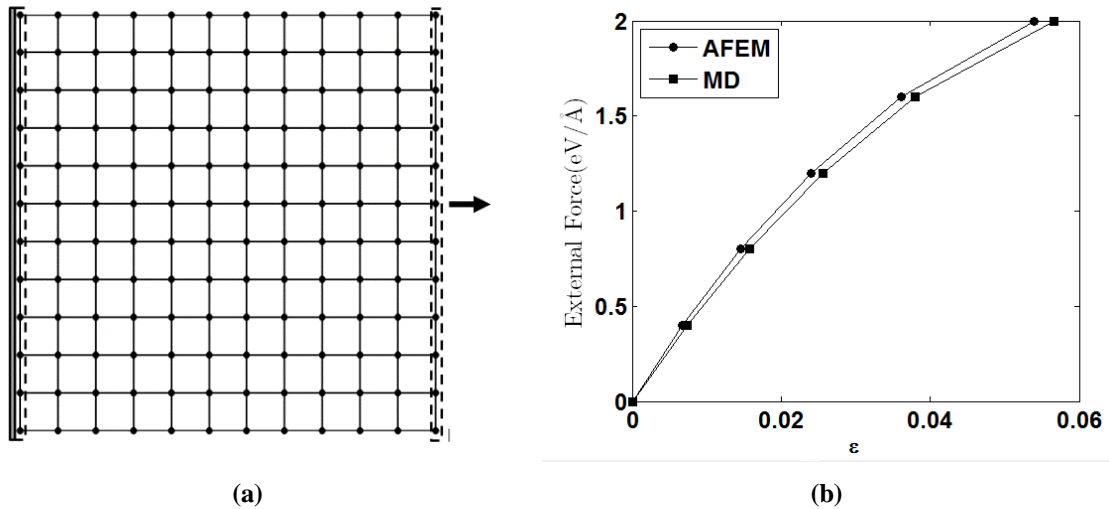


Figure 3.19: (a) Square bravais lattice; (b) Force-strain curves obtained from AFEM and MD.

### 3.4 Remarks

This chapter presents a detailed description of the formulation and implementation of the Atomistic Finite Element Method (AFEM), exemplified in the analysis of one- and two-dimensional atomic domains governed by the Lennard-Jones interatomic potential. The methodology to synthesize element stiffness matrices and load vectors, the potential energy modification of the atomistic finite elements (AFE) to account for boundary edge effects, the inclusion of boundary conditions were carefully described, in a way that the authors had not previously found in the AFEM literature. The conceptual relation between the cut-off radius of interatomic potentials and the number of nodes in the AFE is addressed and exemplified for the 1D case. For the 1D case elements with 3, 5 and 7 nodes were addressed. The AFEM has been used to describe the mechanical behavior of one-dimensional atomic arrays as well as two-dimensional lattices of atoms. The reported studies also included the analysis of pristine domains, as well as domains with missing atoms, defects, or vacancies. Almost all results were compared with classical molecular dynamic simulations (MD) performed using a commercial package. The results have been very encouraging in terms of accuracy and in the computational effort necessary to execute both methodologies, AFEM and MD. The methodology presented can be extended to other potential, like Tersoff (Tersoff, 1987), REBO (Brenner, 1990),

AIREBO (Stuart, 2000), which have been applied to model nanostructures composed of graphene and materials alike.

## 4 TERSOFF POTENTIAL

In the previous chapter was discussed about the Lennard Jones potential, which it's useful and more accurate in modeling simple structure with non-bonded atoms. Several applications in materials science, considering nanomaterials as graphene sheet require many-body potential formulations (Novoselov et al., 2004). The interatomic potential Tersoff (1987) was proposed to simulate systems as graphene, which is a single layer of carbon atoms connected by covalent bonds. The energy stored on the bond between atoms  $i$  and  $j$  depends on the bond length,  $r_{ij}$ , and also on the relative position of second nearest-neighbor atoms, which are connected by the bending angle  $\theta$ . The energy stored on the bond between atoms  $i$  and  $j$  is given by:

$$V_{ij} = f_c(r_{ij}) [V_{ij}^R(r_{ij}) + B_{ij} V_{ij}^A(r_{ij})] \quad (4.1)$$

The terms  $V_{ij}^R$  and  $V_{ij}^A$  represent the repulsive and attractive pair potential as a function of the bond length  $r_{ij}$ .

$$V_R(r_{ij}) = A \exp(-\lambda^1 r_{ij}) \quad (4.2)$$

$$V_A(r_{ij}) = -B \exp(-\lambda^2 r_{ij}) \quad (4.3)$$

The function  $f_c(r_{ij})$  is a cut-off function, which switches off the atomic interaction when a prescribed interatomic distance is exceeded. A typical expression for  $f_c(r_{ij})$  is given by:



$$f_c(r_{ij}) = \begin{cases} 1, & r_{ij} < R - D \\ \frac{1}{2} - \frac{1}{2} \sin \left[ \frac{\pi}{2} \frac{(r_{ij} - R)}{D} \right], & R - D < r_{ij} < R + D \\ 0, & r_{ij} > R + D \end{cases} \quad (4.4)$$

The parameters  $A$ ,  $B$ ,  $\lambda^1$ ,  $\lambda^2$ ,  $R$  and  $D$  are defined according to physical properties of the atomic systems. For carbon-carbon interactions these parameters are given in Table 4.1 ( Tersoff 1988).

**Table 4.1: Parameters for carbon-carbon interactions.**

$A = 1393.6 \text{ eV}$	$B = 346.74 \text{ eV}$	$\lambda^1 = 3.4879$
$\lambda^2 = 2.2119$	$\beta = 1.5724 \times 10^{-7}$	$n = 0.72751$
$c = 3.8049 \times 10^4$	$d = 4.3484$	$h = -0.57058$
$R = 1.95 \text{ \AA}$	$D = 0.15 \text{ \AA}$	

The term  $B_{ij}$  in Equation (4.1) expresses the measure of the bond order, which is related to the number of neighboring atoms and the connecting angles.

$$B_{ij} = \left( 1 + \beta^n \zeta_{ij}^n \right)^{\left( \frac{1}{2n} \right)} \quad (4.5)$$

The parameters  $\beta^n$  and 'n' are given in Table 4.1, and the function  $\zeta_{ij}^n$  is given by,

$$\zeta_{ij}^n = \sum_{k \in i,j} f_c(r_{ik}) g(\theta_{ijk}) \quad (4.6)$$

The function  $f_c(r_{ik})$  is the cut-off function already described in Equation (4.4). The function  $g(\theta_{ijk})$  takes into consideration the bending angle  $\theta_{ijk}$  and is given by,

$$g(\theta_{ijk}) = 1 + \frac{c^2}{d^2} - \frac{c^2}{\left[ d^2 + (h - \cos\theta_{ijk})^2 \right]} \quad (4.7)$$

The parameters  $c$ ,  $d$  and  $h$  are given in Table 4.1. Figure 4.1 illustrates the definition of the bending angle  $\theta_{ijk}$  for a graphene sheet. It is the angle between bonds  $i$ - $j$  and  $i$ - $k$ . Through the bending angle, the atoms  $k$  affect the energy stored between atoms  $i$  and  $j$ .

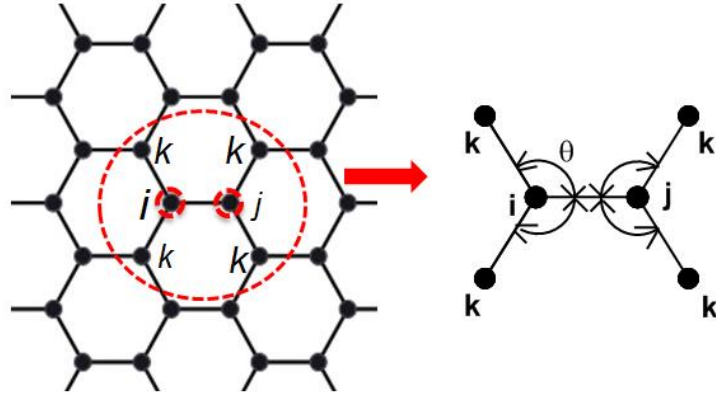


Figure 4.1: Part of graphene sheet.

#### 4.1 Atomic Element

Figure 4.2(a) shows a graphene sheet and within the mesh, the atomic finite element proposed by Liu et al. (2004). A single atomic finite element separated from the mesh is shown in Figure 4.2(b). The element has 10 atoms. The central atom (1) interacts with three nearest neighbours, 2, 5, 8 and six second nearest neighbours 3, 4, 6, 7, 9 and 10. All the calculations for the atomic finite element are in relation to the central atom, atom number 1. In the present article the Tersoff potential is considered to calculate the total energy of system. It has many-body (non-local) nature. It means that the first nearest neighbours 2, 5, 8 as well as the second nearest neighbours 3, 4, 6, 7, 9, and 10 affect the calculation of the total energy of the atom 1. The second nearest neighbours are connected through the angle bending. This is illustrated in Figure 4.2(c) showing the angle bending  $\theta_{123}$  considering the bond 1-2. The cosine is given by the Eq. (4.8) (Kim, 2006),

$$\cos(\theta_{123}) = \frac{\overline{1,2}^2 + \overline{2,3}^2 - \overline{1,3}^2}{2 \cdot \overline{1,2} \cdot \overline{2,3}} \quad (4.8)$$

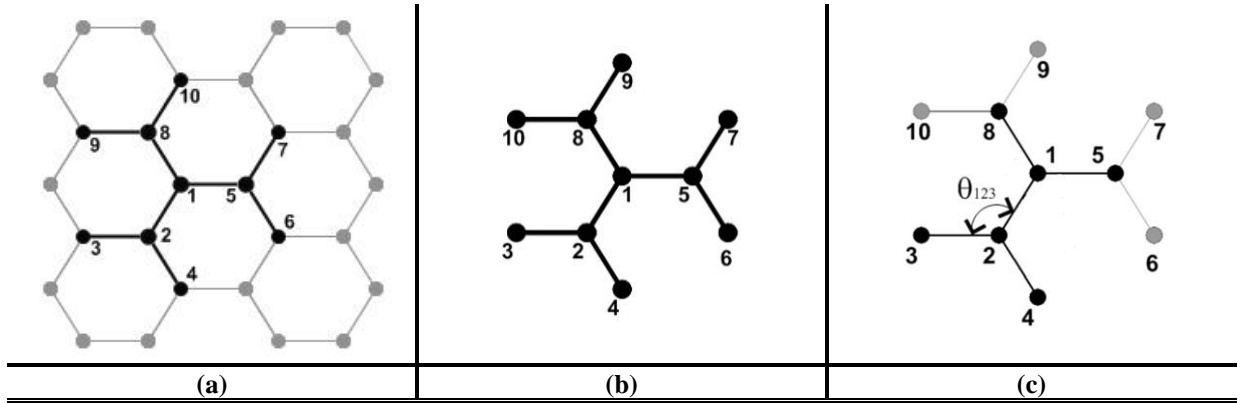
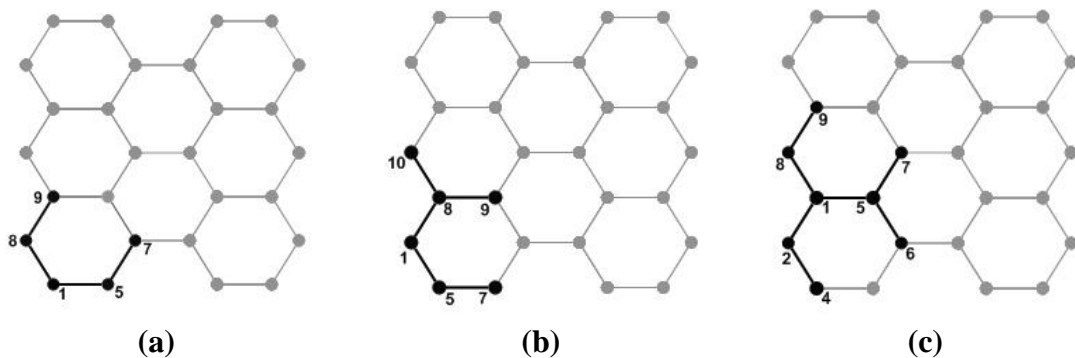
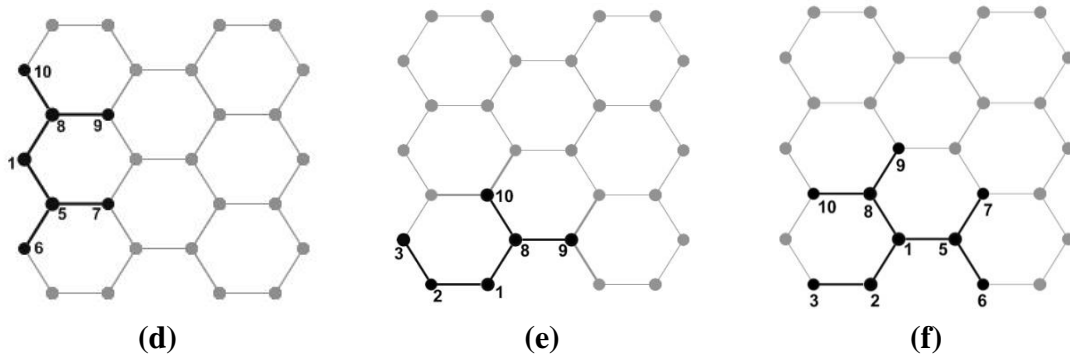


Figure 4.2: (a) Graphene sheet, (b) AFEM element, (c) Atomic finite element with angle bending

**The modified atomic element.** Now the issue of the modified atomic finite element is addressed. This concept, that was not described by previous authors that worked and implemented AFEM, is crucial to proper account for the boundary conditions in bounded meshes and in meshes with missing atoms or vacancies. A set of modified elements are shown in dark black lines in Figures 4.3(a) to 4.3(f). As can be perceived, according to the position that the central atoms (1) takes in the boundary of the mesh, some first or second order neighboring atoms are missing. Consider Figure 4.3(a) as an example. In this element the atoms numbered 2, 3, 4, 6 and 10 are missing. Therefore, the energy contribution from the atoms 2, 3, 4, 6, and 10 must be eliminated from the total energy calculation of the element when determining the element stiffness matrix and the non-equilibrium force vector. The same procedure applies for all other elements shown.





**Figure 4.3: Modified atomic elements.**

When considering meshes with vacancies or missing atoms, the same reasoning applies. The atomic elements around the vacancies are also modified or incomplete elements and this must be taken into account in the energy calculations leading to the element matrix and load vector.

Once is revised the atomic finite element and introduced the concept of modified atomic element, the next topic presents the calculation of the total energy of the complete atomic finite element using the Tersoff potential.

## 4.2 AFEM Implementation

In the chapter 3, section 3.2, was presented all the steps for the AFEM implementation. In this section is presented only the part of the calculation of the total energy of the atomic finite element, Figure 4.2(b), used to model the graphene sheet using the Tersoff potential. Initially, the bond length  $r_{ij}$  and the cut-off function are calculated,

The bond lengths:

$$r_{12} = r_{18} = r_{15} = 1.396 \text{ \AA} \quad (4.9)$$

$$r_{13} = r_{14} = r_{16} = r_{17} = r_{19} = r_{110} = 2.418 \text{ \AA} \quad (4.10)$$

The cut-off function:

$$f_c(r_{ij}) = \begin{cases} 1, & r_{ij} < 1.8 \\ \frac{1}{2} - \frac{1}{2} \sin \left[ \frac{\pi}{2} \frac{(r_{ij} - R)}{D} \right], & 1.8 < r_{ij} < 2.1 \\ 0, & r_{ij} > 2.1 \end{cases} \quad (4.11)$$

Substituting the values (4.9) and (4.10) into Equation (4.11) gives

$$f(r_{12}) = 1, f(r_{15}) = 1, f(r_{18}) = 1 \quad (4.12)$$

$$f(r_{13}) = 0, f(r_{14}) = 0, f(r_{16}) = 0, f(r_{17}) = 0, f(r_{19}) = 0, f(r_{110}) = 0 \quad (4.13)$$

Based on the Eq. (4.12) and Eq. (4.13) the total energy ( $E_{\text{tot}}$ ) of a central atom, 1, is given by the sum of energies of the bonds 1-2, 1-5 and 1-8,

$$E_{\text{tot}} = f(r_{ij})(E_{12} + E_{15} + E_{18}) \frac{1}{2} \quad (4.14)$$

The energy expression in relation to the bond 1-2:

$$E_{12} = (V_{12}^R + B_{12} V_{12}^A) \quad (4.15)$$

The energy expression in relation to the bond 1-5:

$$E_{15} = (V_{15}^R + B_{15} V_{15}^A) \quad (4.16)$$

The energy expression in relation to the bond 1-8:

$$E_{18} = (V_{18}^R + B_{18} V_{18}^A) \quad (4.17)$$

In order to simplify the demonstration of the calculation of the total energy of the atomic finite element, only the calculation of the energy related to the bond 1-2 is demonstrated. The following equations are related to the bond 1-2.

Repulsive function:

$$V_R(r_{12}) = A \exp(-\lambda^1 r_{12}) \quad (4.18)$$

Attractive function:

$$V_A(r_{12}) = -B \exp(-\lambda^2 r_{12}) \quad (4.19)$$

The term  $B_{ij}$  expresses the measure of the bond order, which is related with the number of neighbors and the angle. The bond order between the atoms 1-2 is given by,

$$B_{ij} = \frac{(b_{12} + b_{21})}{2} \quad (4.20)$$

Term  $b_{12}$ :

$$b_{12} = \left(1 + \beta^n \zeta_{12}^n\right)^{\left(\frac{1}{2n}\right)} \quad (4.21)$$

$$\zeta_{12}^n = \sum_{k \neq i,j} (f_c(r_{15})g(\theta_{125}) + f_c(r_{18})g(\theta_{128})) \quad (4.22)$$

Term  $b_{21}$ :

$$b_{21} = \left(1 + \beta^n \zeta_{21}^n\right)^{\left(\frac{1}{2n}\right)} \quad (4.23)$$

$$\zeta_{21}^n = \sum_{k \neq i, j} (f_c(r_{23})g(\theta_{213}) + f_c(r_{24})g(\theta_{214})) \quad (4.24)$$

All the steps are repeated considering the bonds 1-5 and 1-8 in order to obtain the total energy of the atomic finite element. The considered Tersoff parameters can be found in Table 4.1 (Tersoff, 1988).

### 4.3 Results and discussions

#### 4.3.1 Molecular dynamics simulations

In order to validate the AFEM implementation the force-strain curve of pristine armchair and zigzag graphene sheets are compared to molecular dynamics (MD) simulations, which were performed using the canonical ensemble (NVT) implemented in the Large-scale atomic/molecular massively parallel simulator (LAMMPS) package (Plimpton et al., 1995). The Tersoff potential simulations were carried out at a temperature of 1 K. Non-periodic boundary conditions were used. The time integration step for the MD simulation is 0.05 fs. AFEM is performed, considering the distance between two carbon atoms as 1.396 Å in the equilibrium position (Stuart et al., 2000). The Tersoff parameters used are given in Table 4.1.

#### 4.3.2 Verification of the accuracy of AFEM

In this section the mechanical behaviour of single layer graphene sheets obtained from AFEM simulations is presented and the AFEM implementation will be validated. In order to validate the AFEM implementation, the stress-strain curves of pristine bulk graphene sheets under tension are compared with molecular dynamics (MD) simulation results considering the parameters detailed in the section 4.3.1.

The strain measure is defined as the average of the displacements  $u_i$  for a number of  $n_a$  atoms divided by the original mesh length  $L_0$ :

$$\varepsilon = \frac{\frac{1}{n_a} \sum_{i=1}^{n_a} u_i}{L_0} \quad (4.25)$$

The stress  $\sigma$  is approximated by dividing the sum of the external forces applied at the atoms  $n_a F_{\text{ext}}$  by an assumed area  $A$ . This area is considered to be formed by the length of mesh orthogonal to the traction direction,  $L_y$ , and a thickness  $t$ . In computing the stresses, the thickness of the sheet was assumed as 0.34 nm, which is the equilibrium distance between two parallel graphene sheets:

$$\sigma = \frac{n_a F_{\text{ext}}}{A} = \frac{n_a F_{\text{ext}}}{L_y t} \quad (4.26)$$

Two pristine graphene sheets having armchair and zigzag edges with dimensions of 23.7 Å x 21.8 Å (228 atoms) and 41.2 Å x 39.4 Å (660 atoms) were subjected to uniaxial tension loading to examine the accuracy and size effects of AFEM.

**Validation and mesh dependency.** In the first study, atomic meshes corresponding to the 228 and 660 atoms cases are shown in Figures 4.4(a), 4.4(b) and 4.5(a) with the tensile loading configurations for the armchair and zigzag directions.. Modified Newton-Raphson method was used to solve the Equation (2.7) with load steps of 0.1 eV/ Å.

Figures 4.4(c), 4.4(d) and 4.5(b) shows a comparison of the stress-strain curves of pristine graphene sheets obtained from AFEM and MD simulations for uniaxial tensile loading in the armchair and zigzag directions based on the Tersoff potential. The AFEM and MD results agree very closely until strain reaches 0.1 and thereafter show minor deviation with MD showing slightly higher softening. Minor oscillations are quite natural in MD simulations as the response is determined through a dynamic analysis and nominal stress does not contain a correction for the kinetic energy of the system (Dewapriya, 2012). AFEM results are quite smooth as they correspond to a quasi-static analysis. Some deviations are observed at higher strains closer to the ultimate strength as MD is able to better simulate the initial bond



breaking until the solution becomes unstable and sample reach failure point (Dewapriya and Rajapakse, 2014). It is therefore observed that failure strains from MD simulations are slightly higher and ultimate strengths are slightly smaller. AFEM in the current form does not capture bond breaking as well as MD but the behaviour shown in Figures 4.4(c), 4.4(d) and 4.5(b) confirms that it is able to capture the failure stress and strain predicted by MD with good accuracy.

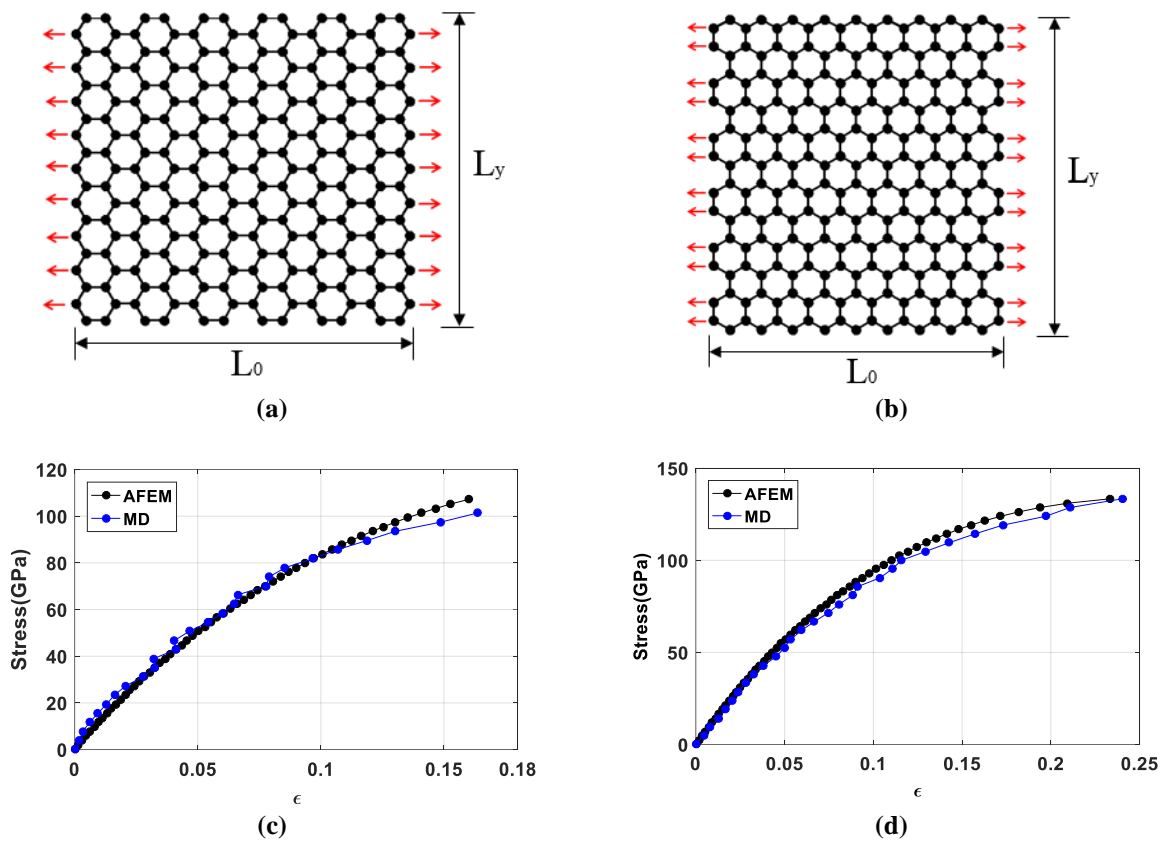


**Figure 4.4:** (a) Pristine graphene sheet with 228 atoms and armchair edges, (b) Pristine graphene sheet with 228 atoms and zigzag edges, (c) and (d) Stress-strain curves obtained from AFEM and MD for armchair and zigzag sheets based on Tersoff potential

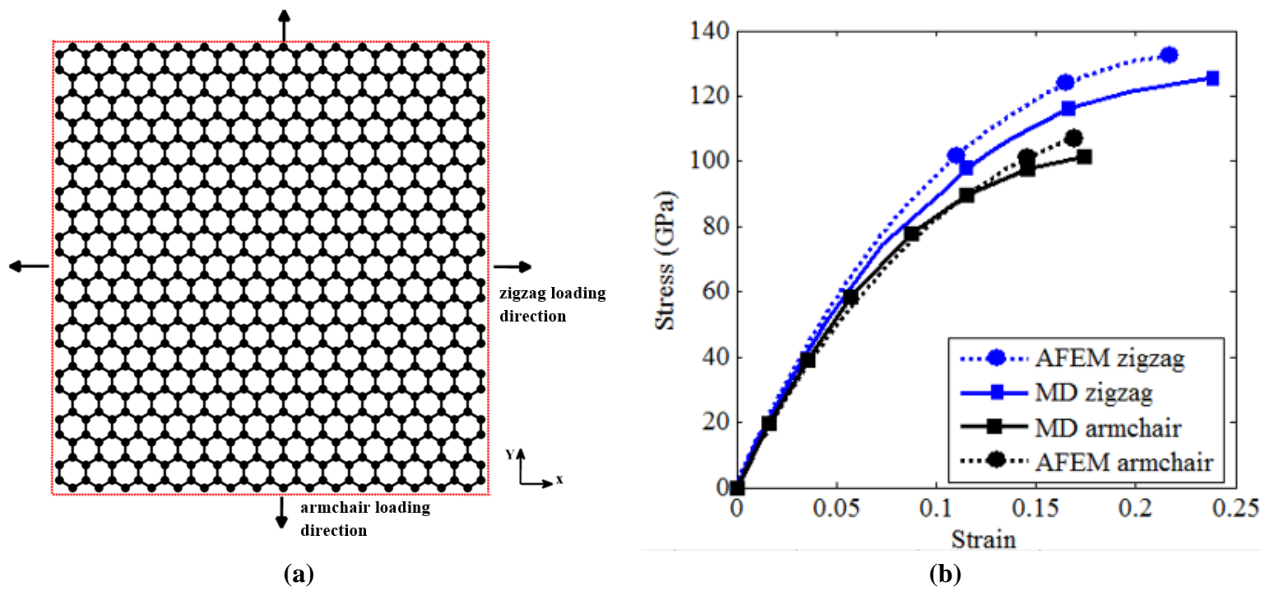


Figure 4.5: (a) Pristine graphene sheet with 660 atoms and armchair and zigzag edges, (c) Stress-strain curves obtained from AFEM and MD for armchair and zigzag sheets based on Tersoff potential.

Figures 4.6(a) and 4.6(b) show a comparison of the stress-strain curves of pristine graphene sheets obtained from AFEM for uniaxial tensile loading in the armchair and zigzag directions based on the Tersoff potential. Note that engineering (nominal) stress and strain are used in the calculations. The results for 228 and 660 atoms meshes showed hardly any differences confirming that the considered mesh sizes were sufficient to model the behaviour of bulk graphene.

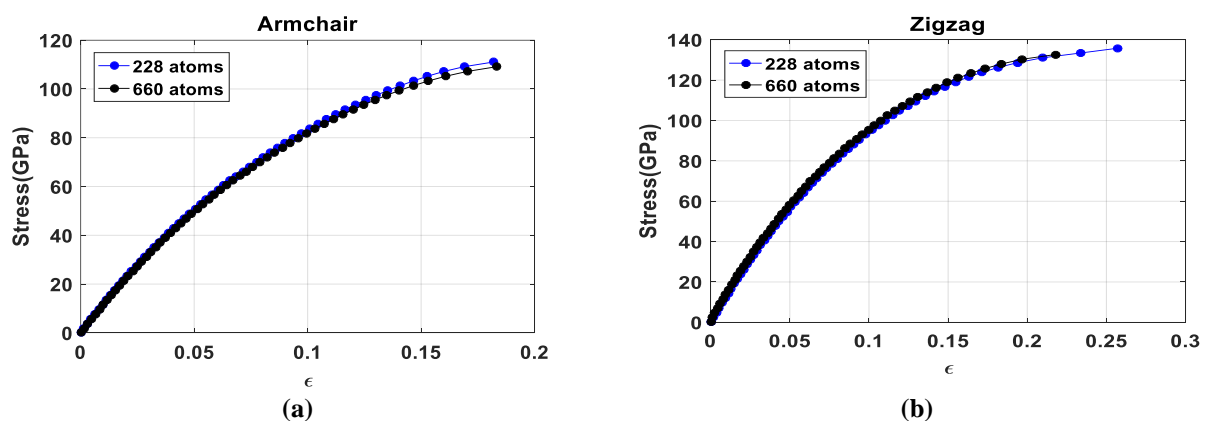


Figure 4.6: (a) Shows a comparison of the stress-strain curves of graphene sheets with 228 and 660 atoms and armchair edges obtained from AFEM, (b) shows a comparison of the stress-strain curves of graphene sheets with 228 and 660 atoms and zigzag edges obtained from AFEM

Although the results in Fig. 4.5(b) for AFEM and MD simulations are generally in good agreement, it is known that Tersoff potential has certain weaknesses in modelling carbon atom systems (Stuart et al. 2000). In the section 5, the second generation REBO potential results will be presented and compared to Tersoff potential results.

### 4.3.3 Effects of chirality

Chirality has a strong influence on the mechanical behavior of graphene sheets. Figure (4.7) shows the stress-strain curves obtained from mesh 2 with 660 atoms, comparing results for the armchair and zigzag orientations. The Figure (4.7) shows that the zigzag orientation is stiffer than the armchair counterpart. It also shows that the fracture strain depends on the chirality. For the present AFEM simulations the strain limit obtained for the zigzag was 0.22 and for the armchair was 0.18. The ultimate Cauchy tensile strength obtained were 109.1 GPa and 132.7 GPa in the armchair and zigzag cases, respectively.

The results obtained by Liu et al. (2007) and by Zhao et al. (2009) are show in Table 4.2. There is a fairly good agreement between the present AFEM calculations and the results reported by the mentioned authors.

**Table 4.2: Fracture strength calculated by atomistic studies.**

Atomistic Studies	Armchair	Zigzag
	Strength (GPa)	Strength (GPa)
Liu et al. (2007)	110	121
Zhao et al. (2009)	102	129
Present work	109.1	132.7

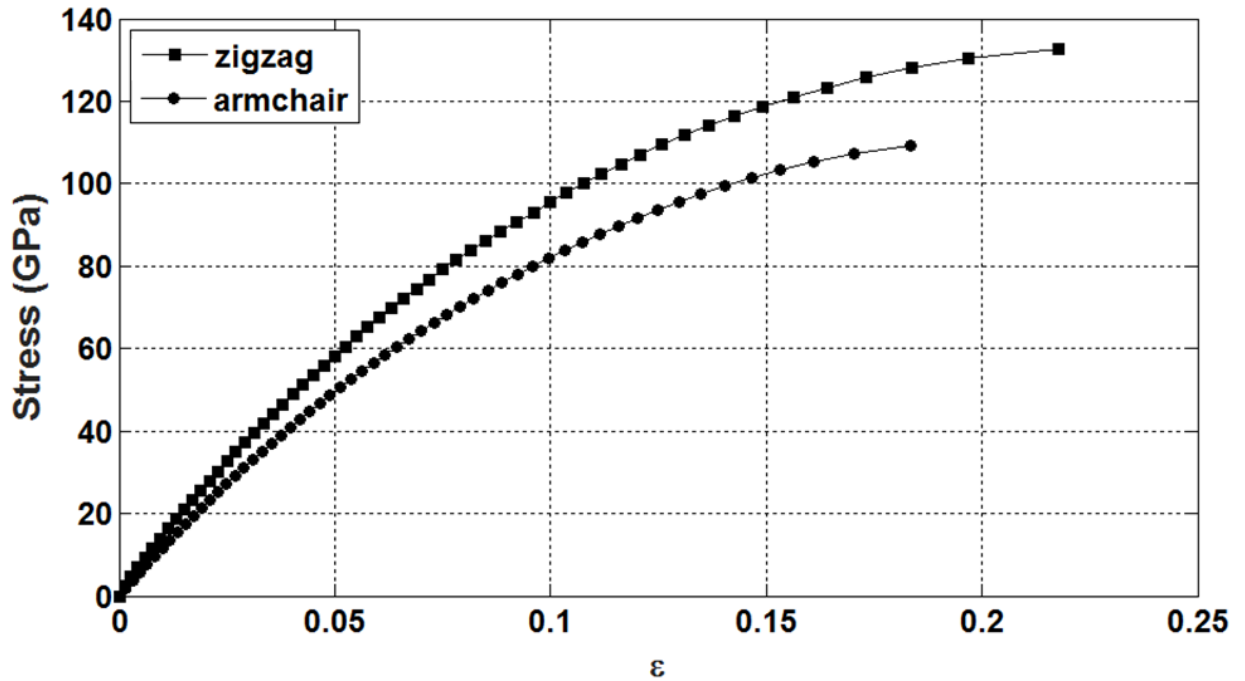


Figure 4.7: Stress-strain curves of the pristine graphene sheet having armchair zigzag edges along x direction.

#### 4.3.4 Effects of vacancy defects

Numerical and theoretical studies have shown that the presence of crack or vacancy defects reduce the ultimate tensile strength of graphene (Dewapriya 2012, Banhart et al., 2011). Furthermore, the ultimate tensile strength is related with the chirality. Figure (4.8) shows a graphene sheet with a defect. A crack of width  $6.98 \text{ \AA}$ , resulting from the exclusion of two atoms is introduced in order to analyse the influence of vacancy defects on the mechanical behaviour of graphene. The original pristine mesh has 660 atoms. Figures 4.9(a) and 4.9(b) show the stress-strain curves obtained from AFEM under uniaxial tensile loading for the case or armchair and zigzag oriented edges. The results in terms of ultimate tensile strength are summarized in Table 4.3. It is clear that the presence of a crack reduces considerably the ultimate tensile strength of the graphene sheet. These curves also show that small vacancy defects have an influence on the ultimate tensile strength of graphene, but practically do not affect rigidity of the sample.

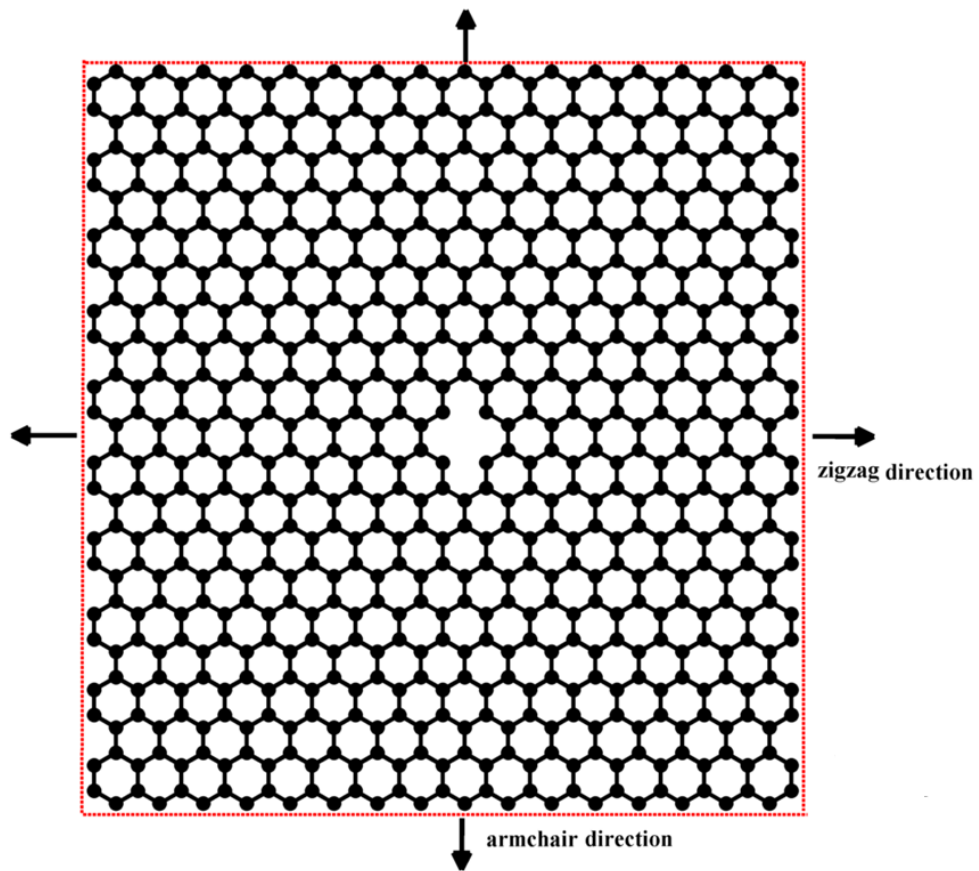
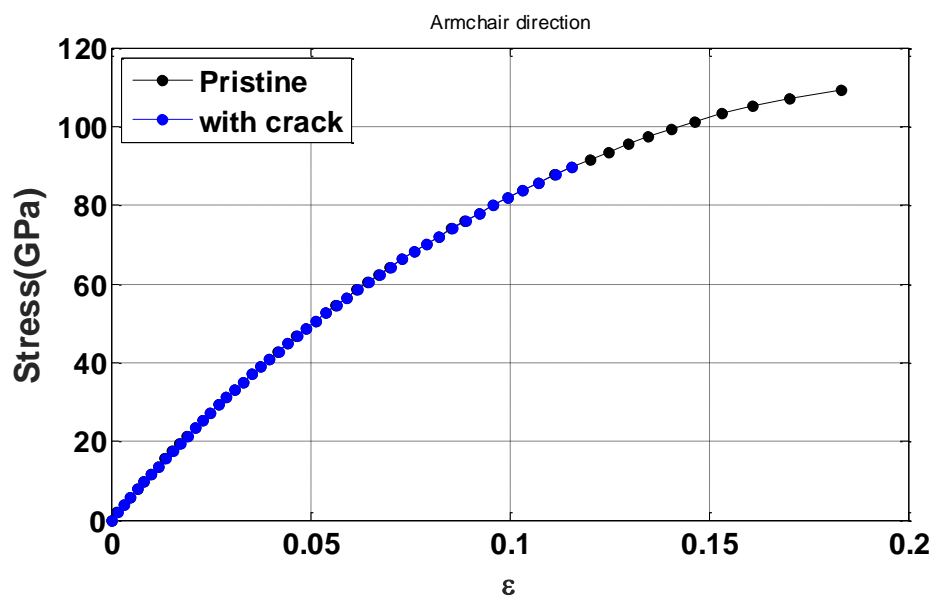


Figure 4.8: Graphene sheet having zigzag and armchair edges with a crack of width  $6.98 \text{ \AA}$ .



(a) Armchair orientation

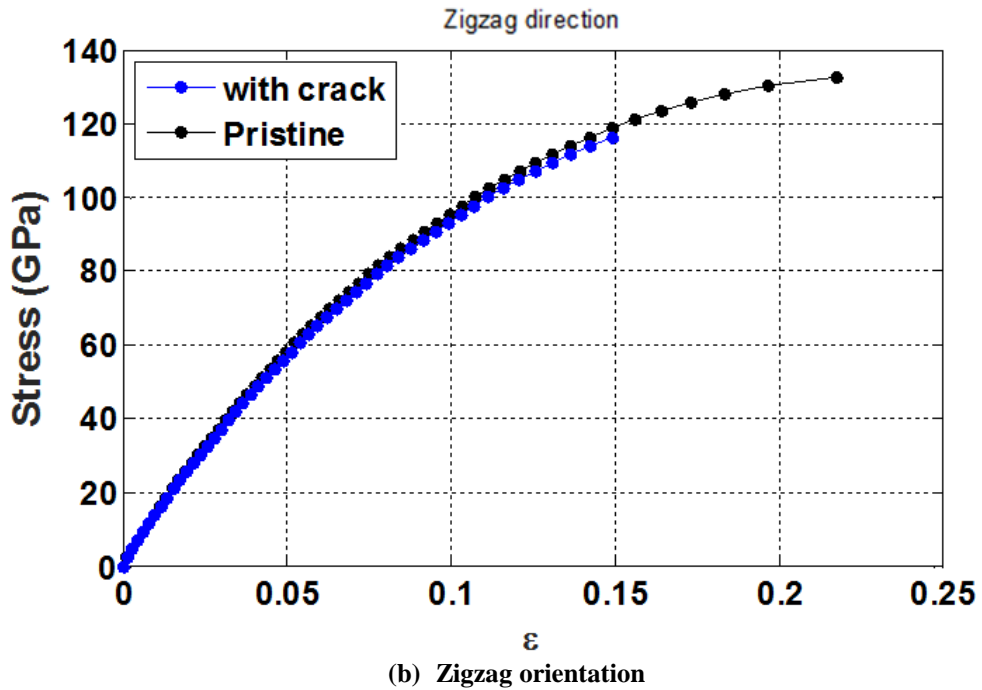


Figure 4.9: Stress-strain relation of the graphene sheet having armchair and zigzag edges with a crack of width 6.98 Å.

Table 4.3: Comparison of ultimate stress-strain results of graphene for the pristine sheet and for the one with vacancy defects.

AFEM results	Armchair		Zigzag	
	$\sigma$ (GPa)	$\epsilon$	$\sigma$ (GPa)	$\epsilon$
<b>Pristine</b>	109.1	0.18	132.7	0.22
<b>With vacancy defects</b>	89.65	0.12	116.4	0.15

#### 4.4 Remarks

This chapter presents a formulation of the AFEM to model the mechanical behavior of graphene sheets using the multi-body Tersoff potential. Special attention is given to description of the modified atomic finite elements in order to account for the proper inclusion of boundary conditions in bounded graphene sheets. These modified elements are also necessary to model defects or vacancies in the graphene domain. This work does not make use of the periodic boundary condition used in many other reported scientific investigations. It analyzes bounded domains with prescribed force boundary conditions. For the best of the authors' knowledge a detailed explanation of the modified atomic finite elements is not

available in the literature. The AFEM formulation was validated by comparison with a classical molecular dynamics software. The proposed AFEM implementation has been applied to investigate the influence of chirality, that is, of the orientation of the graphene edges, armchair or zigzag, on the rigidity and ultimate strength of the graphene. It has been shown that chirality has a pronounced effect on the graphene ultimate strength. The methodology has also been used to assess the influence of vacancies on the rigidity and failure strength of graphene. The performed numerical investigations show that vacancies or the removal of atoms from the pristine mesh has a marked influence on the ultimate strength of the considered graphene sheet.

The results present a good agreement between the two methodologies, MD and AFEM, specially at low to mid strains. For higher strains there are some deviations between both methods. One important aspect is that the limit load, or limit strain reached by each method is distinct. The AFEM behavior for the limit loads shows a mesh dependency. The reasons for these results must be further investigated. Nevertheless some considerations can be advanced. For the solution of the non-linear system given by Equation (2.7), the Newton Raphson method and the modified Newton Raphson method were implemented. Both methods fail when a solution path approaches the limit point. Close to the load limit, the numerical solution does not converge due to the fact that the tangent matrix approached zero value and the system becomes ill-conditioned (Kim, 2015).

## 5 SECOND-GENERATION REACTIVE EMPIRICAL BOND ORDER POTENTIAL

The proposal of this chapter is to apply the atomic-scale finite element method (AFEM), to analyse the mechanical behavior of single-layer graphene sheet by using the second-generation reactive empirical bond order potential energy (Brenner et al., 2012). The energy stored on the bond between atoms  $i$  and  $j$  depends on their separation distance, and also on the relative position of second nearest-neighbor atoms. The energy stored on the bond considering the second generation of REBO is given by:

$$E_{ij}^{\text{REBO}} = f(r_{ij}) (V_{ij}^{\text{R}} + B_{ij} V_{ij}^{\text{A}}) \quad (5.1)$$

This potential consists of the repulsive ( $V_{ij}^{\text{R}}$ ) and the attractive ( $V_{ij}^{\text{A}}$ ) functions, respectively, and defined as:

$$V_{ij}^{\text{R}} = \left[ 1 + \frac{Q_{ij}}{r_{ij}} \right] A_{ij} e^{-\alpha_{ij} r_{ij}} \quad (5.2)$$

$$V_{ij}^{\text{A}} = -\sum_{n=1}^3 B_{ij}^{(n)} e^{-\beta_{ij}^{(n)} r_{ij}} \quad (5.3)$$

where the parameters  $Q_{ij}$ ,  $A_{ij}$ ,  $\alpha_{ij}$ ,  $B_{ij}^{(n)}$  and  $\beta_{ij}^{(n)}$  depend on the atom types  $i$  and  $j$ ;  $r_{ij}$  is the bond length. The term  $f(r_{ij})$  is the cut-off function, which it switches off the interaction when the atom pair exceeds the bond length  $r_{ij}$ , and it's given by



$$f(r_{ij}) = \begin{cases} 1, & r_{ij} < R^{(1)} \\ \frac{1 + \cos \left[ \frac{\pi (r_{ij} - R^{(1)})}{(R^{(2)} - R^{(1)})} \right]}{2}, & R^{(1)} < r_{ij} < R^{(2)} \\ 0, & R^{(2)} < r_{ij} \end{cases} \quad (5.4)$$

The term  $B_{ij}$  corresponds to the bond order term. It's related with the number of neighbors and the angle, which it's related with the forming and breaking of the bonds between of the atoms. The expression for  $B_{ij}$  is:

$$B_{ij} = \frac{1}{2} [b_{ij}^{\sigma\pi} + b_{ji}^{\sigma\pi}] + b_{ij}^{\pi} \quad (5.5)$$

$$b_{ij}^{\pi} = \Pi_{ij}^{rc} + b_{ij}^{dh} \quad (5.6)$$

The term  $b_{ij}^{\sigma\pi}$  is composed by covalent bond interactions, and by the angular function  $g(\cos\theta_{jik})$ , which include the contribution from the second nearest neighbour according to the cosine of the angle of the bonds between atoms  $ik$  and  $ij$ .

$$b_{ij}^{\sigma\pi} = \left[ 1 + \sum_{k \neq i,j} f_{ik}(r_{ik}) g(\cos\theta_{jik}) e^{\lambda_{ijk}} + P_{ij}(N_i^C, N_i^H) \right]^{\frac{1}{2}} \quad (5.7)$$

According to Brenner et al. (2002) the parameters  $P_{ij}$  and  $\lambda$  are taken to be zero for solid-state carbon. The equations (5.8) – (5.14) show the angular function in three regions of bond angle  $\theta$ ,

For  $0^\circ < \theta < 109.476^\circ$

$$g(\cos\theta_{jik}) = G(\cos\theta_{jik}) + Q(N_i!) [\gamma(\cos\theta_{jik}) - G(\cos\theta_{jik})] \quad (5.8)$$

$$G(\cos\theta_{jik}) = 0.5024 \cos^5(\theta) + 1.4297 \cos^4(\theta) + 2.0313 \cos^3(\theta) + 2.2544 \cos^2(\theta) + 1.4068 \cos(\theta) + 0.3755 \quad (5.9)$$

$$\gamma(\cos\theta_{jik}) = -0.0401 \cos^5(\theta) + 1.272 \cos^4(\theta) - 0.5597 \cos^3(\theta) - 0.4331 \cos^2(\theta) + 0.4889 \cos(\theta) + 0.2719 \quad (5.10)$$

For  $109.476^\circ < \theta < 120^\circ$

$$g(\cos\theta_{jik}) = G(\cos\theta_{jik}) \quad (5.11)$$

$$G(\cos\theta_{jik}) = 36.2789 \cos^5(\theta) + 71.8829 \cos^4(\theta) + 57.5918 \cos^3(\theta) + 24.0970 \cos^2(\theta) + 5.6774 \cos(\theta) + 0.7073 \quad (5.12)$$

For  $120^\circ < \theta < 180^\circ$

$$g(\cos\theta_{jik}) = G(\cos\theta_{jik}) \quad (5.13)$$

$$G(\cos\theta_{jik}) = -1.3424 \cos^5(\theta) - 4.928 \cos^4(\theta) - 6.83 \cos^3(\theta) - 4.346 \cos^2(\theta) - 1.098 \cos(\theta) + 0.0026 \quad (5.14)$$

For a better understanding about the bond angle  $\theta_{ijk}$ , the Figure (5.1) shows part of graphene sheet considering the angle bending. The atoms k affect the energy stored between atoms i and j, and j and i.

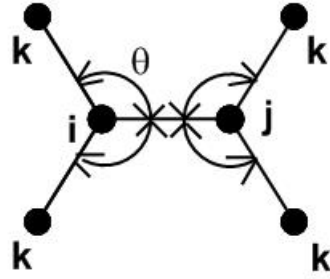


Figure 5.1: Part of graphene sheet

The function  $Q(N_i^t)$  is given by

$$Q(N_i^t) = \begin{cases} 1 & N_i^t < 3.2 \\ \left[1 + \cos(2\pi(N_i^t - 3.2))\right]/2 & 3.2 < N_i^t < 3.7 \\ 0 & N_i^t > 3.7 \end{cases} \quad (5.15)$$

The term  $N_i^t$  is the sum of the carbon atoms number and the hydrogen atoms number, in this case  $N_i^H$  is zero,

$$N_i^t = N_i^C + N_i^H \quad (5.16)$$

$$N_i^C = \sum_{k(\neq i,j)}^{\text{carbon atoms}} f_{ik}(r_{ik}) \quad (5.17)$$

The term  $\Pi_{ij}^{rc}$  is a three-dimensional cubic spline, which depends on the number of carbon atoms that are neighbors of atoms  $i$  and  $j$  and the nonconjugated bonds.

$$\Pi_{ij}^{rc} = F_{ij}(N_i^t, N_j^t, N_{ij}^{\text{conj}}) \quad (5.18)$$

$$N_{ij}^{\text{conj}} = 1 + \left[ \sum_{k(\neq i,j)}^{\text{carbon atoms}} f_{ik}(r_{ik}) F(x_{ik}) \right]^2 + \left[ \sum_{l(\neq i,j)}^{\text{carbon atoms}} f_{jl}(r_{jl}) F(x_{jl}) \right]^2 \quad (5.19)$$

$$F(x_{ik}) = \begin{cases} 1 & x_{ik} < 2 \\ \left[1 + \cos(2\pi(x_{ik} - 2))\right]/2 & 2 < x_{ik} < 3 \\ 0 & x_{ik} > 3 \end{cases} \quad (5.20)$$

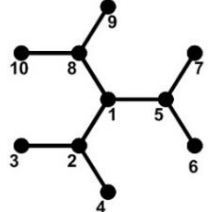
$$x_{ik} = N_k^t - f_{ik}(r_{ik}) \quad (5.21)$$

The term  $b_{ij}^{\text{dh}}$  in Eq. (5.6) is zero for graphene due to its planar configuration. All the parameters considered can be found in Stuart et al. (2000).

## 5.1 Atomic Element

The same atomic finite element considered using the Tersoff potential will be considered using the second generation REBO potential. Table 5.1 shows the AFEM element, which considers the first and second nearest neighbour interaction. The central atom (1) interacts with three nearest neighbours (2, 5 and 8) and six second nearest neighbours (3, 4, 6, 7, 9 and 10). The total energy ( $E_{\text{tot}}$ ) of the complete atomic element obtained from AFEM and from MD are in agreement.

**Table 5.1: AFEM element and total energy value obtained from AFEM and MD**

	Total Energy	
	AFEM	MD
	-7.8073 eV	-7.8073 eV

The important concept of modified atomic finite element was discussed and illustrated in the chapter 4, section 4.1.

## 5.2 AFEM Implementation

In the chapter 3, section 3.2, was presented all the steps for the AFEM implementation. In this section is presented only the calculation of the total energy of the atomic finite element using the second generation of REBO potential. Initially, the bond length  $r_{ij}$  and the cut-off function are calculated,

The bond lengths:

$$r_{12} = r_{18} = r_{15} = 1.396 \text{ \AA} \quad (5.22)$$

$$r_{13} = r_{14} = r_{16} = r_{17} = r_{19} = r_{110} = 2.418 \text{ \AA} \quad (5.23)$$

The cut-off function:

$$f(r_{ij}) = \begin{cases} 1, & r_{ij} < R^{(1)} \\ \frac{1 + \cos\left[\frac{\pi(r_{ij} - R^{(1)})}{(R^{(2)} - R^{(1)})}\right]}{2}, & R^{(1)} < r_{ij} < R^{(2)} \\ 0, & R^{(2)} < r_{ij} \end{cases} \quad (5.24)$$

$$R^{(1)} = 1.7 \text{ \AA}, \quad R^{(2)} = 2 \text{ \AA} \quad (5.25)$$

Substituting the values (5.22), (5.23) and (5.25) into Equation (5.24) gives

$$f(r_{12}) = 1, \quad f(r_{15}) = 1, \quad f(r_{18}) = 1 \quad (5.26)$$

$$f(r_{13}) = 0, \quad f(r_{14}) = 0, \quad f(r_{16}) = 0, \quad f(r_{17}) = 0, \quad f(r_{19}) = 0, \quad f(r_{110}) = 0 \quad (5.27)$$

The expression of the total energy of complete atomic finite element is given by,

$$E_t^{\text{REBO}} = f(r_{ij}) (E_{12}^{\text{REBO}} + E_{15}^{\text{REBO}} + E_{18}^{\text{REBO}}) \frac{1}{2} \quad (5.28)$$

The others bonds will contribute into the energy calculation through of the angles.

The total energy expression in relation to the bond 1-2:

$$E_{12}^{\text{REBO}} = (V_{12}^{\text{R}} + B_{12} V_{12}^{\text{A}}) \quad (5.29)$$

The total energy expression in relation to the bond 1-5:

$$E_{15}^{\text{REBO}} = (V_{15}^{\text{R}} + B_{15} V_{15}^{\text{A}}) \quad (5.30)$$

The total energy expression in relation to the bond 1-8:

$$E_{18}^{\text{REBO}} = (V_{18}^{\text{R}} + B_{18} V_{18}^{\text{A}}) \quad (5.31)$$

In other to simplify the calculation, the following equations are related to the bond 1-2.

Repulsive function:

$$V_{ij}^{\text{R}} = f(r_{ij}) \left[ 1 + \frac{Q_{ij}}{r_{ij}} \right] A_{ij} e^{-\alpha_{ij} r_{ij}} \quad (5.32)$$

$$V_{12}^{\text{R}} = f(r_{12}) \left[ 1 + \frac{Q}{r_{12}} \right] A e^{-\alpha r_{12}} \quad (5.33)$$

Attractive function:

$$V_{ij}^{\text{A}} = -f(r_{ij}) \sum_{n=1}^3 B_{ij}^{(n)} e^{-\beta_{ij}^{(n)} r_{ij}} \quad (5.34)$$

$$V_{12}^A = -f(r_{12}) \sum_{n=1}^3 B^{(n)} e^{-\beta^{(n)} r_{12}} \quad (5.35)$$

The sum of carbon atoms:

$$N_i^C = \sum_{k(\neq i,j)}^{\text{carbon atoms}} f_{ik}(r_{ik}) \quad (5.36)$$

$$N_1^C = \sum_{k(\neq 1,2)}^{\text{carbon atoms}} f_{1k}(r_{1k}) = f_{13}(r_{13}) + f_{14}(r_{14}) + f_{15}(r_{15}) + f_{16}(r_{16}) + f_{17}(r_{17}) + f_{18}(r_{18}) + f_{19}(r_{19}) + f_{110}(r_{110}) = 2 \quad (5.37)$$

Hydrogen atoms:

$$N_i^H = 0 \quad (5.38)$$

$$N_1^H = 0 \quad (5.39)$$

The term  $N_i^t$  is the sum of the carbon atoms number and the hydrogen atoms number:

$$N_1^t = N_1^C + N_1^H = 2 + 0 = 2 \quad (5.40)$$

The bond order between the atoms i and j is given by,

$$B_{ij} = \frac{1}{2} [b_{ij}^{\sigma\pi} + b_{ji}^{\sigma\pi}] + b_{ij}^{\pi} \quad (5.41)$$

$$B_{12} = \frac{1}{2} [b_{12}^{\sigma\pi} + b_{21}^{\sigma\pi}] + b_{12}^{\pi} \quad (5.42)$$

$$b_{ij}^{\sigma\pi} = \left[ 1 + \sum_{k \neq i,j} f_{ik}(r_{ik}) g(\cos\theta_{jik}) e^{\lambda_{ijk}} + P_{ij}(N_i^C, N_i^H) \right]^{-\frac{1}{2}} \quad (5.43)$$

The parameter  $\lambda_{ijk}$  is taken to be zero for solid-state carbon.

$$\lambda_{ijk} = 0 \quad (5.44)$$

The angular function  $g(\cos\theta_{jik})$  modulates the contribution that each nearest neighbour makes to  $B_{ij}$  according to the cosine of the angle of the bonds between atoms  $ik$  and  $ij$ . The angles bending considering the bond 1-2 are shown in Figure (5.2),

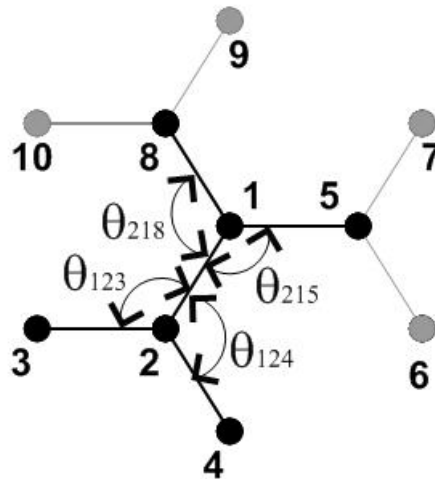


Figure 5.2: Atomic finite element with angle bending

$$b_{12}^{\sigma\pi} = \left[ 1 + f_{15}(r_{15}) g(\cos\theta_{215}) + f_{18}(r_{18}) g(\cos\theta_{218}) + P_{12}(N_1^C, N_1^H) \right]^{-\frac{1}{2}} \quad (5.45)$$

$$b_{12}^{\sigma\pi} = \left[ 1 + f_{15}(r_{15}) g(\cos\theta_{215}) + f_{18}(r_{18}) g(\cos\theta_{218}) + P_{12}(2, 0) \right]^{-\frac{1}{2}} \quad (5.46)$$

Substituting the values (5.37) and (5.39) into  $P_{12}(2, 0)$ ,

$$P_{12}(2, 0) = -0.027603 \quad (5.47)$$



Repeating the steps (5.43) to (5.46), considering the same bond 1-2, but considering 2-1,

$$\mathbf{b}_{21}^{\sigma\pi} = \left[ 1 + f_{23}(\mathbf{r}_{23})g(\cos\theta_{123}) + f_{24}(\mathbf{r}_{24})g(\cos\theta_{124}) + P_{21}(N_2^C, N_2^H) \right]^{\frac{1}{2}}$$

$$N_i^C = \sum_{k(\neq i,j)}^{\text{carbon atoms}} f_{ik}(\mathbf{r}_{ik}) \quad (5.48)$$

$$N_2^C = \sum_{k(\neq 1,2)}^{\text{carbon atoms}} f_{ik}(\mathbf{r}_{ik}) = f_{23}(\mathbf{r}_{23}) + f_{24}(\mathbf{r}_{24}) + f_{15}(\mathbf{r}_{25}) + f_{26}(\mathbf{r}_{26}) + f_{27}(\mathbf{r}_{27}) + f_{28}(\mathbf{r}_{28}) + f_{29}(\mathbf{r}_{29}) + f_{210}(\mathbf{r}_{110}) = 2 \quad (5.49)$$

$$\mathbf{b}_{21}^{\sigma\pi} = \left[ 1 + f_{23}(\mathbf{r}_{23})g(\cos\theta_{123}) + f_{24}(\mathbf{r}_{24})g(\cos\theta_{124}) + P_{21}(2, 0) \right]^{\frac{1}{2}} \quad (5.50)$$

$$P_{21}(2, 0) = -0.027603 \quad (5.51)$$

Calculating the term  $\mathbf{b}_{ij}^{\pi}$ :

$$\mathbf{b}_{ij}^{\pi} = \Pi_{ij}^{\text{rc}} + \mathbf{b}_{ij}^{\text{dh}} \quad (5.52)$$

$$\mathbf{b}_{12}^{\pi} = \Pi_{12}^{\text{rc}} + \mathbf{b}_{12}^{\text{dh}} \quad (5.53)$$

The term  $\mathbf{b}_{ij}^{\text{dh}}$  is zero for graphene due to its planar configuration,

$$\mathbf{b}_{ij}^{\text{dh}} = 0 \quad (5.54)$$

Calculation of the term  $\Pi_{12}^{\text{rc}}$ :

$$\Pi_{12}^{\text{rc}} = F_{ij}(N_1^t, N_2^t, N_{12}^{\text{conj}}) \quad (5.55)$$

$$N_{ij}^{\text{conj}} = 1 + \left[ \sum_{k(\neq i,j)}^{\text{carbon atoms}} f_{ik}(r_{ik}) F(x_{ik}) \right]^2 + \left[ \sum_{l(\neq i,j)}^{\text{carbon atoms}} f_{jl}(r_{jl}) F(x_{jl}) \right]^2 \quad (5.56)$$

For  $k = 8$  and  $5$ , and  $l = 3$  and  $4$ :

$$N_{12}^{\text{conj}} = 1 + \left[ f_{18}(r_{18}) F(x_{18}) + f_{15}(r_{15}) F(x_{15}) \right]^2 + \left[ f_{23}(r_{23}) F(x_{23}) + f_{24}(r_{24}) F(x_{24}) \right]^2 \quad (5.57)$$

$$x_{ik} = N_k^t - f_{ik}(r_{ik}) \quad (5.58)$$

For  $k = 8, 5, 3$  and  $4$ :

$$x_{18} = N_8^t - f_{18}(r_{18}) = 2 - 1 = 1 \quad (5.59)$$

$$x_{15} = N_5^t - f_{15}(r_{15}) = 2 - 1 = 1 \quad (5.60)$$

$$x_{23} = N_3^t - f_{23}(r_{23}) = 0 - 1 = -1 \quad (5.61)$$

$$x_{24} = N_4^t - f_{24}(r_{24}) = 0 - 1 = -1 \quad (5.62)$$

$$F(x_{ik}) = \begin{cases} 1 & x_{ik} < 2 \\ \left[ 1 + \cos(2\pi(x_{ik} - 2)) \right] / 2 & 2 < x_{ik} < 3 \\ 0 & x_{ik} > 3 \end{cases} \quad (5.63)$$

$$F(x_{18}) = 1 \quad (5.64)$$

$$F(x_{15}) = 1 \quad (5.65)$$

$$F(x_{23}) = 1 \quad (5.66)$$

$$F(x_{24}) = 1 \quad (5.67)$$

$$\begin{aligned} N_{12}^{\text{conj}} &= 1 + \left[ f_{18}(r_{18})F(x_{18}) + f_{15}(r_{15})F(x_{15}) \right]^2 + \\ &\quad \left[ f_{23}(r_{23})F(x_{23}) + f_{24}(r_{24})F(x_{24}) \right]^2 \\ &= 1 + [1 \cdot 1 + 1 \cdot 1]^2 + [1 \cdot 1 + 1 \cdot 1]^2 = 9 \end{aligned} \quad (5.68)$$

Substituting the  $N_1^t, N_2^t, N_{12}^{\text{conj}}$  values into Eq. (5.55),

$$\Pi_{12}^{\text{rc}} = F_{ij}(N_1^t, N_2^t, N_{12}^{\text{conj}}) = F_{12}(2, 2, 9) = 0 \quad (5.69)$$

The same procedure is followed for the bonds 1-5 and 1-8 in order to calculate the total energy of the AFEM element. All the considered parameters can be finding in S.J. Stuart et al. (2000).

### 5.3 Results and discussions

#### 5.3.1 Molecular dynamics simulations

In order to validate the AFEM implementation the force-strain curve of pristine armchair and zigzag graphene sheets are compared to molecular dynamics (MD) simulations, which were performed using the canonical ensemble (NVT) implemented in the Large-scale atomic/molecular massively parallel simulator (LAMMPS) package (Plimpton et al., 1995). The second generation REBO potential simulations were carried out at a temperature of 1 K. Non-periodic boundary conditions were used. The time integration step for the MD simulation is 0.05 fs. AFEM is performed, considering the distance between two carbon atoms as 1.396

Å in the equilibrium position (Stuart et al., 2000). In this study, a set of parameter values considered can be found in (Stuart, 2000).

### 5.3.2 Verification of the accuracy of AFEM

In this section the mechanical behaviour of single layer graphene sheets obtained from AFEM simulations is presented and the AFEM implementation will be validated. In order to validate the AFEM implementation, the stress-strain curves of pristine bulk graphene sheets under tension are compared with molecular dynamics (MD) simulation results considering the parameters detailed in the section 5.3.1. The strain measure  $\epsilon$  and the stress  $\sigma$  are defined as shown in Equations (4.25) and (4.26).

Two pristine graphene sheets having armchair and zigzag edges with dimensions of 23.7 Å x 21.8 Å (228 atoms) and 41.2 Å x 39.4 Å (660 atoms) were subjected to uniaxial tension loading to examine the accuracy and size effects of AFEM.

**Validation and mesh dependency.** In the first study, atomic meshes corresponding to the 228 and 660 atoms cases are shown in Figures 5.3(a), 5.3(b) and 5.4(a) with the tensile loading configurations for the armchair and zigzag directions. Modified Newton-Raphson method was used to solve the Equation (2.7) with load steps of 0.1 eV/ Å.

Figures 5.3(c), 5.3(d) and 5.4(b) shows a comparison of the stress-strain curves of pristine graphene sheets obtained from AFEM and MD simulations for uniaxial tensile loading in the armchair and zigzag directions based on the second generation REBO potential. The AFEM and MD results agree very closely until strain reaches 0.1 and thereafter show minor deviation with MD showing slightly higher softening. Minor oscillations are quite natural in MD simulations as the response is determined through a dynamic analysis and nominal stress does not contain a correction for the kinetic energy of the system (Dewapriya, 2012). AFEM results are quite smooth as they correspond to a quasi-static analysis. Some deviations are observed at higher strains closer to the ultimate strength as MD is able to better simulate the initial bond breaking until the solution becomes unstable and sample reach failure point (Dewapriya and Rajapakse, 2014). It is therefore observed that failure strains from MD simulations are slightly higher and ultimate strengths are slightly smaller. AFEM in

the current form does not capture bond breaking as well as MD but the behaviour shown in Figures 4.4(c), 4.4(d) and 4.5(b) confirms that it is able to capture the failure stress and strain predicted by MD with good accuracy.

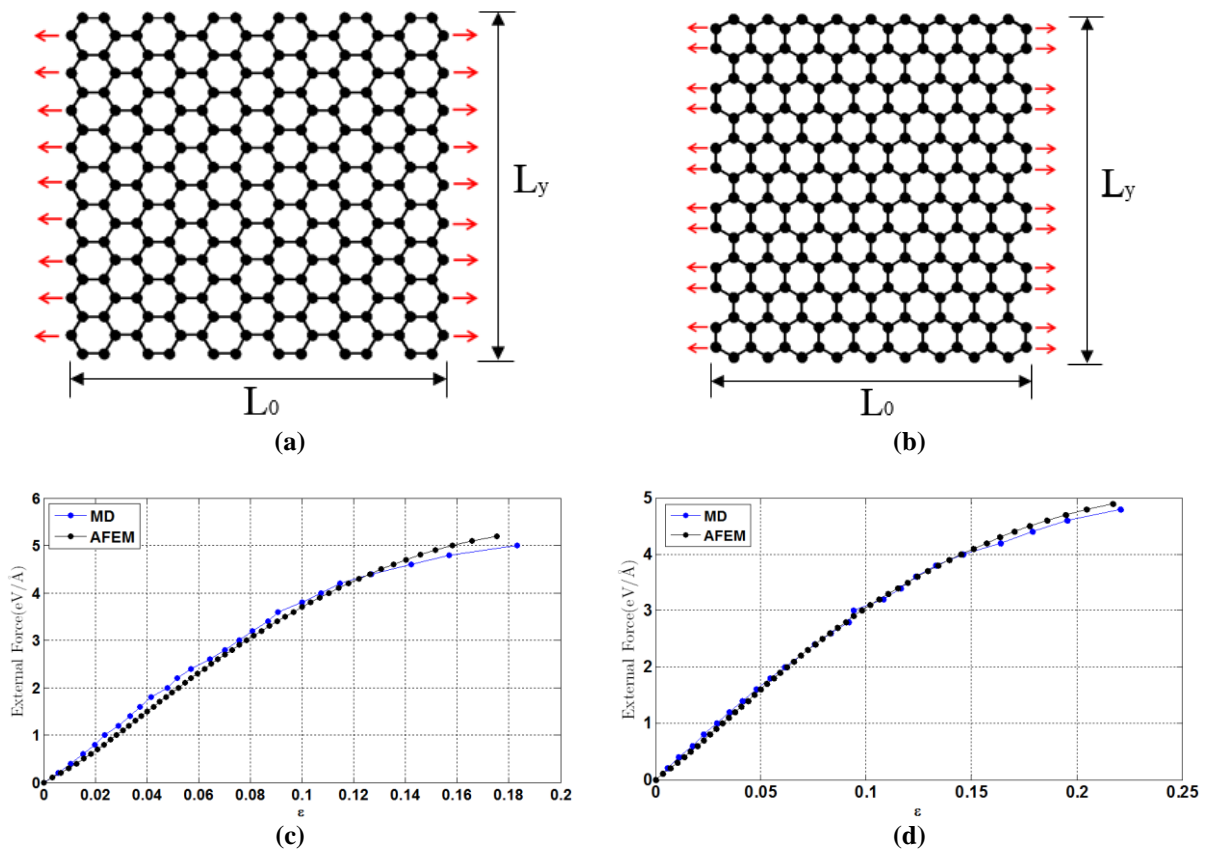


**Figure 5.3: (a) Pristine graphene sheet with 228 atoms and armchair edges, (b) Pristine graphene sheet with 228 atoms and zigzag edges, (c) and (d) Stress-strain curves obtained from AFEM and MD for armchair and zigzag sheets based on Tersoff potential**

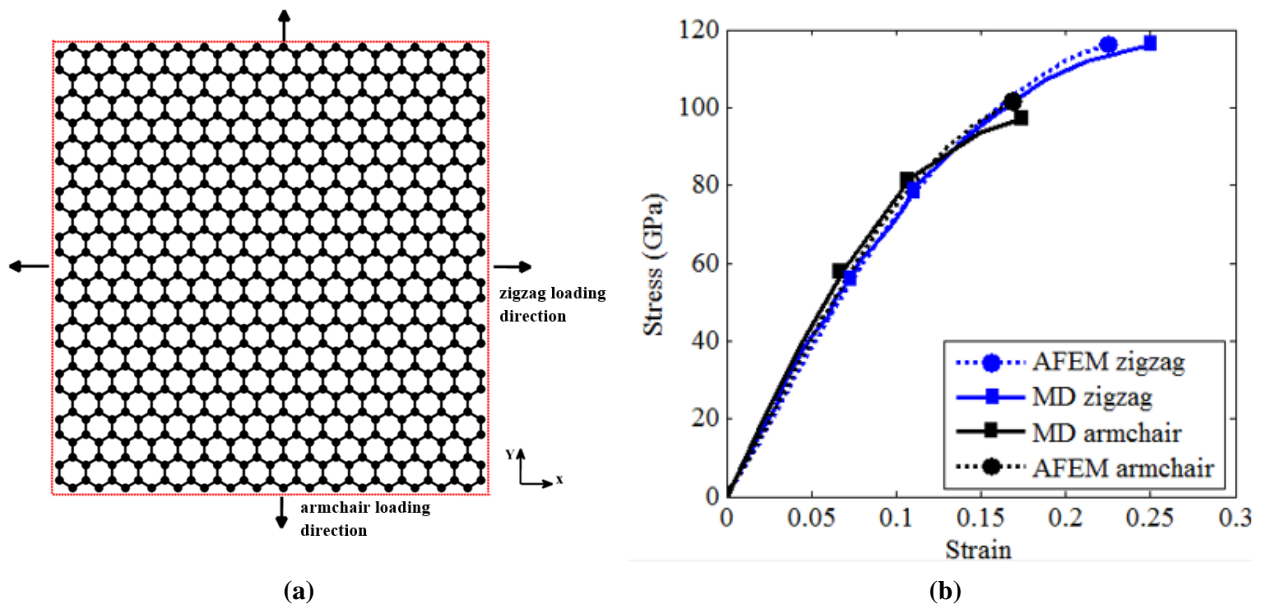


Figure 5.4: (a) Pristine graphene sheet with 660 atoms and armchair and zigzag edges, (c) Stress-strain curves obtained from AFEM and MD for armchair and zigzag sheets based on Tersoff potential.

Figures 5.5(a) and 5.5(b) shows a comparison of the stress-strain curves of pristine graphene sheets obtained from AFEM for uniaxial tensile loading in the armchair and zigzag directions based on the Tersoff potential. Note that engineering (nominal) stress and strain are used in the calculations. The results for 228 and 660 atoms meshes showed hardly any differences confirming that the considered mesh sizes were sufficient to model the behaviour of bulk graphene.

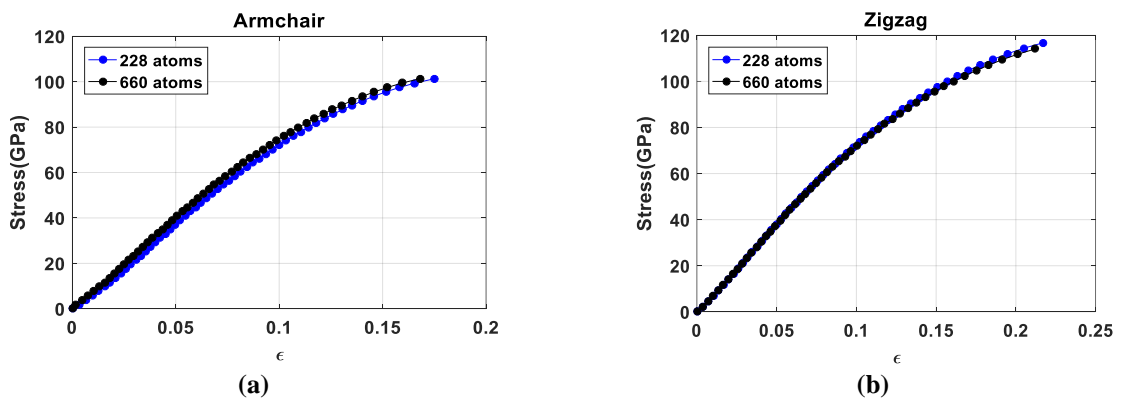


Figure 5.5: (a) Shows a comparison of the stress-strain curves of graphene sheets with 228 and 660 atoms and armchair edges obtained from AFEM, (b) shows a comparison of the stress-strain curves of graphene sheets with 228 and 660 atoms and zigzag edges obtained from AFEM

### 5.3.3 Effects of chirality

Chirality has a strong influence on the mechanical behavior of graphene sheets. Figure (5.6) shows the stress-strain curves obtained from mesh 2 with 660 atoms, comparing results for the armchair and zigzag orientations. The Figure (5.6) shows that the zigzag orientation is stiffer than the armchair counterpart. It also shows that the fracture strain depends on the chirality. For the present AFEM simulations the strain limit obtained for the zigzag was 0.22 and for the armchair was 0.17. The ultimate Cauchy tensile strength obtained were 101.3 GPa and 116.4 GPa in the armchair and zigzag cases, respectively.

The results obtained by Liu et al. (2007) and by Zhao et al. (2009) are show in Table 5.2. There is a fairly good agreement between the present AFEM calculations and the results reported by the mentioned authors.

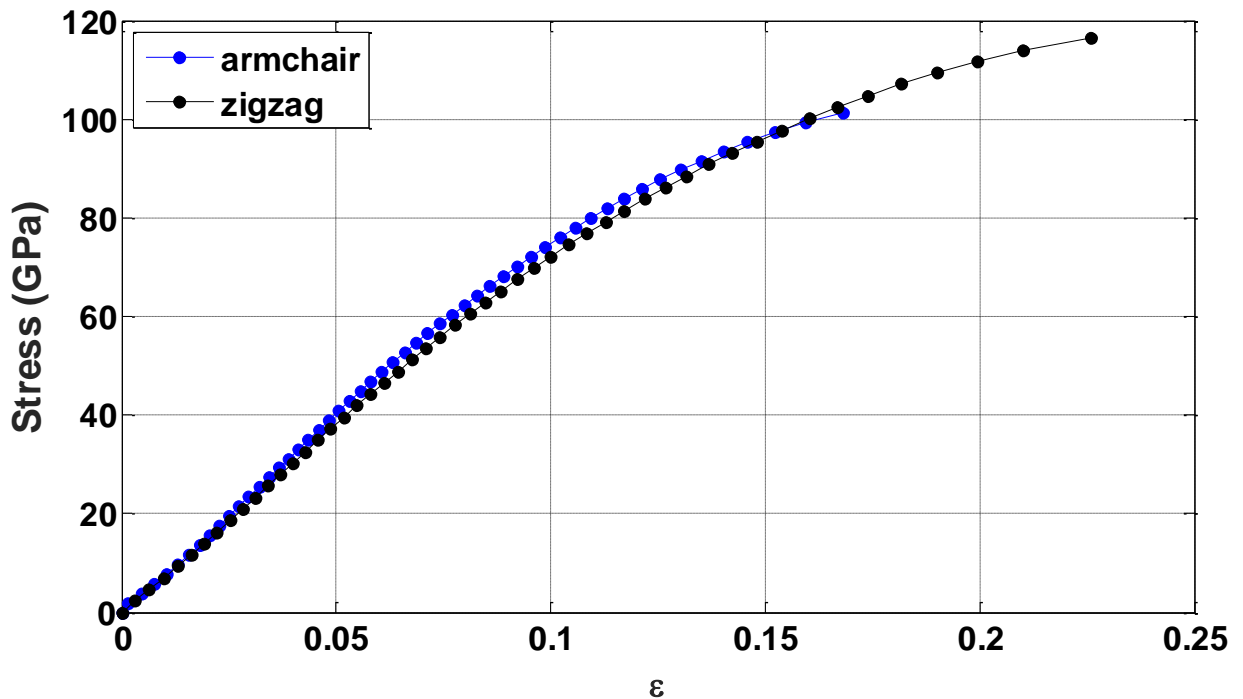


Figure 5.6: Stress-strain curves of the pristine graphene sheet having armchair zigzag edges along x direction.

**Table 5.2: Fracture strength calculated by atomistic studies.**

Atomistic Studies	Armchair	Zigzag
	Strength (GPa)	Strength (GPa)
Liu et al. (2007)	110	121
Zhao et al. (2009)	102	129
Present work	101.3	116.4

There are clear differences in the stress-strain curves presented in Figures 4.7 and 5.6 for the different chiralities and potentials. These differences are illustrated in Fig. 5.7 where the AFEM-based stress-strain curves obtained from the two different potential functions are compared with an independent MD simulation reported in the literature (Zhao et al. 2009).

Figure 5.7 shows that the stress-strain curves based on Tersoff potential has a strong chirality dependence whereas the results from the second generation REBO potential is nearly independent of the chirality except for the different tensile strengths and failure strains. The second generation REBO results in Fig. 5.7 agree quite closely with the results of Zhao et al. (2009), who used the orthogonal tight-binding method and molecular dynamic simulations based on the AIREBO potential (Stuart et al., 2000) to obtain their stress-strain curves. AIREBO is a more advanced version of the REBO potential and the second generation REBO results obtained from AFEM is as good as the AIREBO solutions although the AFEM computational cost is only a fraction of the MD computation cost. The deficiencies of the Tersoff potential in modelling the behaviour of graphene is clear from the Fig. 5.7 and it is therefore not used in Graphene NanoRibbons (GNR) modelling that also it will be showed in the section 5.3.5.



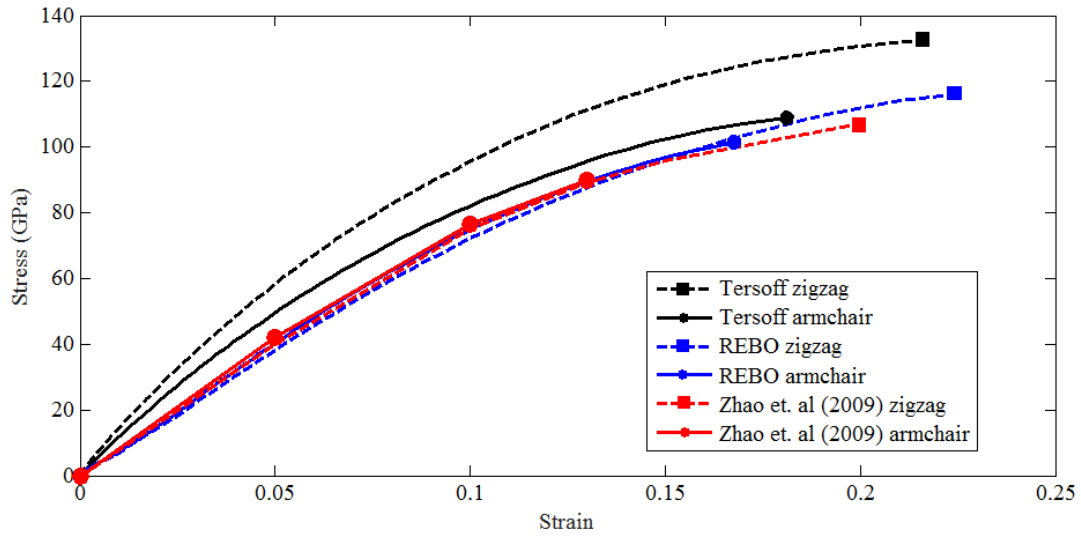


**Figure 5.7 Comparison of stress-strain curves of pristine bulk graphene obtained from AFEM using Tersoff and second generation REBO potentials with AIREBO potential based MD results.**

The ultimate tensile strength obtained from AFEM is 101.3 GPa and 116.4 GPa in the armchair and zigzag cases respectively. The fracture strain also depends on the chirality and is 0.17 and 0.23 in the armchair and zigzag directions respectively. The elastic modulus is 0.67 TPa for armchair and 0.71 TPa for zigzag. Zhao et al. (2009) used MD simulation and reported fracture strain and tensile as 0.13 and 90 GPa in the armchair direction, and 0.2 and 107 GPa in the zigzag direction. Lee et al. (2008) reported, based on experimental measurements, an elastic modulus and intrinsic breaking strength of  $1 \pm 0.1$  TPa and  $130 \pm 10$  GPa respectively for bulk graphene. Liu et al. (2007) using ab initio calculations reported an elastic modulus of 1.050 TPa and tensile strengths of 110 and 121 GPa in the armchair and zigzag directions respectively. Based on ab initio calculations, an elastic modulus of 1.11 TPa (Liera et al. 2000) and  $1.24 \pm 0.01$  TPa (Konstantinova et al. 2006) has been reported in the literature. Using atomistic simulations, Terdalkar et al. (2010) reported an elastic modulus of 0.84 TPa. Gao (2014) presented a comprehensive review of MD simulations of graphene and highlighted the differences between properties reported by different methods. The results obtained from the AFEM based on the second generation REBO potential agree quite well with the above reported solutions tensile strength but lower for the elastic modulus. It should be noted that results from various studies (both experimental and simulations) reported in the literature do not agree perfectly with each other due to different simulation conditions and assumptions (Gao, 2014). Generally, the tensile strength reported is in the range 90-130 GPa and elastic modulus around 0.7-1.1 TPa.

Further comparisons of stress-strain curves of bulk graphene obtained from AFEM based on the second generation REBO potential is shown in Fig. 5.8 where the MD simulation results of Dewapriya (2012) and Malakouti and Montazeri (2016) are used. The present results agree closely with Dewapriya (2012) who used the AIREBO potential but deviate from Malakouti and Montazeri (2016) at higher strains whose results appeared to be based on the first generation REBO potential. Based on these comparisons, it is clear that AFEM based on the second generation potential is able to accurately simulate the tensile response of bulk graphene.

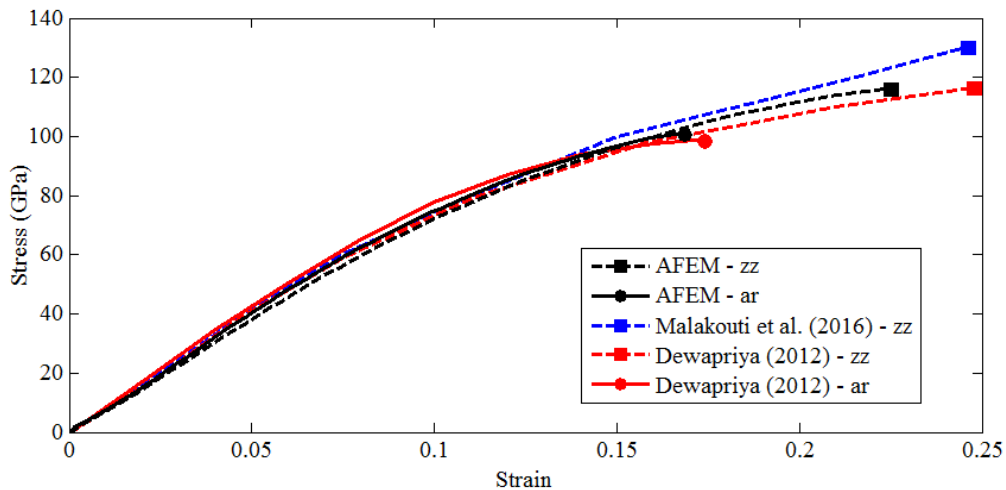


**Figure 5.8.** Comparison of stress-strain curves from AFEM with additional MD results from literature.

### 5.3.4 Effects of vacancy defects

Numerical and theoretical studies have shown that the presence of crack or vacancy defects reduce the ultimate tensile strength of graphene (Dewapriya 2012, Banhart et al., 2011). Furthermore, the ultimate tensile strength is related with the chirality. Figure (5.9) shows a graphene sheet with a defect. A crack of width  $6.98 \text{ \AA}$ , resulting from the exclusion of two atoms is introduced in order to analyse the influence of vacancy defects on the mechanical behaviour of graphene. The original pristine mesh has 660 atoms. Figures 5.10(a) and 5.10(b) show the stress-strain curves obtained from AFEM under uniaxial tensile loading for the case or armchair and zigzag oriented edges. The results in terms of ultimate tensile strength are

summarized in Table 5.3. It is clear that the presence of a crack reduces considerably the ultimate tensile strength of the graphene sheet. These curves also show that small vacancy defects have an influence on the ultimate tensile strength of graphene, but practically do not affect rigidity of the sample.

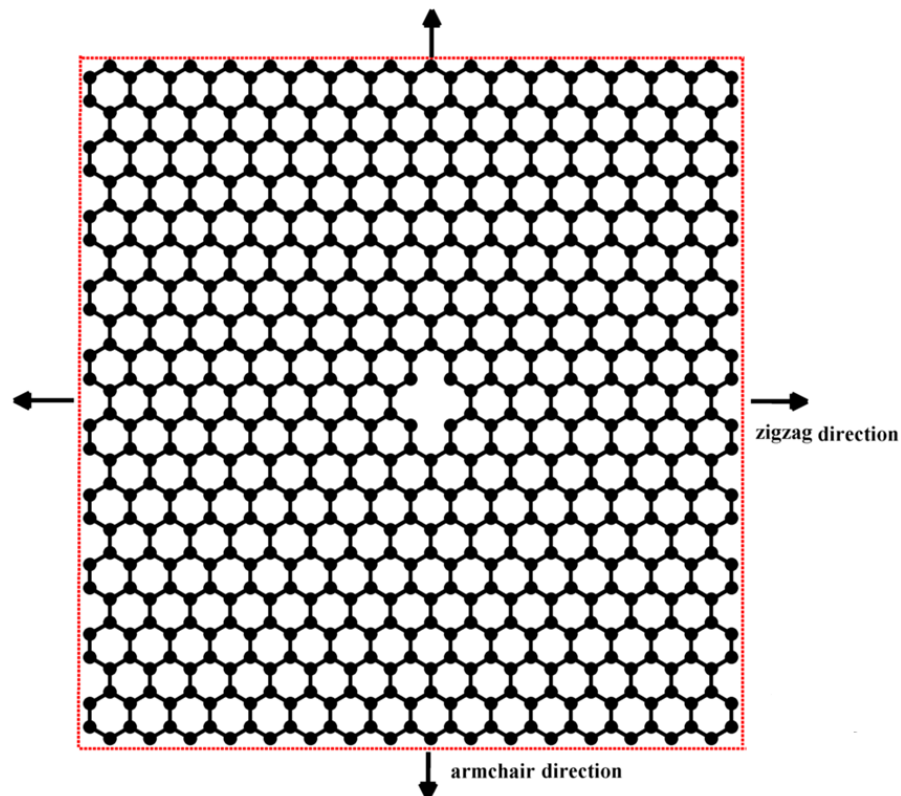
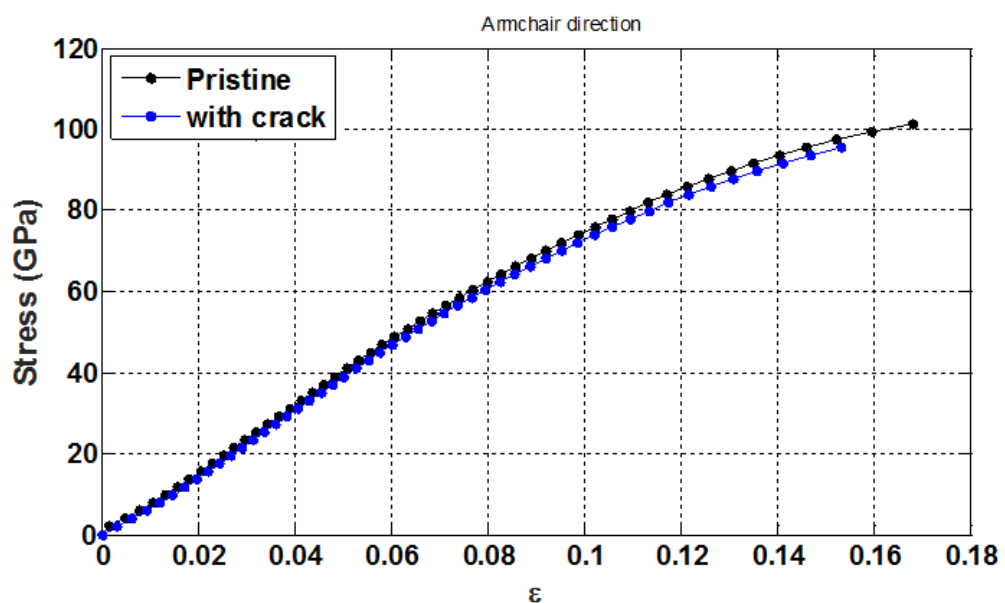


Figure 5.9: Graphene sheet having zigzag and armchair edges with a crack of width 6.98 Å.



(a) Armchair orientation

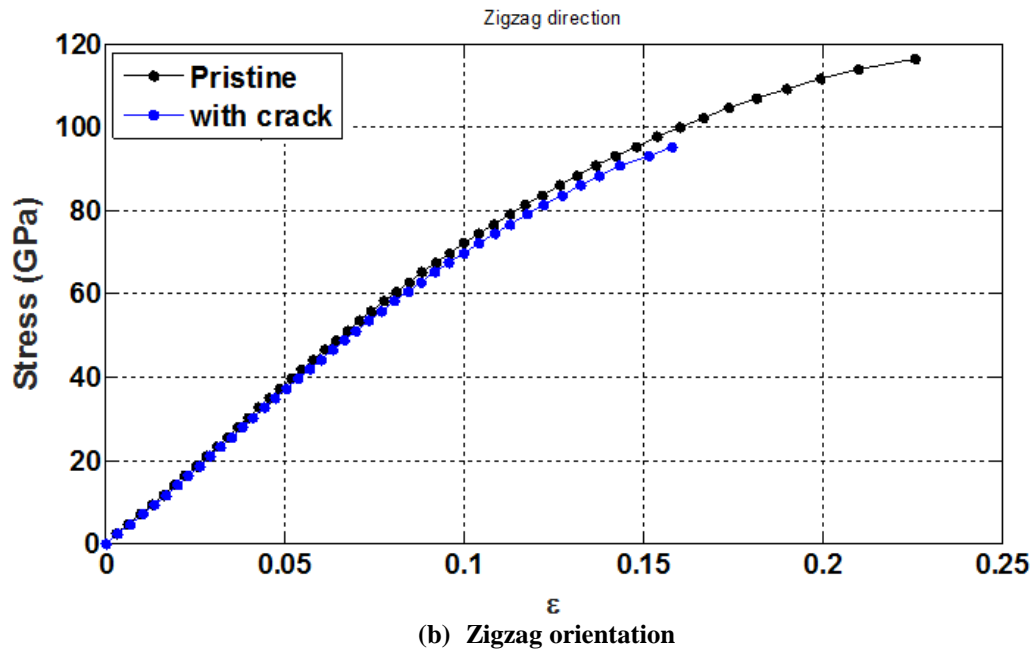


Figure 5.10: Stress-strain relation of the graphene sheet having armchair and zigzag edges with a crack of width 6.98 Å.

Table 5.3: Comparison of ultimate stress-strain results of graphene for the pristine sheet and for the one with vacancy defects.

AFEM results	Armchair		Zigzag	
	$\sigma$ (GPa)	$\epsilon$	$\sigma$ (GPa)	$\epsilon$
Pristine	101.3	0.17	116.4	0.22
With vacancy defects	95.5	0.15	95.4	0.16

### 5.3.5 Modelling of mechanical behaviour of graphene nanoribbons

Experimental characterization of Graphene NanoRibbons (GNRs) is still an expensive task and computational simulations are therefore seen as a practical option to study the properties and mechanical response of GNRs. Design of GNR elements in various nanotechnology devices can be approached through molecular dynamics simulations. This study demonstrates that the Atomic-scale Finite Element Method (AFEM) based on the second generation REBO potential is an efficient and accurate alternative to the molecular dynamics simulation of GNRs. Special atomic finite elements are proposed to model graphene edges. Extensive comparisons are presented with MD solutions to establish the accuracy of

AFEM. It is also shown that the Tersoff potential is not accurate for GNR modeling. The study demonstrates the influence of chirality and size on design parameters such as tensile strength and stiffness. Graphene is stronger and stiffer in the zigzag direction compared to the armchair direction. Armchair GNRs shows a minor dependence of tensile strength and elastic modulus on size whereas in the case of zigzag GNRs both modulus and strength show a significant size dependency. The size-dependency trend noted in the present study is different from the previously reported MD solutions for GNRs but qualitatively agrees with experimental results. Based on the present study, AFEM can be considered a highly efficient computational tool for analysis and design of GNRs.

The separation of carbon allotrope “graphene” (a single flat atomic layer of graphite) using mechanical exfoliation (Novoselov et al. 2004) and advances in nanofabrication have opened the door for the bottom-up approach to nanotechnology. In this approach, nanodevices are built from basic atomic structures such as Graphene NanoRibbons (GNRs), Carbon NanoTubes (CNT), etc. Graphene and other nanomaterials allow for the design and fabrication of a new generation of composites and nanoelectromechanical systems with attractive mechanical, electronic and optical properties (Choi and Lee 2016; Chen and Hone 2013).

Several fundamental design-related to issues require attention in the case of GNRs. While most atomistic simulation studies on graphene have focused on bulk graphene where Periodic Boundary Conditions (PBC) are used, GNRs have edges that could have a significant effect on design parameters such as tensile strength and elastic modulus (Fig. 5.11). The common GNR edges are either armchair or zigzag or they could be described by using an arbitrary chiral vector expressed in terms of the hexagonal base vectors  $n_1$  and  $n_2$  shown in Fig. 5.11. CNTs are considered 1-D structures and end effects are not significant in most applications. Furthermore, as shown by Zhao et al. (2009) using MD simulations, the above design parameters are strongly size and chirality dependent. It would therefore be useful to establish the applicability of AFEM as a design tool for GNRs through a comprehensive comparison with MD results and examine the size and chirality dependence of tensile strength and elastic modulus based on AFEM.

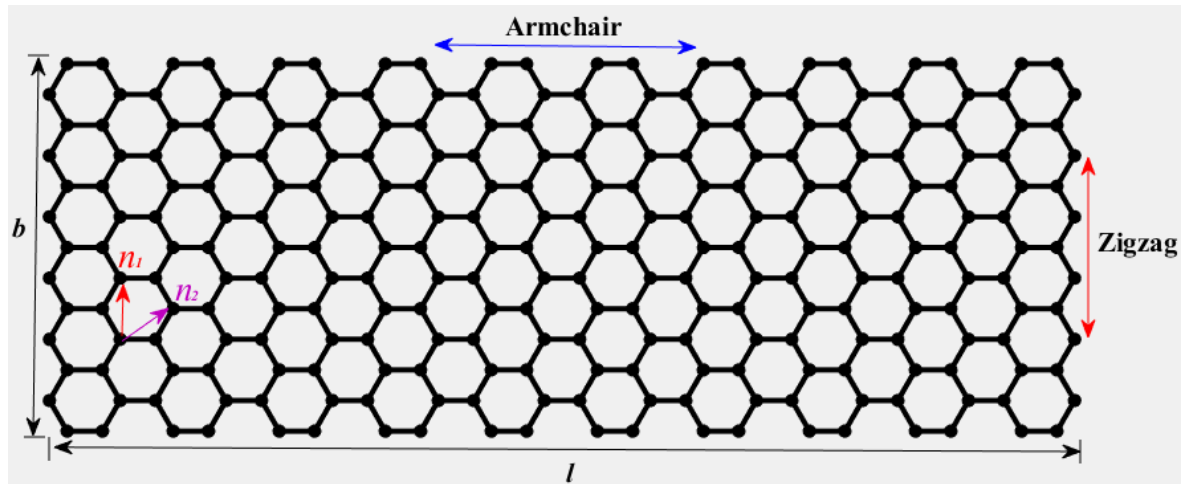
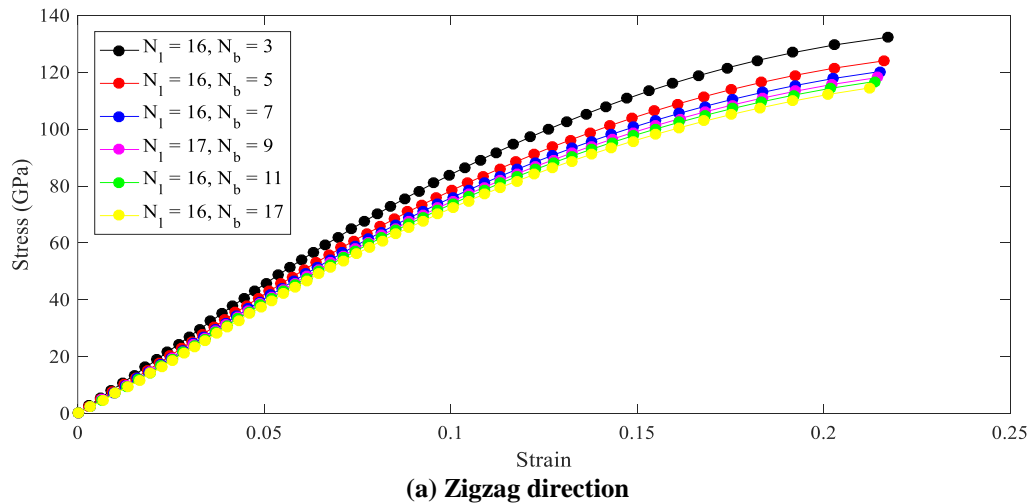


**Figure 5.11: Armchair and zigzag edges of graphene nanoribbon.**

Recent studies by Malakouti and Montazeri (2016) and Gajbhiye and Singh (2015) demonstrated the application of AFEM to analyze pristine and defective bulk graphene sheets and nonlinear frequency response respectively. While both these studies have not examined size-dependency, and edge and chirality effects of GNRs, they are also based on the Tersoff-Brenner (T-B) potential (Brenner 1990; Tersoff 1988). The T-B potential has certain deficiencies as reported by Brenner et al. (2002) and Stuart et al. (2000). In particular, it did not have a double bond or conjugate bond rotation barrier to prevent certain unrealistic bond rotations. The second generation REBO potential (Brenner et al. 2002) leads to a significantly better description of bond energies, lengths, and force constants for hydrocarbon molecules, as well as elastic properties thus enabling simulation of complex deformation patterns. It also accounts for forces associated with rotation about dihedral angles for carbon-carbon double bonds.

Based on the literature review and based on all the comparisons between AFEM and MD simulations considering Tersoff potential and second generation REBO potential, we demonstrated the deficiencies of Tersoff potential in modelling bulk graphene and we showed that AFEM based on the second generation REBO is a very efficient and accurate approach to simulate the mechanical response of GNRs. In this section, we focus on the size-dependency of tensile strength and elastic modulus of GNRs of different width to length ratios. Through these studies, we demonstrate that AFEM can be used as an accurate and efficient simulation tool for design of GNRs.

**Mechanical Behaviour of GNRs.** The mechanical behavior of GNRs of different dimensions is examined to study the effects of size and chirality on the elastic modulus and tensile strength. The results are based on the AFEM using the second generation REBO potential. The geometry of a typical GNR is shown in Fig. 5.11 where  $l$  and  $b$  denotes the length and width; and  $N_l$  and  $N_b$  denote the number of hexagonal cells in the length and width directions respectively. In the numerical study,  $N_l = 16$  with  $N_b$  equal to 3, 5, 7, 9, 11 and 17 are used to study the size effects of GNRs. Figure 5.12 shows the stress-strain curves of zigzag and armchair GNRs with varying values of  $N_b$ . Figure 5.13 shows the variation of tensile strength and elastic modulus with  $N_b$ . It is found that armchair GNRs shows little size-dependency of design properties whereas the size dependency is more prominent in the case of zigzag GNRs. This behavior agrees with the MD results reported by Zhao et al. (2009) for square GNRs and Chu et al. (2014) for both square and rectangular GNRs. Zigzag GNRs becomes stiffer as the width is reduced and the tensile strength is also increased as shown in Fig. 5.13. Zigzag GNRs have a higher tensile strength compared to armchair similar to the case of bulk graphene.



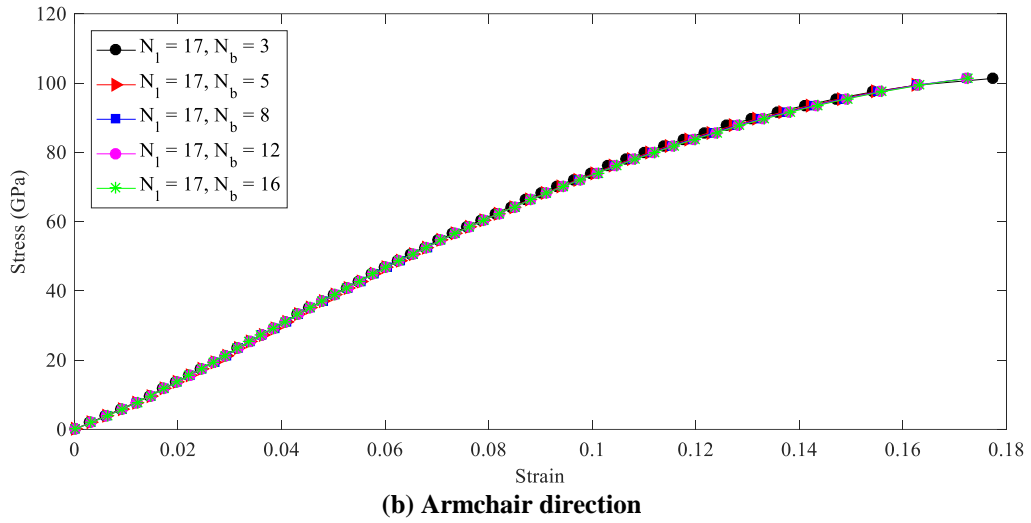


**Figure 5.12: Stress-strain curves of armchair and zigzag GNRs**

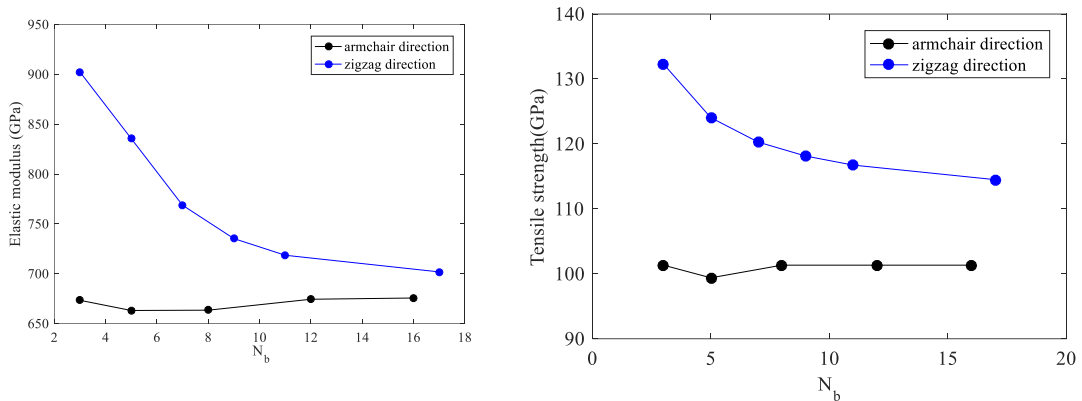


**Figure 5.13. Variation of elastic modulus and tensile strength of GNRs with different widths.**

However, it is interesting to note that the size dependency trend seen in Fig. 5.13 for tensile strength and elastic modulus of zigzag GNRs is different from the trend observed by Zhao et al. (2009) and Chu et al. (2014) who reported increases in tensile strength and elastic modulus as the size of GNR increases eventually approaching the bulk values. Although Zhao et al. (2009) used square GNRs in their simulation, Chu et al. (2014) used both square and rectangular GNRs to confirm their results. In order to investigate this difference, we present a comparison of MD results based on the second generation REBO potential with our AFEM results for GNRs in Fig. 5.14. The accuracy of AFEM solutions is again clear from Fig. 5.14. The trend we notice in Fig. 5.13 is similar to the experimental results of Shin et al. (2006) who determined the elastic modulus of single nanofibers with an ellipsoidal cross-section using an atomic force microscope. Their results confirm a substantial increase in the elastic modulus as the diameter of the fiber decreased similar to the trend noted in Fig. 5.13. It



is generally reported in the literature as the size decreases the properties improve in the case of nanomaterials. Such behaviour is accounted for by an increase in the number of boundary atoms with higher energies compared to the number of internal atoms.

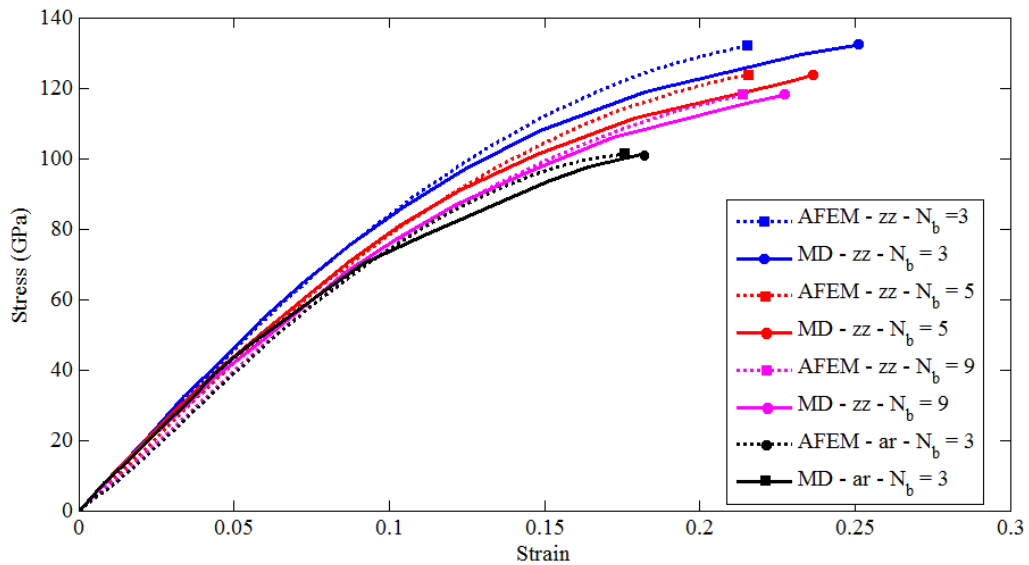


Figure 5.14. Comparison of GNR stress-strain curves obtained from AFEM with MD results.

## 5.4 Remarks

This chapter presents a formulation of the AFEM to model the mechanical behavior of bulk graphene sheets, as well as the GNRs using the multi-body second generation REBO potential. It's considered the same description of the modified atomic finite elements in order to account for the proper inclusion of boundary conditions in bounded graphene sheets and also necessary to model defects or vacancies in the graphene domain. This work does not make use of the periodic boundary condition used in many other reported scientific investigations. It analyzes bounded domains with prescribed force boundary conditions. The AFEM formulation was validated by comparison with a classical molecular dynamics software. The results present a good agreement between the two methodologies, MD and AFEM, specially at low to mid strains. For higher strains there are some deviations between both methods. Important aspects were discussed in the remarks of section 4.4.

The proposed AFEM implementation has been applied to investigate the influence of chirality, that is, of the orientation of the graphene edges, armchair or zigzag, on the rigidity and ultimate strength of the graphene. It has been shown that chirality has a pronounced effect on the graphene ultimate strength. The methodology has also been used to assess the influence of vacancies on the rigidity and failure strength of graphene. The performed numerical investigations show that vacancies or the removal of atoms from the pristine mesh has a marked influence on the ultimate strength of the considered graphene sheet. Additionally, the atomic-scale finite element method was successfully applied to study the mechanical response of GNRs.

## 6 GENERAL CONCLUSIONS

In this thesis, we presented a detailed description of the formulation and implementation of the Atomistic Finite Element Method (AFEM) considering three different potential fields: Lennard Jones potential, Tersoff potential and second generation REBO potential.

The section 3 presents a detailed description of the formulation and implementation of the Atomistic Finite Element Method (AFEM), exemplified in the analysis of one- and two-dimensional atomic domains governed by the Lennard-Jones interatomic potential. The methodology to synthesize element stiffness matrices and load vectors, the potential energy modification of the atomistic finite elements (AFE) to account for boundary edge effects, the inclusion of boundary conditions were carefully described, in a way that the authors had not previously found in the AFEM literature. The conceptual relation between the cut-off radius of interatomic potentials and the number of nodes in the AFE is addressed and exemplified for the 1D case. For the 1D case elements with 3, 5 and 7 nodes were addressed. The AFEM has been used to describe the mechanical behavior of one-dimensional atomic arrays as well as two-dimensional lattices of atoms. The reported studies also included the analysis of pristine domains, as well as domains with missing atoms, defects, or vacancies. Almost all results were compared with classical molecular dynamic simulations (MD) performed using a commercial package. The results have been very encouraging in terms of accuracy and in the computational effort necessary to execute both methodologies, AFEM and MD.

In the sections 4 and 5, the atomic-scale finite element method was applied to study the mechanical response of bulk graphene and in the section 5 the mechanical response of GNRs was also studied. Extensive comparisons with MD simulations reported in the literature are presented for bulk graphene stress-strain curves. It is found that both AFEM and MD based on Tersoff potential are not capable of modelling the tensile behavior of graphene. The AFEM based on the second generation REBO potential shows high accuracy in modelling the tensile response of bulk graphene. Comparisons with MD solutions reported in the literature show that the tensile strength predicted by AFEM is about 5-10 % higher than the results corresponding to MD. Failure strains predicted by AFEM are generally higher than the MD results. The difference between AFEM and corresponding MD results become more visible

closer to tensile failure point and hardly any difference is noted in the initial small strain range. Armchair GNRs show negligible size-dependency whereas size-effects are significant in the case of zigzag GNRs. In terms of the chirality effects, zigzag GNRs are stiffer and stronger than armchair GNRs and similar behavior is also noted for bulk graphene.

## **List of publication**

### **Articles in indexed Journals:**

Damasceno, D. A.; Mesquita, E.; Rajapakse, RNKD. Mechanical Behavior of Nano Structures Using Atomic-Scale Finite Element Method (AFEM). *Latin American Journal of Solids and Structures*, 2017, accepted.

Damasceno, D. A.; Mesquita, E.; Rajapakse, R. K. N. D.; Pavanello, R. *International Journal of Mechanics and Materials in Design*, 2017, under review.

### **Full Papers and Abstracts in Conference Proceedings:**

Damasceno, D. A.; Dewapriya, M. A. N.; Rajapakse, R. K. N. D.; Mesquita, E. Atomic-scale finite element modelling of graphene with vacancy defects. In: *ASCE Engineering Mechanics Institute International Conference*, 2015, Hong Kong, China.

Damasceno, D. A.; Dewapriya, M. A. N.; Mesquita, E.; Rajapakse, R. K. N. D. Study of crack propagation of graphene using atomic-scale finite element method. In: *1st Pan-American Congress on Computational Mechanics*, 2015, Buenos Aires, Argentina.

Damasceno, D. A.; Rajapakse, R. K. N. D.; Mesquita, E.; Mechanical behavior of atoms using atomic-scale finite element method. In: *Proceedings of the XXXVI Iberian Latin-American Congress on Computational Methods in Engineering, ABMEC*, 2015, Rio de Janeiro, Brasil.

Damasceno, D. A.; Mesquita, E.; Rajapakse, R. K. N. D.; Pavanello, R. Mechanical behavior of graphene sheet using atomic-scale finite element method. In: *24th International Congress of Theoretical and Applied Mechanics*, 2016, Montreal, Canadá.

Damasceno, D. A.; Mesquita, E.; Rajapakse, R. K. N. D.; Pavanello, R. The atomistic studies of mechanical behavior of graphene sheet using Tersoff potential. In: *7th International Conference on Mechanics and Materials in Design*, 2017, Albufeira (Algarve), Portugal.

Damasceno, D. A.; Mesquita, E.; Rajapakse, R. K. N. D.; Pavanello, R. The atomistic studies of mechanical behavior of graphene sheet with armchair and zigzag edges. In: *3rd EMI International Conference*, 2017, Rio de Janeiro, Brasil.

Damasceno, D. A.; Mesquita , E.; Rajapakse, R. K. N. D.; Pavanello, R. Assessment of the Accuracy of Atomic-scale Finite Element Method Using Different Potential Fields. In: 9th international conference on materials for advanced technologies, 2017, Singapura.

## 7 FUTURE WORKS

Based on this study, in the following future works are suggested:

- Implementation of AIREBO potential in order to solve more realistic problems. The AIREBO potential is considered to be one of the best available to simulate hydrocarbon systems such as graphene since it considers both covalent and non-bonded interactions between atoms.
- Modelling of large multiscale problems by using the combination of AFEM and FEM.
- Application of the AFEM to study the mechanical behavior of others nanomaterials, or the interactions of graphene sheet with presence of other kind of atom;
- Extend the AFEM implementation for modelling of problems in three dimensions;

## References

Adri C. T. van Duin, Siddharth Dasgupta, Francois Lorant, William A. Goddard, 2001. ReaxFF: A Reactive Force Field for Hydrocarbons. **The Journal of Physical Chemistry A**, v. 105, p. 9396–9409.

Alder, B. J.; Wainwright, T. E. Studies in Molecular Dynamics. I. General Method. **J. Chem. Phys.**, v. 31, p. 459, 1959.

Binnig, G.; Quate, C. F.; Gerber, Ch. Atomic force microscope. **Phys. Rev. Lett**, v. 56, n. 9, p. 930–933, 1986.

Binnig, G.; Rohrer, H. Scanning tunneling microscopy. **Surface Science**, v. 126, n. 1, 236–244, 1983.

Brenner, D. W. Empirical potential for hydrocarbons for use in simulating the chemical vapor deposition of diamond films. **Phys. Rev. B**, v. 42, p. 9458, 1990.

Bunch, J. S.; Van Der Zande, A. M.; Verbridge, S. S.; Frank, I. W.; Tanenbaum, D. M.; Parpia, J. M.; Craighead, H. G.; Mceuen, P. L. Electromechanical resonators from graphene sheets. **Science**, v. 315, n. 5811, p. 490–3, 2007.

Brenner, D.W.; Shenderova, O. A.; Harrison, J. A.; Stuart S. J.; Ni, B.; Sinnott, S. B. A second-generation reactive empirical bond order (REBO) potential energy expression for hydrocarbons. **J. Phys. Condens. Matter**, v. 14, p. 783–802, 2002.

Cancino, J.; Marangoni, V. S.; Zucolotto, V. Nanotecnologia em medicina: aspectos fundamentais e principais preocupações. **Quim. Nova**, v. 37, n. 3, p. 521–526, 2014.

Cecchi, M. Morandi; Rispoli, V.; Venturin, M. An atomic-scale finite element method for single-walled carbon nanotubes. In: **Applied and Industrial Mathematics in Italy III**, vol. 82, p. 449–460, 2009.

Chen, C.; Hone, J. Graphene Nanoelectromechanical Systems. In: **Proceedings of the IEEE**, v. 101, n. 7, 2013.

Chen, C.; Rosenblatt S.; Bolotin, K. I.; Kalb, W.; Kim, P.; Kymissis, I.; Stormer, H. L.; Heinz, T. F.; and Hone, J. Performance of monolayer graphene nanomechanical resonators with electrical readout. **Nat Nanotechnol**, vol. 4, n. 12, p. 861–867, 2009.

Choi, W., Lee, J-W. (eds.). **Graphene: Synthesis and Applications**, CRC Press, 2016.

Chu, Y., Ragab, T., Gautreau, P., Basaran, C.: Mechanical Properties of Hydrogen Edge–Passivated Chiral Graphene Nanoribbons. **Journal of nanomechanics and micromechanics**. 5, 04015001-1 - 04015001-8, 2015.

Dewapriya, M.A.N.: Molecular dynamics study of effects of geometric defects on the mechanical properties of graphene. **Master’s thesis**, University of British Columbia, (2012).

Dewapriya, M.A.N.; Rajapakse, R.K.N.D. Molecular dynamics simulations and continuum modeling of temperature and strain rate dependent fracture strength of graphene with vacancy defects. **Int. J. Fracture**. doi: 10.1115/1.4027681, 2014.

Dingerville, R.; Qu, J.; Cherakoui, M. Surface free energy and its effect on the elastic behavior of nano-sized particles wires and films. **J. Mech. Phys. Solid.**, v. 53, p. 1827, 2005.

Dirac, P.A.M. **The Principles of Quantum Mechanics**. Clarendon Press, Oxford, 1981.

Feynman, R.P. There’s Plenty of Room at the Bottom. Feynman, R. **Lecture at the California Institute of Technology**, [www.zyvex.com/nanotech/feynman.html](http://www.zyvex.com/nanotech/feynman.html), 1959.

Gao, G. Atomistic Studies of Mechanical Properties of Graphene. **Polymers**, doi:10.3390/polym6092404, 2014.

Garcia-Sanchez, D.; Van Der Zande, A. M.; Paulo, A. S.; Lassagne, B.; Mceuen, P. L.; Bachtold, A. Imaging mechanical vibrations in suspended graphene sheets. **Nano letters**, v.8, n. 5, p.1399-403, 2008.

Goettler, L. A.; Lee, K. Y.; Thakkar, H. Layered silicate reinforced polymer nanocomposites: development and applications, **Polym. Rev.**, v. 47, n. 2, p. 291-317, 2007.



Guo, X. ; Leung, A.Y.T. ; He, X.Q. ; Jiang, H. ; Huang, Y. Bending buckling of single-walled carbon nanotubes by atomic-scale finite element. **Composites: Part B**, vol. 39, n. 1, p. 202–208, 2008.

Gupta, Swaroopa Rani N. Advances in Molecular Nanotechnology from Premodern to Modern Era. **IJMSE**, vol. 2, n. 2, 2014.

Gurtin, M.E.; Murdoch, A. I. A continuum theory of elastic material surfaces, **Arch. Ration. Mech. Anal.**, v. 57, p. 291, 1975.

Haile, J. M. **Molecular Dynamics Simulation**. Wiley, New York, 1992.

Hu, Y.; Shenderova, O. A.; Hu, Z.; Padgett, C. W.; Brenner, D. W. ), Carbon nanostructures for advanced composites. **Rep. Prog. Phys.**, v. 69, n. 6, p.1847-1895, 2006.

Iijima, S. Helical microtubules of graphitic carbon. **Nature**, v. 354, p. 56–58, 1991.

Jones, J. E. On the determination of molecular fields—II. From the equation of state of a gas. In: **Proceedings of the Royal Society A**, v. 106, p. 463–477, 1924.

Kim, K. The Atomic-scale Finite Element Method for Analyzing Mechanical Behavior of Carbon Nanotube and Quartz. M.Sc. Dissertation, Virginia Polytechnic Institute, 2006.

Kim, NH. Introduction to Nonlinear Finite Element Analysis, New York, **Springer US**, 2015.

Konstantinova E.; Dantas S. O.; Barone P. M. V. B. Electronic and elastic properties of two-dimensional carbon planes. **Phys. Rev. B**, v. 74, 2006.

Kroto, H. W.; Heath, J. R.; O'Brien, S. C.; Curl, R. F.; Smalley, R. E. C60: Buckminsterfullerene. **Nature**, v. 318, n. 6042, p. 162-163, 1985.

Lee, C.; Wei, X.; Kysar, J. W.; Hone, J. Measurement of the elastic properties and intrinsic strength of monolayer graphene. **Science**, v. 321, p. 385 - 8, 2008.

Leung, A. Y. T.; Guo, X.; and He, X. Q. Postbuckling of carbon nanotubes by atomic-scale finite element. **J. Appl. Phys**, vol. 99, n.12, 2006.

Liera, G.V., Alsenoyb, C.V., Dorenc V.V., Geerlingsd P.: Ab initio study of the elastic properties of single-walled carbon nanotubes and graphene. **Chemical Physics Letters**. 326, 181-185, 2000.

Liu, B.; Jiang, H.; Huang, Y.; Qu, S.; Yu, M. F. Atomic-scale finite element method in multiscale computation with applications to carbon nanotubes. **Phys. Rev. B**, v. 72, 035435, 2005.

Liu, B.; Huang, Y.; Jiang, H.; Qu, S.; Hwang, K. C. The atomic-scale finite element method. **Comp. Meth. Appl. Mech. Engrg**, v. 193, n. 17, p. 1849-1864, 2004.

Liu, C.; Rajapakse, R.K.N.D. Continuum models incorporating surface energy for static and dynamic response of nanoscale beams. **IEEE Trans. Nanotechnology**, v. 9, p. 422, 2010.

Liu, F.; Ming, P.M.; Li, J. Ab initio calculation of ideal strength and phonon instability of graphene under tension. **Phys. Rev. B**, v. 76, 2007.

Lu, Z.; Ma, L.; Tan, J.; Wang, H.; Ding, X. Transparent multi-layer graphene/polyethylene terephthalate structures with excellent microwave absorption and electromagnetic interference shielding performance. **Nanoscale**, v. 8, p. 16684-16693, 2016.

Malakouti, M. ; Montazeri, A. Nanomechanics analysis of perfect and defected graphene sheets via a novel atomicscale finite element method. **Superlattices Microstruct**, vol. 94, p.1-12, 2016.

Maranganti, R.; Sharma, P. Length scales at which classical elasticity breaks down for various materials. **Phy. Rev. Lett.**, v. 98, n. 19, 195504, 2007.

Miller, R. E.; Shenoy, V. B. Size-dependent elastic properties of nanosized structural elements. **Nanotechnology** , v. 11, p. 139 - 147, 2000.

Njuguna, J. ; Pielichowski, K. Polymer nanocomposites for aerospace applications: properties. **And. Eng. Mater.**, v. 5, n. 11, p. 769-778, 2003.

Novoselov, K. S.; Fal'Ko, V. I.; Colombo, L.; Gellert, P. R.; Schwab, M. G.; Kim, K. A roadmap for graphene. **Nature**, v. 490, n. 7419, p. 192, 2012.

Novoselov, K. S.; Geim, A. K.; Morozov, S. V.; Jiang, D.; Zhang, Y.; Dubonos, S. V.; Grigorieva, I. V.; Firsov, A. A. Electric field effect in atomically thin carbon films. **Science**, v. 306, n. 5696, p. 666 – 9, 2004.

Sapsathiarn, Y.; Rajapakse, R.K.N.D. A model for large deflections of nanobeams and experimental comparison, **IEEE Trans. Nanotech.**, v. 11, p. 247, 2012.

Smit, B. Phase diagrams of Lennard-Jones fluids. **J. Chem. Phys.**, v. 96 (11), p. 8639, 1992.

Souza, J. E. P. Nanodispositivos baseados em grafeno. 2012. Tese (doutorado em física) - Instituto de física, Universidade de São Paulo, São Paulo, 2012.

Stuart, Steven J.; Tutein, Alan B.; Harrison, Judith A. A reactive potential for hydrocarbons with intermolecular interactions. **J. Chem. Phys.**, v. 112, n. 14, p. 6472 -6486, 2000.

Tadmor, E.B., Miller, R.E. Modeling materials: **continuum, atomistic, and multiscale techniques**. Cambridge University Press, New York, 2011.

Taniguchi, N. On the basic concept of nanotechnology. In: **Proceedings of the International Conference on Production Engineering**, Tokyo, Part II, Japan Society of Precision Engineering, 1974, p. 18-23.

Tao, Jixiao ; Sun, Yuzhou Mortazavi, Bohayra. The Elastic Property of Bulk Silicon Nanomaterials through an Atomic Simulation Method. **J Nanomater**, vol. 2016, p. 6, 2016.

Tersoff, J. New empirical approach for the structure and energy of covalent systems. **Phys. Rev. B.**, v. 37, p. 6991, 1987.

Tersoff, J. Empirical interatomic potential for carbon with applications to amorphous carbon. **Phys. Rev. Lett.**, v. 61, p. 2879, 1988.

Terdalkar, S.S.; Huang, S.; Yuan, H.Y.; Rencis, J.J.; Zhu, T.; Zhang, S.L. Nanoscale fracture in graphene. **Chem. Phys. Lett.**, v. 494, p. 218–222, 2010.

The Royal Society and the Royal Academy of Engineering. **Nanoscience and Nanotechnologies: Opportunities and Uncertainties**. London, UK, 2004.

Van Duin, Adri C. T.; Dasgupta, Siddharth; Lorant, Francois; Goddard, William A. Iii. ReaxFF: A Reactive Force Field for Hydrocarbons. **J. Phys. Chem. A**, v. 105, n. 41, p. 9396–9409, 2001.

Zhao, H.; Min, K.; Aluru, N.R. Size and chirality dependent elastic properties of graphene nanoribbons under uniaxial tension. *Nano Lett.* **2009**, 9, 3012–3015.

Yazdanbakhsh, A.; Grasley, Z.; Tyson, B.; Al-Rub, R. A. Carbon nano filaments in cementitious materials: some issues on dispersion and interfacial bond. In: **Proceedings of the American Concrete Institute**, v. 267, p. 21-34, 2009.

## APPENDIX A – Lennard Jones derivatives

$$\frac{dU(\mathbf{r}_{ij})}{dx_i} = 4\epsilon \left[ -6 \frac{\sigma^{12}(2x_i - 2x_j)}{\left((x_i - x_j)^2 + (y_i - y_j)^2\right)^7} + 3 \frac{\sigma^6(2x_i - 2x_j)}{\left((x_i - x_j)^2 + (y_i - y_j)^2\right)^4} \right] \quad (\text{A.1})$$

$$\frac{dU(\mathbf{r}_{ij})}{dy_i} = 4\epsilon \left[ -6 \frac{\sigma^{12}(2y_i - 2y_j)}{\left((x_i - x_j)^2 + (y_i - y_j)^2\right)^7} + 3 \frac{\sigma^6(2y_i - 2y_j)}{\left((x_i - x_j)^2 + (y_i - y_j)^2\right)^4} \right] \quad (\text{A.2})$$

$$\frac{d^2U(\mathbf{r}_{ij})}{dx_i dx_i} = 4\epsilon \left( \begin{aligned} & \left( \frac{6\sigma^6}{\left((x_i - x_j)^2 + (y_i - y_j)^2\right)^4} - \frac{12\sigma^{12}}{\left((x_i - x_j)^2 + (y_i - y_j)^2\right)^7} - \dots \right) \\ & \frac{12\sigma^6(2x_i - 2x_j)^2}{\left((x_i - x_j)^2 + (y_i - y_j)^2\right)^5} + \frac{42\sigma^{12}(2x_i - 2x_j)^2}{\left((x_i - x_j)^2 + (y_i - y_j)^2\right)^8} \end{aligned} \right) \quad (\text{A.3})$$

$$\frac{d^2U(\mathbf{r}_{ij})}{dx_j dx_j} = -4\epsilon \left( \begin{aligned} & \left( \frac{6\sigma^6}{\left((x_i - x_j)^2 + (y_i - y_j)^2\right)^4} - \frac{12\sigma^{12}}{\left((x_i - x_j)^2 + (y_i - y_j)^2\right)^7} - \dots \right) \\ & \frac{12\sigma^6(2x_i - 2x_j)^2}{\left((x_i - x_j)^2 + (y_i - y_j)^2\right)^5} + \frac{42\sigma^{12}(2x_i - 2x_j)^2}{\left((x_i - x_j)^2 + (y_i - y_j)^2\right)^8} \end{aligned} \right) \quad (\text{A.4})$$

$$\frac{d^2U(\mathbf{r}_{ij})}{dy_i dy_i} = 4\epsilon \left( \begin{aligned} & \left( \frac{6\sigma^6}{\left((x_i - x_j)^2 + (y_i - y_j)^2\right)^4} - \frac{12\sigma^{12}}{\left((x_i - x_j)^2 + (y_i - y_j)^2\right)^7} - \dots \right) \\ & \frac{12\sigma^6(2y_i - 2y_j)^2}{\left((x_i - x_j)^2 + (y_i - y_j)^2\right)^5} + \frac{42\sigma^{12}(2y_i - 2y_j)^2}{\left((x_i - x_j)^2 + (y_i - y_j)^2\right)^8} \end{aligned} \right) \quad (\text{A.5})$$

$$\frac{d^2U(\mathbf{r}_{ij})}{dy_j dy_i} = -4\varepsilon \left( \frac{\frac{6\sigma^6}{\left((x_i - x_j)^2 + (y_i - y_j)^2\right)^4} - \frac{12\sigma^{12}}{\left((x_i - x_j)^2 + (y_i - y_j)^2\right)^7} - \dots}{\frac{12\sigma^6(2y_i - 2y_j)}{\left((x_i - x_j)^2 + (y_i - y_j)^2\right)^5} + \frac{42\sigma^{12}(2y_i - 2y_j)}{\left((x_i - x_j)^2 + (y_i - y_j)^2\right)^8}} \right) \quad (\text{A.6})$$

$$\frac{d^2U(\mathbf{r}_{ij})}{dy_i dx_i} = (-4)\varepsilon \left( \frac{12\sigma^6(2x_i - 2x_j)(2y_i - 2y_j)}{\left((x_i - x_j)^2 + (y_i - y_j)^2\right)^5} - \frac{42\sigma^{12}(2x_i - 2x_j)(2y_i - 2y_j)}{\left((x_i - x_j)^2 + (y_i - y_j)^2\right)^8} \right) \quad (\text{A.7})$$

$$\frac{d^2U(\mathbf{r}_{ij})}{dy_j dx_i} = 4\varepsilon \left( \frac{12\sigma^6(2x_i - 2x_j)(2y_i - 2y_j)}{\left((x_i - x_j)^2 + (y_i - y_j)^2\right)^5} - \frac{42\sigma^{12}(2x_i - 2x_j)(2y_i - 2y_j)}{\left((x_i - x_j)^2 + (y_i - y_j)^2\right)^8} \right) \quad (\text{A.8})$$